LOCALIZATION AND TRACKING IN WIRELESS MIMO SYSTEMS
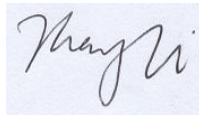
ZHANG LI

A THESIS SUBMITTED FOR THE DEGREE OF

DOCTOR OF PHILOSOPHY

NUS GRADUATE SCHOOL FOR INTEGRATIVE SCIENCES AND
ENGINEERING

NATIONAL UNIVERSITY OF SINGAPORE

2013

Declaration

I hereby declare that this thesis is my original work and it has been written by me in its entirety. I have duly acknowledged all the sources of information which have been used in the thesis.

This thesis has also not been submitted for any degree in any university previously.

Zhang Li
01 Nov 2013

To my parents.

Acknowledgements

I would like to express my sincere gratitude to my supervisor, Prof. Lawrence Wong Wai-Choong, who has given me his continuous support during my PhD candidature. He provided me the invaluable opportunity to study, and I am very grateful for his guidance and the trust in my ability to carry out research independently. I have been benefited from his sharing of experiences, and the insights and advices provided during our discussions.

I would like to express my heartfelt appreciation to my co-supervisor, Dr. Chew Yong Huat, for his guidance and encouragement since the beginning of my PhD candidature. His knowledge, patience and motivational thoughts have always inspired me to move forward. He has devoted a lot of efforts in the thesis, without which its completion is not possible.

I would also like to thank my thesis advisory committee members, Prof. Hari Krishna Garg and Dr. Zhang Rui, for their efforts and critical yet beneficial comments during the PhD qualification examination.

Words cannot express my thankfulness to my parents and my wife. Their love, care, support and encouragement are the source of my strength. I am also grateful to my younger sister, who has been accompanying our parents when I am far from home.

I would also like to thank the lab officers, Mr Song Xianlin and Ms Guo Jie, for providing assistance in carrying out my research.

Last but not least, I would like to thank all my friends in IDMI Ambient Intelligence Lab, for their friendships and many of the happiness hours working together.

Contents

Summary

Due to the demands for location-based services, localization and tracking of a mobile terminal (MT) have attracted much attention recently. Various approaches have been proposed, some of which are developed using the existing communications infrastructure. When performing localization and tracking in multiple-input multiple-output (MIMO) systems, the space-time processing capability which MIMO can provide not only enhances the estimation accuracy, but also enable the ability to develop more unique methods than when single-antenna systems are used. In this thesis, we aim to exploit the additional enhancements in location estimation and accuracy which MIMO systems can provide. The space-time processing techniques together with the prior channel state information (CSI) are used to enhance the performance of location systems. We also study a MT tracking method based on the space-time processing capability of MIMO systems.

We first propose a precoder design strategy to enhance the estimation of angle-of-arrival (AoA) and location. Starting from deriving a new asymptotic error variance bound for the MUSIC (MUltiple SIgnal Classification) algorithm, we propose an optimal precoder to achieve the bound. As it is impractical to realize such optimal precoder, we further propose a more feasible precoder design, which leverages on the feedback CSI estimated at the receiver. Both precoder schemes perform similarly and exhibit improvements in performance when compared with the case without precoder. Furthermore, the precoder technique is applied to a known AoA-based localization method, and the improvement on the accuracy of the location estimate is studied numerically through simulations.

With the objective of minimizing Cramer-Rao lower bound (CRLB) of the time-of-arrival (ToA) estimator, we next study the impact of signal pre-processing on the ToA estimation performed in MIMO systems. Transmit beamforming is adopted when the CSI at the transmitter (CSIT) is available, while space-time block code (STBC) is employed as the transmit diversity technique for the case

without CSIT. We demonstrate that the accuracy of the ToA estimator is enhanced with the availability of CSIT and the number of antennas.

A maximum a posterior (MAP) based channel estimation algorithm is also proposed to jointly estimate the temporal and spatial domain channel parameters for single-input multiple-output (SIMO) systems. The proposed algorithm leverages on prior knowledge of the statistics of the channel parameters used in the extended Saleh-Valenzuela (SV) model, and uses the expectation-maximization (EM) algorithm to reduce computational complexity. We also discuss how the algorithm can be extended and applied to MIMO systems.

Finally, we propose a novel efficient three-step tracking approach. An algorithm based on the space-time correlation of the received signal is first developed to estimate the radial velocity (both the speed and direction) of the MT. The extend Kalman filter (EKF) based tracking method is next adopted to estimate the current location of the MT by using the estimated parameters and the previous location estimate. Finally, the MUSIC algorithm is applied to obtain additional high-resolution AoA (HR-AoA) estimate and we show how this partial location information can be fused with the tracking results to further improve tracking accuracy. The performances of the algorithms are studied through simulations.

List of Figures

List of Tables

List of Symbols

Symbol	Meaning
M	number of antennas at the transmitter
N	number of antennas at the receiver
L	number of multipath components
$x(t)$	signal stream before transmit signal pre-processing
$\mathbf{x}(t)$	signal vector before transmit signal pre-processing
$s(t)$	transmitted signal at the transmitter with single antenna
$\mathbf{s}(t)$	transmitted signal vector at the transmitter antenna array
$\mathbf{y}(t)$	signal vector impinging on the receiver antenna array
$\mathbf{r}(t)$	received signal vector at the receiver antenna array
$\mathbf{u}(t)$	received signal vector at the receiver array without noise
$g(t)$	signal stream after receive beamforming
$\mathbf{z}(t)$	white noise vector at the receiver, with each entry being a Gaussian random variable with zero mean and variance N_0
N_0	power spectral density of white noise
$\mathbf{c}_T(\cdot)$	steering vector of transmitter antenna array
$\mathbf{c}_R(\cdot)$	steering vector of receiver antenna array
$\mathbf{C}_T(\cdot)$	steering matrix of transmitter antenna array
$\mathbf{C}_R(\cdot)$	steering matrix of receiver antenna array
d_h	distance between two adjacent antennas in a uniform linear array (ULA)
λ_s	carrier wavelength
$\Omega_{T,l}$	angle-of-departure (AoD) of the lth path
$\Omega_{R,l}$	angle-of-arrival (AoA) of the lth path
$\omega_{R,l}$	phase difference of the signal with AoA $\Omega_{R,l}$ impinging on two adjacent antennas in a ULA, $\omega_{R,l} = 2\pi d_h \cos \Omega_{R,l}/\lambda_s$
α_l	complex path gain of the lth path

Symbol	Meaning
$\mathbf{H}$	channel matrix, with the truncated singular value decomposition (SVD) as $\mathbf{H} = \mathbf{U}_h \mathbf{\Lambda}_h \mathbf{V}_h^H$
$\mathbf{H}_b$	channel matrix exclusive of the receiver antenna array, with the truncated SVD as $\mathbf{H}_b = \mathbf{U}_b \mathbf{\Lambda}_b \mathbf{V}_b^H$
$\lambda_{h,l}$	the lth singular value of $\mathbf{H}$
$\lambda_{b,l}$	the lth singular value of $\mathbf{H}_b$
$\mathbf{Q}$	covariance matrix of the transmitted signal vector $\mathbf{s}(t)$
$\mathbf{P}$	covariance matrix of the signal $\mathbf{y}(t)$
$\mathbf{F}$	precoder matrix
$\mathbf{\Sigma}_b$	power allocation matrix in the optimal precoder, $\mathbf{\Sigma}_b = \mathrm{diag}\{\sigma_{b,1}, \ldots, \sigma_{b,L}\}$
$\mathbf{\Sigma}_h$	power allocation matrix in the practical precoder, $\mathbf{\Sigma}_h = \mathrm{diag}\{\sigma_{h,1}, \ldots, \sigma_{h,L}\}$
P_T	total transmitted signal power
P_R	total received signal power
E_s	power of a transmitted signal stream
K_x	number of uncorrelated signal streams in $\mathbf{x}(t)$
I	number of samples
$\mathbf{I}_n$	$n \times n$ identity matrix
λ_L	Lagrange multiplier
θ_d	AoA difference of a pair of signals
$\theta_{3\mathrm{dB}}$	3 dB beamwidth of an antenna array
(x_m, y_m)	location of a mobile terminal (MT) in a 2-D space
(x_f, y_f)	location of a fixed terminal (FT) in a 2-D space
N_f	number of FTs involved in a localization process
L_n	number of multipath components between the nth FT and the MT
σ_d	standard derivation of a distance measurement
$\mathbf{w}_T$	transmit beamforming vector
$\mathbf{w}_R$	receive beamforming vector
ζ	equivalent channel coefficient which involves the effects due to the channel and the transmit and receive beamforming
λ_h	singular value of channel matrix $\mathbf{H}$ of a single-path channel
$a(t)$	pulse with unit energy

Symbol	Meaning
$A(f)$	Fourier transform of $a(t)$
β_a	effective bandwidth of $a(t)$
b_l	data symbol taking the value of either -1 or $+1$
T_s	symbol duration
$\mathbf{J}_\Theta$	Fisher information matrix with respect to the parameter Θ
$\mathbf{H}_f$	feedback channel matrix
σ_f	the quality of $\mathbf{H}_f$, e.g. $\sigma_f^2 = 0.1$ indicates 10% error in $\mathbf{H}_f$
$\Gamma, \gamma, \Phi, \phi, \sigma$	parameters of the extended Saleh-Valenzuela (SV) model
$h(\cdot)$	channel impulse response (CIR)
L_c	number of clusters in the clustered channel model
K_l	number of rays in the lth cluster in the clustered channel model
$\Theta_{T,l}$	mean AoD of the lth cluster in the clustered channel model
$\varphi_{T,kl}$	AoD of the kth ray in the lth cluster relative to $\Theta_{T,l}$ in the clustered channel model
$\Omega_{T,kl}$	AoD of the kth ray in the lth cluster in the clustered channel model, $\Omega_{T,kl} = \Theta_{T,l} + \varphi_{T,kl}$
$\Theta_{R,l}$	mean AoA of the lth cluster in the clustered channel model
$\varphi_{R,kl}$	AoA of the kth ray in the lth cluster relative to $\Theta_{R,l}$ in the clustered channel model
$\Omega_{R,kl}$	AoA of the kth ray in the lth cluster in the clustered channel model, $\Omega_{R,kl} = \Theta_{R,l} + \varphi_{R,kl}$
T_l	time-of-arrival (ToA) of the lth cluster in the clustered channel model
τ_{kl}	ToA of the kth ray in the lth cluster in the clustered channel model
α_{kl}	complex path gain of the kth ray in the lth cluster in the clustered channel model
σ_{kl}	standard derivation of α_{kl}
$\mathbf{w}_{kl}(t)$	signal transmitted through the kth ray in the lth cluster, the set of signals forms the complete data
v	speed of the MT
ψ	moving direction of the MT
v_0	radial speed of the MT

Symbol	Meaning
Ω_0	line-of-sight (LOS) AoA seen at the FT
Ω_R	mean AoA of the multipath components seen at the FT
c	speed of light
f_c	carrier frequency
f_D	Doppler frequency
f_0	Dopper frequency due to radial velocity
$C_r(n-m,\tau)$	space-time correlation of two received signals arriving at the nth and mth antennas respectively, with time difference τ
K	Rician factor
κ	parameter of the von-Mises distribution
ϑ	state vector in the extended Kalman filter (EKF) based tracking
A_w	relative reliability of the EKF output compared with the high-resolution AoA (HR-AoA) estimate
ρ	memory level in the Gauss-Markov mobility model
j	$\sqrt{-1}$
i,k,l,m,n	indices
$(\cdot)^T$	transposition of the argument
$(\cdot)^*$	complex conjugate of the argument
$(\cdot)^H$	Hermitian transpose of the argument
$(\cdot)^\dagger$	Moore-Penrose pseudoinverse of the argument
$\mathrm{tr}(\cdot)$	matrix trace
$(\cdot)_{i,k}$	i,k element of a matrix
$\mathrm{E}_x\{\cdot\}$	expectation with respect to x
$\mathrm{diag}(\cdot)$	function that constructs a diagonal matrix with entries of the argument along the main diagonal
$\Re\{\cdot\}$	real part of a complex number
$\|\cdot\|$	absolute value of a complex number
$\|\cdot\|$	vector norm
$\|\cdot\|_F$	Frobenius norm
$\angle$	operator to take the phase angle of a complex number
$p(\cdot)$	probability of a random variable
$\delta(\cdot)$	Delta function
$I_0(\cdot)$	zeroth-order modified Bessel function of the first kind

List of Abbreviations

3GPP	3rd Generation Partnership Project
AoA	angle-of-arrival
AoD	angle-of-departure
CIR	channel impulse response
CRLB	Cramer-Rao lower bound
CSI	channel state information
CSIR	channel state information at the receiver
CSIT	channel state information at the transmitter
EKF	extended Kalman filter
EM	expectation-maximization
ESPRIT	estimation of signal parameters via rotational invariance techniques
FT	fixed terminal
GPS	Global Positioning System
HR-AoA	high-resolution angle-of-arrival
KF	Kalman filter
LOS	line-of-sight
LS	least square
MAP	maximum a-posterior
MIMO	multiple-input multiple-output
ML	maximum likelihood
MRC	maximum ratio combining
MT	mobile terminal
MUSIC	multiple signal classification
NLOS	non-line-of-sight
PN	pseudo-noise

RF	radio-frequency
RSS	received signal strength
RMSE	root mean square error
SAGE	space-alternating generalized EM
SIC	successive interference cancellation
SIMO	single-input multiple-output
SISO	single-input single-output
SNR	signal-to-noise ratio
STBC	space-time block code
SV	Saleh-Valenzuela
SVD	singular value decomposition
TDoA	time-difference-of-arrival
ToA	time-of-arrival
ULA	uniform linear array
UWB	ultra-wideband

Chapter 1

Introduction

1.1 Background

Due to the increasing demand for both commercial and government services which require the location of a mobile terminal (MT) in a wireless network, the development of radio-frequency (RF) based localization systems has attracted increasing attention in the past few decades. These systems provide a new technique of automation called automatic object location detection [1], upon which many applications can be built, such as facilitate proximity advertisement, location-sensitive billing, intelligent transport tracking system, location information in emergency systems and localization of nodes in wireless sensor networks. Various localization systems have been developed, and depending on their functionalities, they can be classified into two categories, namely dedicated localization systems and communication infrastructure based systems, respectively. The first approach develops a system which primarily focuses on wireless location applications. For example, the Global Positioning System (GPS) is a satellite-based navigation system which finds the location of an object represented by longitude and latitude in the globe when at least four satellites can be involved in the localization process. The advantage of this approach is that the physical specifications and the quality of location sensing results can be easily controlled. The second approach is to use the existing communication infrastructure to locate a MT. Some examples include the current standards for the Third Generation Partner Project (3GPP) and ultra-wideband (UWB). The combination of localization and communication

functionalities has the advantage of low cost and fast deployment.

According to the measuring principles and positioning algorithms, the current localization techniques are classified into two categories, namely trilateration/triangulation and fingerprinting-based localization [1]. The first category is the classic method which first measures the channel parameters such as time-of-arrival (ToA), time-difference-of-arrival (TDoA), angle-of-arrival (AoA), received signal strength (RSS), etc., and then uses trilateration or triangulation to estimate the location. ToA estimate can infer the measurement of distance between a MT and a fixed terminal (FT), and at least three FTs and ToA estimates are required to perform trilateration. The ToA estimation techniques have been mature, and it is well accepted due to the low requirement on devices when implemented. In recent years, the use of UWB technique has significantly improved the resolution of estimating the ToA of first-arriving path [2]. However, this method has two major drawbacks. Firstly, the object and all the reference nodes must be precisely synchronized, otherwise, a small timing error may lead to a large distance error. Secondly, the ToA estimation consumes very large bandwidth in order to achieve a high accuracy. The use of TDoA eliminates the requirement of synchronizing the MT clock with the FT clocks, because it measures the time difference between the signals arriving at two FTs. From each TDoA measurement, it can be inferred that the MT is located along a corresponding hyperbola, and therefore, at least two non-redundant TDoA measurements are needed to infer the location of a MT.

When the devices are equipped with an antenna array or a directional antenna, the estimation of AoA can be performed with high accuracy and yet reasonable computational complexity. The techniques mainly include maximum likelihood (ML) based and subspace-based algorithms [3, 4]. Unlike using ToA or TDoA, this method only requires two FTs, and no synchronization is needed. However, the drawbacks include higher cost incurred by the use of antenna array and larger error with increased distances between the MT and the FTs. ToA, TDoA and AoA techniques all require available line-of-sight (LOS) to obtain correct measurements. In the case of non-line-of-sight (NLOS), the performance is degraded and special techniques need to be utilized to mitigate the errors [5–7], which will be reviewed in detail in Chapter 2.

The RSS is another way of inferring the distance information by assuming an appropriate signal propagation model. Similar with ToA, after the distances are calculated, multiple FTs collaborate to localize the MT via trilateration. Since

the RSS information can be easily obtained in the communication devices, it has the advantage of very low system burden and cost. Besides, the NLOS condition does not affect the RSS much, as it only leads to a shadowing effect in the signal power. However, the disadvantage in applying RSS technique is also obvious. In practice, the signal strength often fluctuates severely, especially when the surrounding environment has many scatterers and moving objects, which may result in relatively larger distance estimation error compared with any other technique in this category.

The second category refers to those algorithms that first collect the fingerprints corresponds to various locations (offline stage) and then estimate the position of the MT by matching online measurements with the closest a priori location fingerprint (online stage). During the offline stage, the location coordinates and corresponding fingerprints from nearby FTs are collected, and stored in a database. In the online stage, the location of a MT is derived based on the currently observed fingerprint by selecting the closest stored fingerprint. This technique has been first proposed in [8] using RSS as the fingerprint, and since then many algorithms have been developed under this framework [9]. Channel impulse response (CIR) has also been used as a type of fingerprint in [10, 11]. The fingerprinting technique is very suitable for complex environment, such as indoor scenarios, because the channel in such environments is highly unpredictable. However, this technique has two challenges. One is the time-consuming and labor-intensive offline information collection stage. Another is that the offline training stage needs to be performed every time when the environment has changed.

When there is a need to continuously monitor the movement of a MT, the dynamics model of the MT can be involved in addition to the motion-dependent parameters. Such a tracking process, which is generally described by the motion-dependent parameters together with the dynamics model, helps reduce the frequency in performing location estimation and estimation latency when supporting real-time location monitoring. The Kalman filter (KF) is widely used to infer the locations of a MT at discrete time instants by fusing the motion dynamics and the motion-dependent parameters [12, 13]. The techniques for tracking a MT can be classified into self and remote tracking. In a self tracking system, the MT is usually equipped with inertial/magnetic sensors, such as accelerometers and magnetometers, which are used to estimate the motion-dependent parameters such as speed and direction of movement. The dead-reckoning technique is then adopted to track

its location. The development of microelectromechanical systems (MEMSs) has made the inertial/magnetic sensors small in size and low in cost, thus easily to be integrated into mobile devices. However, the disadvantages includes three aspects. Firstly, due to the noisy measurements, tracking error accumulates quickly over time, especially for a winding path. Although there are some approaches which utilize step detection to improve the accuracy [14, 15], they are only applicable for pedestrian tracking and not efficient to deal with turns. Secondly, the magnetic field of an inertial sensor can easily be distorted by ferrous objects and electrical sources [16, 17]. Thirdly, under some conditions where the energy and computational resources at the MT are limited, it may not be always possible to provide real-time and accurate tracking at the MT alone. On the other hand, the successfully deployed wireless systems have boosted the research interests to develop infrastructure-based techniques to perform remote tracking. It allows the MT to track its relative location with respect to a FT located in its coverage area [18]. A FT can make use of the periodically transmitted beacon signals from the MT to estimate the motion-dependent parameters. The computational complexity is then transferred from MTs to FT. The parameters such as ToA, AoA and velocity, are first estimated on the FT. The location is then derived by KF through the fusion of MT dynamics and the estimated parameters. Therefore, the second and third drawbacks of self tracking system can be eliminated. The disadvantages of the remote tracking system are the requirement of a supporting infrastructure and the sensitivity to the availability of LOS. However, this should not be the major barrier if the system is built on top of the widely deployed cellular and WLAN systems.

1.2 Motivation and Objectives

In recent years, the multiple-input multiple-output (MIMO) systems have emerged as an important technique to provide high data rate communication services. MIMO exploits spatial diversity through the use of smart antenna technology at both the transmitter and the receiver to achieve high spectral efficiency in the next generation cellular networks (4G) and WLANs. Compared to single-antenna systems which provides signal processing capability only in the temporal dimension, MIMO systems create an additional dimension (the spatial dimension)

to perform parameter estimation. Therefore, MIMO systems have attracted remarkable interests in recent years [19]. When applying space-time processing techniques to localization, we can achieve enhanced accuracy and capability through the development of more unique localization methods. On the one hand, the motion dependent parameters, such as AoA, ToA and velocity, can be estimated or improved in accuracy through space-time processing, and the location performance is thus enhanced. On the other hand, MIMO systems enable the use of each of the multipath components for localization under both LOS and NLOS scenarios [20], due to its ability to differentiate the spatial paths. These additional advantages introduced by the space-time processing and low cost widely deployed infrastructure make the development of MIMO-based localization techniques important and justifiable.

In MIMO communication systems, many advanced processing techniques take advantage of the channel state information (CSI) at the transmitter or the receiver to achieve high data rate [21]. For instance, accurate CSI at the receiver (CSIR) is required for space-time coding technique to achieve high performance [22]. If the CSI at the transmitter (CSIT) is available, the precoding technique can be adopted to further enhance the performance by pre-processing the signal before transmission [23]. Since the purpose of location-dependent parameters estimation is to extract the parameter information about a channel, it would be helpful to investigate how to make full use of the CSI to assist in estimation, so that enhanced location-dependent parameters estimation and localization can be achieved. However, to the best knowledge of the author, the CSI has never been utilized for such a purpose in MIMO systems. Therefore, the first objective of the thesis is to study the benefits of applying prior CSI to location dependent parameters (i.e. AoA and ToA) estimation and localization. In Chapters 3 and 4, we take advantage of instantaneous CSIT to pre-process the signal before transmission to achieve enhanced AoA and ToA estimation respectively. Localization improvement is evaluated by applying enhanced AoA. In Chapter 5, we demonstrate that the prior statistical information on the parameters in the extended Saleh-Valenzuela (SV) channel model makes maximum a posterior (MAP) estimation possible, and increases the accuracy compared with the case when no prior channel information is used.

When it is required to continuously monitor the location of a MT, tracking can be a means to reduce the frequency in performing regular localization and estima-

tion latency. The complexity of tracking is a major consideration when designing a tracking system. If the MT has limited power, the energy consumption is also a key problem for real-time service. Since MIMO enables an additional dimension of signal processing, it is expected to make certain functions possible. Therefore, our second objective is to exploit the MIMO features for designing a low complexity and more energy-efficient tracking system. The targeted solution should have two advantages. Firstly, the estimation of the required motion-dependent parameters should have low computational complexity. Secondly, the system is a remote-tracking system where the task is mainly accomplished in the FT instead of the MT to reduce MT energy consumption. In Chapter 6, we propose a three-step tracking approach performed at the FT, consisting of motion-parameters estimation based on space-time correlation of the received signal, extended KF (EKF) based tracking to find the location, and AoA-assisted performance enhancement which requires additional AoA information but can be estimated less frequently.

1.3   Contributions of the Thesis

In this thesis, we exploit the additional enhancement in estimation accuracy which a MIMO system can provide. Space-time processing techniques with prior CSI are applied to improve the estimation accuracy of location dependent parameters, such as AoA, ToA and joint AoA/ToA. Furthermore, we also study the tracking system based on the space-time processing technique in MIMO systems and propose a three-step approach. The motion dependent parameters (i.e. radial velocity) are estimated based on space-time processing at the FT with low complexity, and EKF is used to find the location. Additional AoA information which can be made available in a MIMO system is utilized to assist in the tracking process to achieve enhanced accuracy. To be more specific, the thesis includes four contributions as follow.

The first contribution is the development of precoder design strategies to improve the accuracy in AoA estimation using the MUSIC (MUltiple SIgnal Classification) algorithm for localization. While all the previous efforts on AoA estimation and improvement in accuracy focus only on the processing of the received signal, we raise a question of whether it is possible to improve the estimation accuracy by pre-processing the transmitted signal at the transmitter. The idea on

pre-processing the transmitted signal by taking advantage of the available CSIT comes from the precoding technique which is exploited in MIMO communication systems to enhance the system capacity. Although the use of precoder in the reported work is to increase the achievable system capacity [23], we apply it to improve parameter estimation accuracy. Specifically, we investigate the asymptotic error variance bound in AoA estimation based on the MUSIC algorithm where the design of transmit signal is possible. We first derive a new asymptotic error variance bound when the MUSIC algorithm is used to estimate the AoA and the transmitted signal can be pre-processed. Next, we propose a precoder design to achieve this bound. However, such an optimal precoder requires CSI exclusive of the effect due to the receiver antenna array which cannot be separately estimated practically. A more feasible precoder design, which leverages on the feedback CSI estimated at the receiver, is next proposed. Using the performance of the optimal precoder as a benchmark, the practical precoder design performs close to the optimal precoder even in the high-resolution scenario. Both precoder schemes exhibit performance improvement compared with the case when no precoder is used. Finally, the performance when the practical precoder is applied to localization is studied through simulations, and the results exhibit a considerable improvement in the accuracy of location estimation.

The second contribution takes advantage of space-time processing technique to enhance the ToA estimation. The general conclusion derived from previous studies on ToA estimation is that at high SNR, the Cramer-Rao lower bound (CRLB) gives a good performance bound to any of the TOA algorithms developed. This gives rise to a question on how the CRLB of the estimator depends on the transmitted signal characteristics if pre-processing for transmitted signal is possible, and how the final accuracy of the estimator can be improved. The objective of our work is to investigate the impact on the asymptotic performance of the ToA estimator when it is possible to pre-process the transmitted signal in MIMO systems. We first derive the CRLB of the ToA estimator in MIMO systems which is used as a metric to evaluate its performance, and then adopt MIMO beamforming and diversity techniques at the transmitter to minimize the CRLB, in two scenarios where the CSIT are available and not available, respectively. For MIMO with CSIT, transmit beamforming is adopted, while space-time block code (STBC) [24] is utilized as the transmit diversity technique for MIMO without CSIT. Receive beamforming is performed at the receiver under the assumption

7

that the CSIR is always known. We demonstrate through simulation that the case of MIMO with perfect CSIT performs better than the case of MIMO without CSIT, and both have enhanced performances compared with the case of the single-antenna system. The performance is further enhanced with the increase in the number of transmit and receive antennas. Furthermore, when channel information errors exist, performance improvement can still be observed compared with the case where there is no CSIT.

The third contribution involves joint estimation of both spatial and temporal parameters under the same framework. We propose a MAP-based algorithm for joint ToA, AoA and complex amplitude estimation of multipath components in single-input multiple-output (SIMO) systems over the extended SV channel, and then extend it to MIMO systems. Direct solution to the MAP-based algorithm of a MIMO system is usually not possible due to its high computational complexity. On the other hand, by using a ML-based algorithm, the known channel statistics will not be fully exploited for a more accurate solution. We demonstrate that with the prior knowledge of the statistical distributions of the parameters used in the extended SV model, we are able to develop a MAP-based algorithm. In order to reduce the computationally intensive algorithm, the expectation-maximization (EM) algorithm is used to resolve the high dimensional optimization problem into iteratively solving multiple 3-dimensional (3-D) optimization sub-problems. Our simulation results show that the proposed algorithm outperforms the ML-based algorithm for SIMO systems. Finally, we extend and apply our approach to MIMO systems where the AoA, angle-of-departure (AoD), ToA and complex amplitude are jointly estimated.

The last contribution deals with the tracking problem. Due to the drawbacks of the self tracking system, we focus on a remote tracking approach with space-time processing and MIMO features being applied. We propose a three-step tracking approach performed at the FT where energy consumption is not a concern. The motion-dependent parameters, i.e. the radial velocity of the MT, which includes both the speed and direction, are first estimated from the received samples obtained at the FT antennas. With a suitable channel model identified, we show that both the radial speed and direction of a MT can be jointly estimated from the phase of the complex space-time correlation, and has low computational complexity. The EKF algorithm is then adopted to estimate the current location based on the estimated radial velocity parameters and the previous location esti-

mate. In order to reduce the accumulative error, we propose a novel AoA-assisted performance enhancement scheme which requires the FT to perform the MUSIC-based algorithm to obtain additional high-resolution AoA (HR-AoA) but can be estimated less frequently. Using such partial location information obtains a good compromise between accuracy and system costs, because complete location information usually requires extensive resource, such as computational capability and a number of FTs to perform triangulation [10]. We show how this partial location information can be fused with the erroneous tracking estimate to improve the tracking accuracy of EKF algorithm.

1.4 Organization of the Thesis

The rest of the thesis is organized in the following manner. Chapter 2 reviews the related work in the literature. In Chapter 3, the precoder design strategies are developed to improve the accuracy of the AoA estimation using the MUSIC algorithm. The enhanced AoA estimate is also evaluated in a localization scenario in terms of location accuracy. We next present the enhanced ToA estimation by taking advantage of space-time processing technique in Chapter 4. Then, the MAP-based algorithm for joint spatial and temporal parameters of multipath components is proposed in Chapter 5. After that, we propose a three-step tracking approach performed at the FT consisting of motion dependent parameters estimation based on space-time correlation of the received signal, EKF-based tracking to estimated the location, and HR-AoA based performance enhancement to reduce the accumulative error in Chapter 6. Finally, Chapter 7 concludes the paper and points out future directions.

Chapter 2

Literature Review

In this chapter, we give a literature review on the existing work in the context of localization and tracking. We will focus on reviewing the works which are related to the use of geometric methods to perform localization and tracking.

2.1 AoA-Based Localization

When the devices are equipped with an antenna array or a directional antenna, angle-of-arrival (AoA) estimation can be performed with low computational complexity. With at least two AoA estimates, triangulation is adopted to estimate the location. In this section, various AoA estimation algorithm as well as AoA location estimation approaches are reviewed.

2.1.1 AoA Estimation

Accurate AoA estimation has received a significant amount of attention over the last few decades. It is fundamental in many engineering applications, including wireless communications, radar, radio astronomy, sonar, navigation and tracking of objects. Since the multiple-input multiple-output (MIMO) technique has emerged as an important technique for high data rate communications in the next generation wireless networks, AoA estimation is more feasible by making use of the available antenna array in these MIMO devices. In the literature, the AoA estimation includes two major techniques: spectral-based and parametric

algorithms.

The spectral-based algorithms can be further divided into two categories, namely the beamforming and subspace-based methods, respectively. The beamforming method has been first proposed to estimate the AoA of the source signal [4]. Through the linear combination of the outputs at the antenna elements, the antenna array response is steered to every direction, and the corresponding output power is recorded. The direction with the maximum output power corresponds to the estimated AoA of the source signal. The conventional beamforming (also known as Bartlett beamforming) is an extension of the Fourier-based spectral analysis, where the transformation is performed in the spatial domain. The AoA estimate is obtained as the angle for which the spatial spectral is maximized. This method is computational efficient and can be implemented easily. It also often serves as a classical standard when new array processing algorithms are proposed and compared, and its performance has been evaluated in [25, 26]. The major limitation is that the source signals cannot be resolved if the AoAs are spaced closer than a beamwidth of the antenna array. In order to alleviate this limitation, the Capon beamformer has been proposed [27], and its performance has been discussed in [28]. The Capon beamformer obtains the AoAs of the source signals by minimizing the unwanted power contributed by the noise and the interference from other directions. It outperforms the conventional beamformer for closely spaced sources although its performance still depends on the array aperture and signal-to-noise ratio (SNR). An alternative version of this beamformer has been proposed for uniform linear array (ULA) named as the root Capon which is computational simpler and more accurate.

With the development of array signal processing technique, more accurate spectral-based algorithms have also been proposed, among which the subspace-based algorithms [3, 4] have drawn much attention due to their low computational complexity and high resolution property in performing AoA estimation. This technique utilizes the structure of the spatial correlation matrix of the received signal from the array with spatial white noise. By decomposing the correlation matrix, the signal subspace and noise subspace are constructed, followed by the formulation of the null spectrum function. The values which minimize the null spectral function are the estimated AoAs. The MUSIC (MUltiple SIgnal Classification) algorithm is a representative subspace-based algorithm which has been proposed in [29]. It results in significant performance improvement compared

with the beamforming methods. Since then, considerable research work in either analyzing its performance [30–34] or developing more advanced robust MUSIC algorithms [35, 36] have been proposed. The asymptotic estimation error of MUSIC is shown to be Gaussian distributed for sufficiently large numbers of samples and antenna elements [30]. It is also proven to be a large sample realization of maximum likelihood (ML) algorithm and achieve the Cramer-Rao lower bound (CRLB) asymptotically when the signals are uncorrelated. When the model errors such as imprecisely known noise covariance or array response are present, theoretical analysis has been carried out in [31]. It is shown through simulation that the weighted version of MUSIC performs very near to the CRLB where the weights are optimally chosen to minimize the error variance. With the aim of reducing the required SNR when applying the MUSIC algorithm, the root-MUSIC has been proposed for ULA with lower computational complexity [35]. Furthermore, the use of unitary transformation makes the root-MUSIC much more computationally efficient [37].

In a multipath environment, the MUSIC algorithm can be used to estimate the AoAs of various signal paths impinging on the receiver antenna array simultaneously [38]. The ESPRIT (Estimation of Signal Parameters via Rotational Invariance Techniques) algorithm is another representative subspace-based algorithm developed in [39]. A comprehensive study of the subspace-based algorithms has been performed in [32], where the performances of different algorithms are evaluated in the same framework with different types of error sources. The limitation of this technique is its inefficiency when dealing with correlated signals. Under this condition, the method called spatial smoothing is usually adopted to reduce the correlation of signals before AoA estimation.

While all the previous efforts on spectral-based AoA estimation and improvement in accuracy focus only on the processing of the received signal, in this thesis we have proposed precoder design strategies to pre-process the transmitted signal [40]. The proposed strategies are shown to improve the performance of the MUSIC algorithm significantly.

The second category of AoA estimation algorithm is the parametric approach [3, 4], which overcomes the limitation of subspace-based algorithms in estimating correlated source signals. However, the disadvantage is higher computational complexity, as it usually requires multidimensional search. The parametric approach includes ML-based and maximum a posterior (MAP) based algorithms.
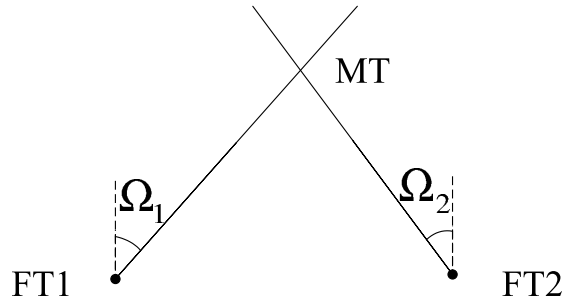
Fig. 2.1: AoA-based localization through triangulation

It assumes the noise to be Gaussian white random process, and the AoAs are estimated by maximizing the likelihood function. Based on the assumption of the property of the source signals impinging on the receiver array, the ML-based approach can be further classified into deterministic and stochastic algorithms. The deterministic ML assumes the source signals are deterministic and unknown, while the stochastic ML models the signals as Gaussian random process, which is shown to approach the CRLB asymptotically.

2.1.2 AoA-Based Location Estimation

In a localization system, the fixed terminal (FT) with known location can use the above mentioned algorithms to estimate the AoA of the source signal transmitted through a line-of-sight (LOS) path. A line of bearing can then be drawn from the FT, which indicates the direction of the MT. If two AoAs are estimated at different FTs respectively, we can draw two bearing lines and the intersection point gives the estimated location of the MT. When more than two FTs are involved into the localization process, the location can be derived using the least square (LS) methods [41]. An example of an AoA-based localization scenario with two FTs is depicted in Fig. 2.1.

One of the earliest research to use AoA for localization has been reported in [42], where a method to navigate autonomous vehicles using the angular information between FT pairs is developed. It demonstrates that accurate position estimation can be obtained through triangulation. In addition, a practical system has been implemented and the performance is evaluated both analytically and experimentally. The authors in [43] have designed and implemented an AoA-based location system where the MT locates itself by measuring the azimuths of

several FTs with known locations using the probabilistic approach. A prototype has been implemented on a PDA device with WLAN support. Their experiments show that by using two FTs, the algorithm can achieve 1.9 meters accuracy in the outdoor environment and 0.85 meters accuracy in the indoor areas. A prototype which uses rotatable directional antenna to estimate the AoA has been developed in [44]. It is shown that the system can be implemented with low cost yet achieve good localization accuracy. In the presence of multipath components, a method which jointly utilizes ML-based amplitude estimation and LS-based time-delay estimation has been proposed to estimate the LOS AoA. Using such an enhanced method, the system can achieve sub-meter accuracy. They have also proposed a scheme in which the directional FTs make use of the time of earliest arrival to detect the LOS component [45]. Based on both the WLAN infrastructure and MIMO channel measurement techniques, an AoA-based localization approach has been studied in [46]. It is demonstrated that with the use of a specific channel parameter estimation algorithm, such as the simplified ML algorithm, AoA and location estimates can be computed with low computational complexity.

The AoA-based localization has also been widely utilized for locating nodes in wireless sensor networks. The authors in [47] have proposed an algorithm for all nodes to determine their locations and orientations in an ad-hoc network. It is assumed that a fraction of nodes have self-localization capabilities and all nodes have AoA estimation capabilities. For such a distributed system, the neighboring nodes communicate with each other and determine the relative AoAs between nodes. Then the triangulation method is adopted to derive the location of regular nodes from the nodes with localization capabilities in a hop by hop manner. In [48], the problem is solved using the semidefinite programming relaxation based method. With a weaker assumption that only the nodes with unknown locations have the AoA estimation capabilities, a probabilistic algorithm has been developed and the AoA estimate errors are modeled by a given distribution [49].

2.2 ToA/TDoA-Based Localization

Localization algorithms developed based on time-of-arrival (ToA) estimates have been widely adopted. For example, the GPS utilizes the ToA estimates between the user equipment and satellites when at least four satellites can be

connected. In this section, ToA and time-difference-of-arrival (TDoA) estimation algorithms and location estimation based on ToA or TDoA estimate are reviewed.

2.2.1 ToA/TDoA Estimation

In the last few decades, various ToA estimation techniques have been proposed, from the conventional correlation-based algorithms to recently developed ultra-wideband (UWB) based estimation techniques.

The conventional correlation-based technique estimates the ToA by maximizing the cross correlation between the received signal and the known template signal [50, 51]. The optimal ToA estimator utilizes a correlation receiver with the received waveform as the template signal and chooses the most appropriate time shift that maximizes the cross correlation value [52]. This method has the advantage of low complexity and does not require any prior information. However, the disadvantages are also obvious. It is not able to resolve closely spaced signals which makes it inefficient to work under multipath environments such as urban areas and indoor areas. Furthermore, its performance is highly sensitive to noise.

Another ToA estimation technique is the deconvolution-based method which is a means of constrained inverse filtering approach [53]. Compared with the conventional correlation-based method, the deconvolution method has improved the ability to resolve closely spaced multipath components. However, it is still not sufficient to achieve high resolution ranging. Furthermore, although the deconvolution-based method shows reduced sensitivity to noise, it is still not robust enough to work under large noise. Besides, its increased complexity results in higher implementation cost.

The above two techniques are both sensitive to multipath effect which can be overcome by using ML-based algorithm. The ML-based algorithm is able to resolve the multipath and estimate the ToAs and path coefficients simultaneously for all multipath components [54]. The generalized ML algorithm is an approach which has been used to estimate the ToA of the first path in a multipath channel environment, and modified versions have been proposed to reduce the computational complexity and dense multipath effect [55, 56]. The authors in [57] have developed an iterative nonlinear programming technique to estimate the unknown parameters sequentially, so that the computational complexity can be further reduced. Compared with the previously mentioned techniques, the major advantage

of this technique is the ability of mitigating multipath effect, as it estimates the parameters of all the paths sequentially. However, this method has high computational complexity, since it involves multidimensional search when solving the optimization problem.

When pre-processing the signal before transmission is possible, we have carried out a study for ToA estimation in MIMO systems [58]. We utilize transmit beamforming and transmit diversity techniques to improve the performance of the ML ToA estimator, for both cases when the channel state information at the transmitter (CSIT) is either available or unavailable.

In recent years, the use of UWB technique has significantly improved the resolution in estimating the short-range ToA of the first-arriving path [2, 57, 59]. UWB approaches are suitable for localization, because it allows not only centimeter accuracy in ranging, but also introduces low implementation cost and low power consumption. According to the manner in which a UWB system accesses the spectrum, UWB systems can be classified into two categories: impulse radio (IR) and multiband orthogonal frequency division multiplexing (MB-OFDM). In the literature, the researchers have developed different ToA estimation algorithms for the two types of UWB techniques. IR UWB transmits signals that occupy the whole frequency band. Based on IR UWB, one possible ToA estimation approach is to use the ML algorithm to estimate all the parameters in the channel model, including the ToAs and path coefficients of all multipath components. However, it usually requires Nyquist sampling rate or higher during implementation, which may not be practical due to the large bandwidth of UWB systems. An alternative approach is the use of an energy detection-based technique which requires only sub-Nyquist rate sampling [59, 60]. In a typical energy detection-based algorithm, the received signal is first passed through a bandpass filter to eliminate the out-of-band noise, and then processed by an energy detector which consists of a square-law device and an integrator. The ToA is determined by finding the first path which exceeds a pre-defined threshold.

For MB-OFDM, the UWB spectrum is accessed by combining the OFDM signals with frequency hopping technique. A correlation-based algorithm has been proposed in [61] which calculates the correlation between two identical half-symbol segments, and the ToA estimate is determined by finding the maximum of the cross correlation. This algorithm has been enhanced through the design of training symbols [62]. When a matched filter is used to correlate the received samples

17

with the transmitted training sequence, the output is the sample spaced discrete time channel. The ToA of the first path can be identified by the strongest sample of the sampled channel [63] or the first path with energy that exceeds a given threshold. An alternative approach is the energy leakage minimization method which is motivated by the idea of minimizing the energy leakage from the first channel path due to mis-sampling [64, 65].

When ToA estimates are performed at all FTs, it is straightforward to obtain the TDoA between any two ToA estimates. Since the MT and the FTs are not synchronized, all the ToA estimates include a timing offset due to the local time difference between the MT and the FTs, in addition to the time of flight. By taking the difference of two ToA estimates, the timing offset can be canceled. Another approach to estimate TDoA is cross-correlation based method [1] which computes the cross correlation between the signals arriving at a pair of selected FTs. The delay which maximizes the cross-correlation function is the desired TDoA corresponding to the pair of FTs. This approach performs well in the single-path environment when white noise is present. However, its performance is affected significantly by multipath conditions and colored noise. Therefore, the generalized cross-correlation method has been proposed to enhance its performance [50]. The signals are first filtered through a pair of receiver prefilter and then cross-correlated.

2.2.2 ToA/TDoA-Based Location Estimation

When using ToA information for localization purpose, the distances from the MT to all FTs are first computed from the ToAs. The location of the MT is then inferred using trilateration with at least three distances (e.g. see Fig. 2.2).

With at least three available ToAs, it is straightforward to use the geometric approach to compute the intersection region of multiple circles inferred from ToAs. The LS algorithm can then be applied, and the location is estimated by minimizing the sum of squared distances from the MT to all FTs [66]. It is often computational intensive to solve such a non-linear function because a numerical search is required, such as Gauss-Newton method. Therefore, the linearization technique has been developed based on Taylor's series expansion. The non-linear LS problem is then converted to iteratively solving linear LS problems [41]. A different linearization approach has been proposed in [67], where the non-linear terms
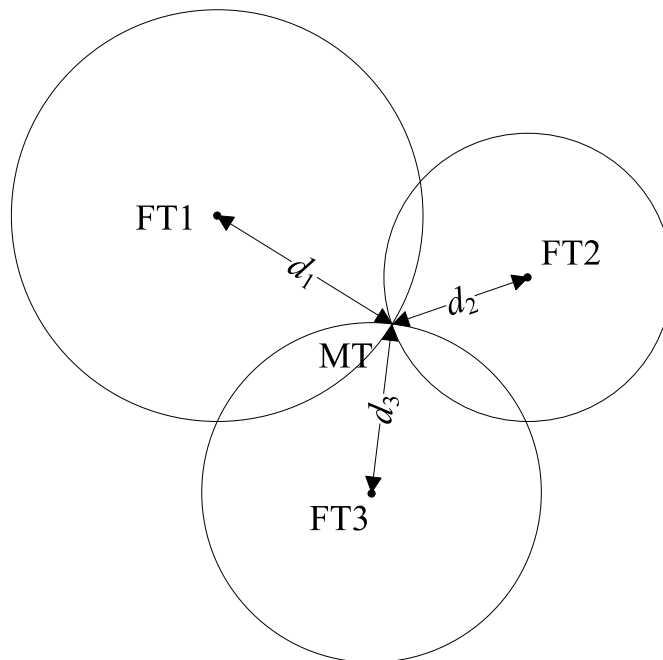
Fig. 2.2: ToA-based localization through trilateration

can canceled by taking the difference between the distance functions between the MT and any two FTs. The linear LS is then applied to find the solution. It is shown that the performance is slightly worse than the Taylor's series LS algorithm when the measurements are corrupted by zero-mean Gaussian noise. But when there is large bias on the measurement, such as non-line-of-sight (NLOS) bias, it exhibits much better performance. The basic LS algorithm can be improved through adding constraint and weights in the cost function in [68]. Weights are assigned to measurements to distinguish their reliabilities, and the constraint is devised from the relation of the range variable and position coordinates. The improved performance is shown to achieve the CRLB at sufficiently high SNR. In addition to LS algorithm, the ML-based approach is also applied for ToA-based localization problem. The ML approach assumes the ToA measurements are corrupted by Gaussian noise, and the position is determined by maximizing the likelihood function. It is statistically able to achieve the CRLB. Although closed form solution is impossible, researchers have proposed a modified ML approach which may achieve the CRLB asymptotically. An approximate ML approach has been developed in [69] which first obtains a rough location estimate for initialization, and then derives the accurate location iteratively.
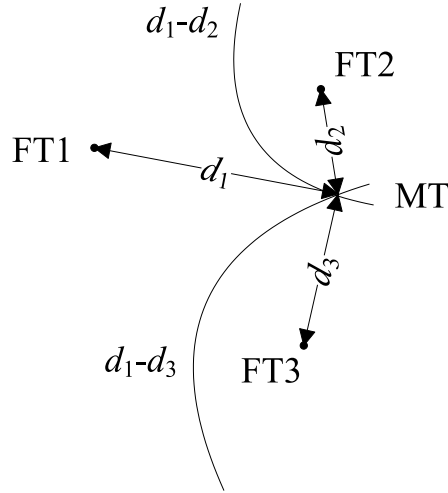
Fig. 2.3: TDoA-based hyperbolic localization

For TDoA-based localization, the differences in the ToAs between the MT and FTs are used to estimate the location. The location is estimated through the intersection of hyperbolic trajectories which is shown in Fig. 2.3. Compared with ToA-based approach, this method only requires synchronization between FTs. The MT and FTs are not necessarily synchronized. Geometrically, each TDoA measurement defines a hyperbola on which the MT may lie in the 2-dimensional (2-D) space. With at least two TDoA measurements, the location of the MT can be determined by finding the intersection of corresponding hyperbolas. Mathematically, we can estimate the location of the MT by solving a set of hyperbolic TDoA equations using the non-linear regression method. The LS algorithm can be applied by formulating the cost function as the sum of the square differences between the measurements and the real values. Alternatively, if we treat each measurement as a random variable which composes of the real value plus a noise component, we can use the ML algorithm to find the location by maximizing the likelihood function. Due to its computational complexity, an alternative approach is to linearize the equations using Taylor's series and solve iteratively [70]. An efficient non-iterative algorithm has been proposed in [71] which is an approximate realization of the ML estimator and is shown to attain the CRLB near the small error region. Compared with the Taylor's series approach, its solution can be expressed in an explicit form and hence it has less complexity. Another challenge with TDoA localization is the pairing problem. A TDoA measurement is

the difference of ToAs for a signal arriving at a pair of FTs. Therefore, with N_f FTs, there are $N_f(N_f - 1)/2$ distinct TDoAs from all possible FT pairs. However, there are only $(N_f - 1)$ non-redundant TDoAs. The authors in [72] have developed an algorithm to optimally convert the full TDoA set to non-redundant set, which is achieved via the standard LS estimation procedure. The accuracy is demonstrated by comparing the CRLBs derived from the full set and the non-redundant set, respectively.

2.3 Hybrid Localization Approach

With the development of channel parameters estimation techniques, various location estimation algorithms which do not rely on a single parameter have been proposed. These algorithms combine two or more kinds of parameters, such as the hybrid TDoA/AoA scheme reported in [73]. In this section, we review the joint parameters estimation techniques as well as hybrid location estimation algorithms in the literature.

2.3.1 Joint Parameters Estimation

With the development of MIMO technology, existing mobile radio communication systems have incorporated various diversity techniques to increase data transmission rate as well as to improve link reliability. As a result, the parameters used to describe such a channel lie not only in the temporal domain, i.e., ToA and fading amplitudes, but also in the spatial domain, i.e., AoA and angle-of-departure (AoD). Estimation of the instantaneous channel parameters is essential in many research areas.

Various highly accurate algorithms have been proposed to jointly estimate the channel parameters for MIMO/SIMO channels. The approaches can be classified into two categories, namely, subspace-based estimation and ML-based estimation. As mentioned in Section 2.1.1, the MUSIC [29] and ESPRIT [39] schemes belong to the first category. A 2-D MUSIC has been proposed to joint estimate AoA and AoD in [74]. In order to avoid the need to perform exhaustive search, an algorithm based on double polynomial root finding procedure has also been proposed to jointly estimate the AoA and AoD with automatic pairing. ESPRIT has been adopted to jointly estimate AoA and ToA in [75]. The proposed algorithm uses

a 2-D ESPRIT-like shift-invariance technique to separate and estimate the AoA and ToA with automatic pairing of two parameter sets from an estimated channel impulse response (CIR). It has been then extended to jointly estimate AoA and AoD for MIMO systems in [76, 77]. In [78], it has been further developed to jointly estimate AoA, AoD, ToA and Doppler shift by exploiting the structure of the CIR matrix. The subspace-based methods generally have relatively low complexity. However, its performance is significantly downgraded by correlated signals. In such cases, spatial smoothing is needed to mitigate the correlation. Further, the ESPRIT-based method requires an antenna array with a translational invariance structure [39].

The ML-based approach provides a more robust solution. However, it is very computational intensive due to the high dimensional search involved in the optimization problem. A computationally efficient algorithm for joint parameters estimation of multipath signals has been developed in [79] based on the expectation-maximization (EM) algorithm. The observed data is first decomposed into signals transmitted through multipath components, and then the parameters of each signal path are estimated separately. Based on the current parameter estimates, it is possible to decompose the observed data better and thus increase the likelihood of the next parameter estimates. This process is repeated iteratively, and therefore the high dimensional problem is converted to iteratively solving low dimensional problems. The SAGE (Space-Alternating Generalized EM) algorithm, which is an extension of EM, has been used to jointly estimate the delay and azimuth in a time-invariant environment [80]. A similar method has been applied to jointly estimate the delay, azimuth, Doppler frequency and complex fading amplitude in a time-variant environment [81]. Its performance has been studied in detail in [82] in synthetic and real channels, and it shows high resolution and fast convergence rate. This algorithm has been extended to jointly estimate the delays, AoAs, AoDs, Doppler frequency and the complex amplitudes for all the paths in MIMO systems in [83]. The ML-based estimation approach generally assumes that we do not have any prior information about the parameters under estimation. In this thesis, a MAP-based algorithm to jointly estimate the channel parameters by taking advantage of prior channel statistical information obtained from the existing channel model, has been developed. The proposed algorithm has been shown to achieve enhanced performance [84].

2.3.2 Hybrid Location Estimation

The hybrid approach is capable of providing more robust solutions in location estimation by combining different parameters, such as hybrid ToA/AoA, TDoA/AoA, etc. The authors in [85] have developed a non-linear constrained optimization based algorithm and a LS-based method, both of which utilize ToA and AoA measurements to estimate the MT's location with bounds on range and angle errors inferred from geometry. The algorithms are shown to outperform the ToA-only approaches. A hybrid ToA/AoA location estimation algorithm has been proposed in [86] for GSM networks. In addition to using the typical ToA/AoA cost functions, the proposed algorithm also incorporates a method which makes use of the values of ToA and AoA to identify the degree of NLOS at each measurement. Appropriate weights related to the degree of NLOS propagation are included to improve the accuracy. Another approach for hybrid ToA/AoA location estimation has been developed in [87]. It uses minimax mean square error criterion and extends the spherical interpolation technique [71] to solve the linear equations for location estimation.

Hybrid TDoA/AoA approach has also been exploited in the literature. By assuming the availability of both TDoA and AoA measurements, the performance improvement over TDoA-only system has been evaluated [88]. The result shows that a significant improvement ($20\% - 60\%$ in most scenarios) can be achieved. Another hybrid TDoA/AoA algorithm has been proposed in [73]. It obtains the solution of the non-linear TDoA/AoA location equations by extending the two-step LS estimator which is originally developed for TDoA localization. The features of CDMA cellular systems, e.g. FTs are precisely synchronized in time, are made use of to achieve low signaling overhead and implementation cost. It is shown to have high location accuracy by simulations.

In a multipath environment, the multipath components usually degrade the localization performance, and thus their effect should be eliminated. However, a hybrid ToA/AoA/AoD approach has been proposed in the literature to perform location estimation by making use of the single-bound multipath components. The approach given in [89] estimates the position of the MT by minimizing the effect of the errors in estimating the multipath parameters. The Taylor's series expansion is adopted to solve the non-linear location equations in an iterative manner. However, the Taylor's series approach requires an accurate initial estimate of the MT's

location in order to guarantee computation convergence. Therefore, the authors in [90] have developed a simple linear LS-based algorithm. They also formulate the ML approach which is shown to be able to achieve the CRLB. Since this approach only utilizes the LOS and single-bound multipath components, a scheme has been proposed in [20] to detect and extract the LOS and single-bound paths from multiple-bound paths. We have adopted this hybrid approach in our work, and the results show that the performance can be further improved if a transmitter pre-processing technique is applied to enhance angle estimation [91].

Some other hybrid algorithms, such as hybrid ToA/received signal strength (RSS) [92] and hybrid ToA/TDoA [93], have also been discussed and the details can be found in the respective references.

2.4 NLOS Problem

The performance of geometric-based localization technique highly depends on the availability of LOS. Therefore, how to identify and mitigate NLOS effect has attracted much attention in the localization field. The previous research on this problem can be classified into the following three categories.

2.4.1 NLOS Identification

The NLOS identification technique identifies the presence of NLOS measurements and discards results from NLOS. If we divide all the measurements into multiple groups, the groups which contain only LOS measurements give consistent location estimates. On the contrary, the groups containing NLOS measurements produce inconsistent location estimates which result in larger residuals[1] compared with consistent estimates. The residual test is a way of NLOS identification. A residual test algorithm has been proposed in [94] for ToA-based localization which is based on the principle that the normalized residuals have a central Chi-Square distribution when all measurements are obtained under LOS, but a non-central distribution when there is NLOS. A hypothesis test comparing the residuals with a threshold is performed to identify the presence of NLOS measurements. This approach can achieve the CRLB when there are more LOS than NLOS measure-

---

[1]In this context, residual means the difference between a location estimate and the average of location estimates produced by all groups of measurements.

ments. An AoA-based residual test has been developed in [6] to identify NLOS by coordinating measurements at all base stations. The proposed approach demonstrates a high successful rate in identifying NLOS measurements. Other channel statistics, such as the kurtosis, the mean excess delay spread, and the root-mean-square delay spread, can also be used for NLOS identification [95] by performing hypothesis test over the respective threshold.

While the above research considers only using one antenna element for NLOS identification, Xu [96] has studied the potential to use the antenna array. Considering a narrowband MIMO system, the spatial correlation of channel coefficients among the antenna elements is used as a metric to identify the presence of NLOS, based on a new MIMO channel model using rough surface theory. In addition, the statistics of the phase difference between two antenna elements has also been studied for NLOS identification. When dealing with a wideband MIMO system which uses OFDM signaling, joint space-time-frequency channel correlation can also be exploited to attain NLOS identification in time-varying, frequency-selective and space-selective radio channels. This makes the NLOS identification for MIMO-based systems exhibit higher accuracy than those based on single antenna, and has been demonstrated in [96].

2.4.2   NLOS Mitigation

Different from the above mentioned NLOS identification approach which discards the NLOS measurements, NLOS mitigation technique includes all measurements to perform localization. However, the degree of NLOS for each measurement is computed and included in the cost function so that the overall NLOS impact is kept at the minimum. A residual weighting algorithm has been developed in [97] which is based on the observation that the residual error is typically larger when NLOS FTs are involved in location estimation. The authors in [98] have also utilized the residual error and proposed an algorithm which first identifies the NLOS measurements and then incorporates them into an objective function by assuming prior distribution of NLOS. However, the above approaches assume only a small portion of the total measurements is obtained under the NLOS condition. The algorithm proposed in [7] overcomes this limitation by assuming the knowledge of prior NLOS statistics. The proposed ML location estimator can achieve high accuracy even in the case when most FTs are NLOS.

2.4.3   NLOS Localization Based on Single-Bound Model

While the above two categories of algorithms try to detect the NLOS errors and reduce their effects, the third category is mainly for MIMO systems, which is able to make use of the spatial domain processing capability to derive the NLOS propagation paths and achieve location estimate [20, 89, 90]. In particular, the single-bound NLOS paths, as well as the LOS path (if available), can be selected from among the multiple-bound paths. The location can then be estimated using one of the hybrid ToA/AoA/AoD approaches: Taylor's series expansion based algorithm [89], LS-based method [20, 90], and ML-based approach [90], which have been reviewed in Section 2.3.2.

2.5   Mobile Terminal Tracking

In the context of MT tracking, the existing techniques can be classified into three categories, namely self tracking, remote tracking and hybrid approach. The self tracking scheme requires the MT to be equipped with inertial/magnetic sensors, such as accelerator and magnetometer, to estimate the motion-dependent parameters. The location is then derived by fusing the estimated parameters and the previous location estimate. For remote tracking systems, a supporting infrastructure with FTs is required. The range or angle information is estimated through communications between the FTs and MT for inferring the location of the MT together with its previous location estimate. The hybrid approach takes advantage of the above two approaches to achieve lower complexity and enhanced accuracy.

2.5.1   Self Tracking

A conventional self tracking system includes two steps. The displacement of the MT during a short interval is first calculated by integrating the acceleration in the estimated direction. The current location estimate is then obtained by adding the displacement to the previous location estimate. This technique is well suited for instrumented vehicles, and it can also be applied to robot navigation and pedestrian tracking [99]. Due to noisy measurements and drift effects in the inertial measurement devices, the error in estimated location accumulates quickly [100]. The effects of biases in the accelerometer data has been studied in [100]

analytically, and a comparison is made between the theoretical results and experimental data taken from commercial accelerometers. Calibration is recommended before applying it in the practical systems. In order to improve the tracking accuracy, a technique named as step-detection [101] has been widely exploited for pedestrian tracking. The scheme in [101] applies the pattern recognition to accelerometer signals to determine a user's step. However, it may suffer large errors when the user is walking up/down stairs. A robust step detection scheme has been developed in [14] which utilizes a two-axis accelerometer and an acceleration pattern of a step, and demonstrates enhanced performance through experiments.

2.5.2 Remote Tracking

For remote tracking techniques, the time, angle or velocity estimates are first obtained through beacon signal transmission between the MT and FTs in the supporting infrastructure. The location of the MT is then derived using the Kalman filter (KF) by fusing the parameter estimates and the previous location estimate. As reviewed in Section 2.1.1 and 2.2.1, the angle and time information can be estimated using these algorithms. The speed can be obtained through estimating the Doppler shift of the transmitted signal at the MT, which has been studied for handoff purpose in wireless communications [102–104]. Joint estimation of Doppler shift and other parameters are also feasible [78, 82], but with high computational complexity. With known parameter information, a joint particle filter and unscented KF (UKF) based algorithm has been proposed in [105] where the LOS/NLOS event is tracked by a particle filter and the location is estimated by UKF. This algorithm has been applied to ToA data to evaluate its performance, and it can be readily extended to AoA or TDoA estimates. Robust EKF-based MT tracking algorithms developed in [106] and [18] also makes use of ToA estimates between the MT and FTs. TDoA estimates have been utilized for MT tracking in [107]. An EKF structure to process hybrid TDoA/AoA measurements for MT positioning and tracking has been given in [108].

The complexity is an important issue when designing a tracking system. Furthermore, if the MT has limited power, it is helpful to transfer the burden from the MT to the FT, which cannot be accomplished in self-tracking system. We have developed a tracking approach by taking advantage of space-time processing which is performed at the FT [109]. We first propose an algorithm to jointly estimate

27

the radial speed and direction at the FT based on the space-time correlation of the received signal with low complexity. An extended KF (EKF) is next adopted to estimate the location based on the estimated parameters, and high-resolution AoA (HR-AoA) is applied to reduce the cumulative errors.

2.5.3 Hybrid Approach

When the MT is equipped with inertial/magnetic sensors and a supporting infrastructure is also available, the above two schemes can be combined to track the MT. The hybrid approach has the advantages of the two approaches. First, the accumulative error can be reduced by performing calibration based on the time or angle measurements within the infrastructure. Second, the infrastructure can have a sparse structure with low cost, because the calibrations need not to be carried out frequently thanks to the self tracking technique. The GPS output is fused with the self tracking results [110, 111] when it is available, which achieves an enhanced performance compared with self tracking only approach. Correction schemes using range measurements in wireless networks have been developed in [10, 112]. Results in [15] show that the self tracking can be significantly improved by performing correction with reasonable frequencies.

2.6 Existing Localization Systems and Solutions

With the development of localization techniques in the last few decades, many practical systems and solutions have been developed and available in the market. This section gives an overview of existing geometric-based systems and solutions.

The most well-known system is GPS which determines the location in terms of longitude and latitude by measuring ToAs and trilateration between the MT and at least four satellites. While GPS is able to effectively used for many localization and navigation applications, its performance is downgraded by scattering environments and the absence of clear view of the sky. Another problem of GPS is its relatively long time to first fix, and therefore it is not able to provide timely services in emergency situations. Assisted-GPA (A-GPS) [113] has been developed to mitigate the limitations, as the cellular networks are also used to assist in the localization process. The MT can request the cellular network to provide satellite information, which enables the MT to acquire satellite signals quickly.

After the MT is connected to the satellites, ToA estimation and trilateration are performed to determine the location. Another enhancement in GPS is differential GPS (DGPS) [114]. Fixed ground-based reference stations are installed to broadcast the common positioning errors in an area, such as ionosphere and troposphere errors, so that the users can correct their estimates. This enables precise localization with accuracy of less than 1 meter if multipath and scattering effects are not severe.

In order to fulfill the location requirements for emergency safety services and other location-based services (LBSs), cellular networks have included localization as a key feature. The localization methods are based on existing communication infrastructure and have been standardized in 3GPP standards. The enhanced cell identity (E-CID) is a method which uses cell identity information to determine the location of a MT and is often augmented by timing advance (TA) and AoA information. The latest standards also support uplink TDoA (UTDoA) and observed TDoA (OTDoA) methods. These two methods are similar and both use hyperbolic trilateration, but the difference is that TDoA measurements are performed at the network for UTDoA and at the MT for OTDoA, respectively. The accuracy of cellular-based localization methods depends on cell density and environments [41].

Due to the high resolution in ToA estimation, UWB-based systems have been developed for commercial applications requiring high precision. Ubisense[2] is an UWB-based localization system which requires the deployment of readers in the target area and tags on the objects to be located. The tags transmit UWB signals to the networked readers where ToA and AoA are measured and LS method is employed for location estimation. The system can be applied to difficult environments, such as manufacturing facilities and warehouses, and provides 1-meter accuracy. Other UWB-based products are also available, such as PulsON from Time Domain[3] and location systems from Aether Wire[4].

Bluetooth is another promising solution for indoor localization due to its high handset penetration, high accuracy and ease of deployment. Nokia has developed precision indoor location technology based on Bluetooth 4.0 location protocol layer. This technology is based on measuring AoD of signals broadcast by

---

[2]Ubisense company. http://www.ubisense.net/
[3]Time Domain Company. http://www.timedomain.com/
[4]Aether Wire & Location, Inc. http://www.aetherwire.com/

dedicated Bluetooth beacons which are deployed in the target area at the installation of the location system. Sub 5-meter accuracy can be achieved using this technology. The Topaz local positioning solution[5] is based on Tadlys Bluetooth infrastructure and accessory products. It is able to achieve 2-meter accuracy and is suitable for tracking humans and assets in indoor environments.

Due to the popularity of WLAN, location systems and solutions have also been developed which can be built on top of WLAN infrastructure. AeroScout[6] has developed WLAN-based location solutions. When performing a location estimation, a WiFi tag and/or standard WiFi client device sends a signal to access points where the signal is transferred to a location engine. The location engine then uses RSS or TDoA algorithms to determine the location. Most of other WLAN-based systems and solutions adopt fingerprinting-based techniques and utilize RSS information as fingerprint. We will not review these fingerprinting-based systems and solutions, as this is beyond the scope of the thesis. Interested reader can refer to [1] for more information.

---

[5]The Topaz local positioning solution. http://www.tadlys.co.il/
[6]AeroScout Company. http://www.aeroscout.com/

Chapter 3

Precoder Design for Enhancing AoA Estimation and Localization

In this chapter, we propose a novel algorithm to improve the accuracy in estimating the angle-of-arrival (AoA) and hence localization. Using the MUSIC (MUltiple SIgnal Classification) algorithm to estimate the AoA, we first derive a new asymptotic error variance bound when the transmitted signal can be pre-processed. We next propose a precoder design to achieve this bound. However, such an optimal precoder requires the transmitter to have the channel state information (CSI) exclusive of the effect due to the receiver antenna array, and this cannot be separately estimated practically. A more feasible precoder design, which leverages on the feedback CSI estimated at the receiver, is next proposed. Using the performance of the optimal precoder which achieves the bound asymptotically as a benchmark, the practical precoder design performs close to the optimal precoder even in the high-resolution scenario[1]. Both precoder schemes exhibit performance improvement compared with the case when no precoder is used. Furthermore, the precoder technique is applied to a known AoA-based localization method, and the improvement on the accuracy of the location estimate is studied through simulations.

---

[1]High-resolution scenario means the AoA difference of a pair of arriving signals is smaller than the 3 dB beamwidth of the receiver antenna array.

3.1 Overview of Precoder Design in MIMO systems

The proposed algorithm is based on the concept of precoder design which has been exploited in multiple-input multiple-output (MIMO) communication systems to achieve enhanced data rate. Therefore, before proceeding to present our proposed algorithm, we first give a brief overview on precoder design.

The MIMO technology has enabled a significant increase in data transmission rate as well as improving link reliability. The performance can be further enhanced if a precoder is used to exploit the available CSI at the transmitter (CSIT) before transmission. It essentially functions as a multimode beamformer, optimally matching the input signal on one side to the channel on the other side [23]. In [115], perfect CSIT has been used to compute the achievable channel capacity. In the scenarios where instantaneous CSIT cannot be tracked reliably, CSIT is usually provided in terms of the channel statistics such as channel mean and covariance matrices (which are also named mean CSIT and covariance CSIT, respectively) [23]. The use of mean CSIT and covariance CSIT to compute channel capacity have been studied in [116–118], and [116, 117, 119], respectively. Vu *et al.* [120] have proposed an algorithm in which both the mean and covariance CSIT are used.

The use of precoder in the reported work focuses on increasing the achievable system capacity. In this chapter, we shall apply it to improve parameter estimation accuracy. Specifically, we investigate the possibility to improve the asymptotic error variance bound in AoA estimation when the MUSIC algorithm is used and if transmit signal design is possible.

3.2 Improving the Performance Bound of MUSIC Algorithm

In this section, we describe the theory behind how the improvement to the asymptotic error variance bound can be made through the transmit signal design.
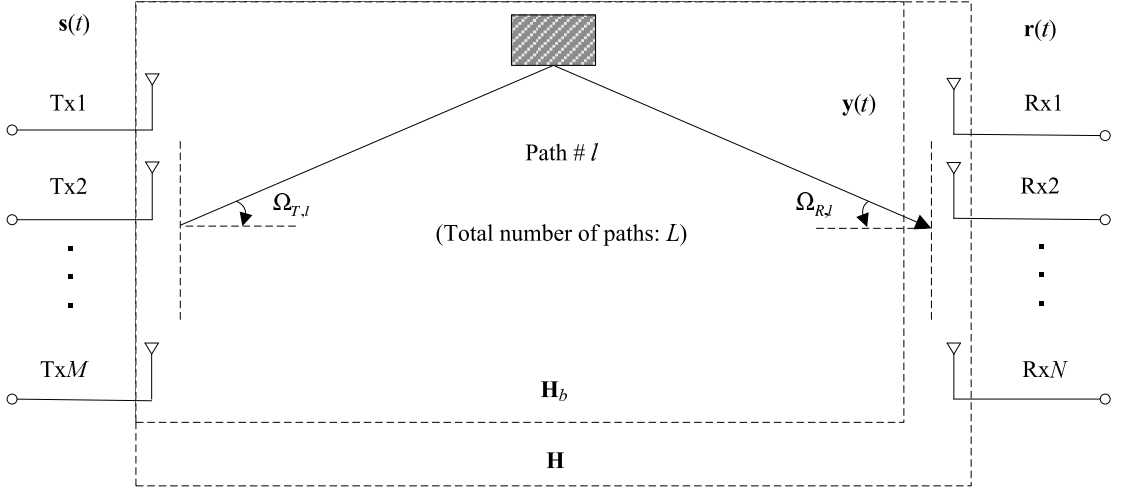
Fig. 3.1: The flat-fading channel model

3.2.1 Channel Model

We consider a time-invariant flat-fading channel as shown in Fig. 3.1. The transmitter and the receiver are each equipped with an uniform linear array (ULA) of M and N omni-directional antennas, respectively. The total number of paths is L. Each path contains three parameters, namely the angle-of-departure (AoD) $\Omega_{T,l}$, AoA $\Omega_{R,l}$ and complex gain α_l. Using the same assumption made in [29], L should be less than $\min(M, N)$ for the purpose of AoA estimation.

The narrowband array assumption [121] is employed here; i.e. the transmit time of the wavefront across the antenna array is assumed to be much smaller than the reciprocal of the signal bandwidth. With this assumption, the steering vector of an array with N elements is defined as $\mathbf{c}(\Omega) = [c_1(\Omega), \ldots, c_N(\Omega)]^T$, where Ω is the direction of the wave. Specifically, for a ULA, it has the following expression:

$$\mathbf{c}(\Omega) = [1, \exp(j2\pi d_h \cos\Omega/\lambda_s), \ldots, \exp(j2\pi(N-1)d_h \cos\Omega/\lambda_s)]^T, \qquad (3.1)$$

where d_h is the distance between two adjacent antennas and λ_s is the wavelength.

For the lth propagation path, the mth transmit antenna gain response due to the AoD $\Omega_{T,l}$ is $c_{T,m}(\Omega_{T,l})$ and the nth receive antenna gain response due to the AoA $\Omega_{R,l}$ is $c_{R,n}(\Omega_{R,l})$. With the transmitted signal denoted by $\mathbf{s}(t) =$

33

$[s_1(t), \ldots, s_M(t)]^T$, the received signal for the nth antenna is expressed as

$$r_n(t) = \sum_{m=1}^{M} \sum_{l=1}^{L} \alpha_l c_{T,m}(\Omega_{T,l}) c_{R,n}(\Omega_{R,l}) s_m(t) + z_n(t), \tag{3.2}$$

where $z_n(t)$ is the complex white Gaussian noise with mean of zero and power spectral density N_0.

We define $\mathbf{C}_T(\mathbf{\Omega}_T)$ and $\mathbf{C}_R(\mathbf{\Omega}_R)$ as the transmit and receive steering matrices with $\mathbf{c}_T(\Omega_{T,l})$ and $\mathbf{c}_R(\Omega_{R,l})$ as the lth column, $l = 1, \ldots, L$, respectively. We further denote $\mathbf{H}_\alpha = \text{diag} \{\alpha_1, \ldots, \alpha_L\}$. Thus, the channel model may be expressed in matrix form as

$$\mathbf{r}(t) = \mathbf{H}\mathbf{s}(t) + \mathbf{z}(t), \tag{3.3}$$

where

$$\mathbf{H} = \mathbf{C}_R(\mathbf{\Omega}_R)\mathbf{H}_\alpha \mathbf{C}_T^T(\mathbf{\Omega}_T),$$
$$\mathbf{r}(t) = [r_1(t), \ldots, r_N(t)]^T,$$
$$\mathbf{z}(t) = [z_1(t), \ldots, z_N(t)]^T.$$

The matrix $\mathbf{H}$ is the channel matrix and can be estimated at the receiver. We also define $\mathbf{H}_b = \mathbf{H}_\alpha \mathbf{C}_T^T(\mathbf{\Omega}_T)$, which is the component of the channel matrix exclusive of the receiver array. The signal impinging on the receive antenna array is $\mathbf{y}(t)$, and is expressed as $\mathbf{y}(t) = \mathbf{H}_b\mathbf{s}(t)$. For convenience, we omit the time index t hereafter.

3.2.2 Performance Bound

We use the sum of the error variances for the L AoAs estimates as the metric to evaluate the performance of the MUSIC algorithm. As shown in [30], when the receiver is a ULA and N increases, the sum of the variances approaches the following limit

$$\begin{aligned}
\text{var}_{MU}(\boldsymbol{\omega}_R) &= \sum_{l=1}^{L} \text{E}_{\hat{\omega}_{R,l}}\left[(\hat{\omega}_{R,l} - \omega_{R,l})^2\right] \\
&= \frac{6N_0}{IN^3}\text{tr}\left(\mathbf{P}^{-1}\right), \tag{3.4}
\end{aligned}$$

where $\boldsymbol{\omega}_R = [\omega_{R,1}, \ldots, \omega_{R,L}]$ is the parameter vector under estimation, with $\omega_{R,l} = 2\pi d_h \cos \Omega_{R,l}/\lambda_s$, $l = 1, \ldots, L$, and $\hat{\omega}_{R,l}$ is the estimate of $\omega_{R,l}$. I denotes the number of samples used when performing the estimation. $\mathbf{P} = \mathrm{E}_{\mathbf{y}}[\mathbf{y}\mathbf{y}^H]$ is the covariance matrix of $\mathbf{y}$.

Conventionally, the MUSIC algorithm does not involve signal pre-processing at the transmitter. The novelty of this work is to examine if pre-processing of transmitted signal is possible through CSI feedback, and how the bound given in (3.4) can be improved. Defining $\mathbf{Q} = \mathrm{E}_{\mathbf{s}}[\mathbf{s}\mathbf{s}^H]$ which is the covariance matrix of the transmitted signal $\mathbf{s}$, we have $\mathbf{P} = \mathbf{H}_b \mathbf{Q} \mathbf{H}_b^H$. The problem can be formulated as minimizing the error variance under the transmit power constraint as follow:

$$\min_{\mathbf{Q}} \quad \mathrm{tr}\left((\mathbf{H}_b \mathbf{Q} \mathbf{H}_b^H)^{-1}\right)$$
$$\text{subject to} \quad \mathrm{tr}\,(\mathbf{Q}) = P_T$$
$$\mathbf{Q} \succeq \mathbf{0} \tag{3.5}$$

where P_T is the total transmission power, and the second constraint means that $\mathbf{Q}$ should be positive semidefinite. We have ignored the scaling factor in the objective function since it does not affect the final solution. The design problem now becomes how we can obtain the optimal transmit covariance matrix $\mathbf{Q}$.

Theorem 1. *Let the truncated singular value decomposition (SVD) of $\mathbf{H}_b$ be given by $\mathbf{H}_b = \mathbf{U}_b \mathbf{\Lambda}_b \mathbf{V}_b^H$, where $\mathbf{U}_b$ and $\mathbf{V}_b$ are $L \times L$ and $M \times L$ matrices with the property $\mathbf{U}_b^H \mathbf{U}_b = \mathbf{I}_L$ and $\mathbf{V}_b^H \mathbf{V}_b = \mathbf{I}_L$, respectively, and $\mathbf{\Lambda}_b$ is a $L \times L$ diagonal matrix with its diagonal elements being the singular values of $\mathbf{H}_b$ permutated in decreasing order. Then the optimal transmit covariance matrix that minimizes the cost function in (3.5) should take the form $\mathbf{Q} = \mathbf{V}_b \mathbf{\Sigma}_b \mathbf{V}_b^H$, where $\mathbf{\Sigma}_b$ is a diagonal matrix.*

Proof. Substituting the truncated SVD into the cost function in (3.5), we have

$$\mathrm{tr}\left((\mathbf{H}_b \mathbf{Q} \mathbf{H}_b^H)^{-1}\right) = \mathrm{tr}\left((\mathbf{U}_b \mathbf{\Lambda}_b \mathbf{V}_b^H \mathbf{Q} \mathbf{V}_b \mathbf{\Lambda}_b^H \mathbf{U}_b^H)^{-1}\right). \tag{3.6}$$

Since $\mathbf{U}_b$ and $\left(\mathbf{\Lambda}_b \mathbf{V}_b^H \mathbf{Q} \mathbf{V}_b \mathbf{\Lambda}_b^H\right)$ are both full rank, (3.6) can be simplified to

$$
\begin{aligned}
&\mathrm{tr}\left(\left(\mathbf{U}_b^H\right)^{-1}\left(\mathbf{\Lambda}_b\mathbf{V}_b^H\mathbf{Q}\mathbf{V}_b\mathbf{\Lambda}_b^H\right)^{-1}\mathbf{U}_b^{-1}\right) \\
=\ &\mathrm{tr}\left(\left(\mathbf{\Lambda}_b\mathbf{V}_b^H\mathbf{Q}\mathbf{V}_b\mathbf{\Lambda}_b^H\right)^{-1}\right) \\
=\ &\mathrm{tr}\left(\mathbf{\Lambda}_b^{-2}\mathbf{\Sigma}_b^{-1}\right),
\end{aligned} \tag{3.7}
$$

where $\mathbf{\Sigma}_b = \mathbf{V}_b^H \mathbf{Q} \mathbf{V}_b$.

Next, we need to prove that $\mathbf{\Sigma}_b$ should be diagonal for (3.7) to be minimized. We use the following lemma [122].

Lemma 1. *If* $\mathbf{U}$ *and* $\mathbf{V}$ *are* $n \times n$ *positive semidefinite Hermitian matrices with eigenvalues* $\lambda_i(\mathbf{U})$ *and* $\lambda_i(\mathbf{V})$, *respectively, arranged in decreasing order, and the eigenvalues of the product matrix* $\mathbf{U}\mathbf{V}$ *are* $\lambda_i(\mathbf{U}\mathbf{V})$, *then*

$$
\mathrm{tr}(\mathbf{U}\mathbf{V}) = \sum_{i=1}^n \lambda_i(\mathbf{U}\mathbf{V}) \geq \sum_{i=1}^n \lambda_i(\mathbf{U})\lambda_{n-i+1}(\mathbf{V}). \tag{3.8}
$$

From the proof in [119], we know that if matrix $\mathbf{U}$ in Lemma 1 is diagonal, the equality in (3.8) holds only when matrix $\mathbf{V}$ is also diagonal, and vice versa. In addition, the arrangement of diagonal elements of the two matrices should be in the reverse order.

Applying Lemma 1 and the above conclusion to (3.7), the fact that $\mathbf{\Lambda}_b^{-2}$ is diagonal implies that $\mathbf{\Sigma}_b^{-1}$ must be diagonal, so that the equality in (3.8) holds and (3.7) obtains its minimum. So $\mathbf{\Sigma}_b$ is also diagonal. Besides, the diagonal elements of $\mathbf{\Sigma}_b^{-1}$ must be arranged in the reverse order with that for $\mathbf{\Lambda}_b^{-2}$. Thus, we have

$$
\begin{aligned}
\mathbf{V}_b^H\mathbf{Q}\mathbf{V}_b &= \mathbf{\Sigma}_b \\
\Rightarrow\ \mathbf{Q} &= \mathbf{V}_b\mathbf{\Sigma}_b\mathbf{V}_b^H.
\end{aligned} \tag{3.9}
$$

Thus, Theorem 1 is proved. $\square$

By applying Theorem 1, the solution which also fulfills the two constraints given in (3.5) can be computed as follows.

We denote $\mathbf{\Sigma}_b = \mathrm{diag}\left\{\sigma_{b,1}, \ldots, \sigma_{b,L}\right\}$ and $\mathbf{\Lambda}_b = \mathrm{diag}\left\{\lambda_{b,1}, \ldots, \lambda_{b,L}\right\}$, where $\lambda_{b,l}, l = 1, \ldots, L$ are the nonzero singular values of $\mathbf{H}_b$. Substituting (3.9) into

(3.6), we have

$$\text{tr}\left(\left(\mathbf{H}_b\mathbf{Q}\mathbf{H}_b^H\right)^{-1}\right) = \sum_{l=1}^{L}\frac{1}{\lambda_{b,l}^2\sigma_{b,l}}. \tag{3.10}$$

Furthermore, the power constraint can be simplified to $\text{tr}(\mathbf{Q}) = \sum_{l=1}^{L}\sigma_{b,l} = P_T$. The simplified objective function may then be expressed as

$$\min_{\sigma_{b,l},l=1,\ldots,L} \quad \sum_{l=1}^{L}\frac{1}{\lambda_{b,l}^2\sigma_{b,l}}$$
$$\text{subject to} \quad \sum_{l=1}^{L}\sigma_{b,l} = P_T$$
$$\sigma_{b,l} \geq 0, l = 1,\ldots,L \tag{3.11}$$

The Hessian matrix of the cost function in (3.11) is a diagonal matrix as follows

$$\mathbf{H}_e = \begin{bmatrix} 2\lambda_{b,1}^{-2}\sigma_{b,1}^{-3} & \cdots & 0 \\ \vdots & \ddots & \vdots \\ 0 & \cdots & 2\lambda_{b,L}^{-2}\sigma_{b,L}^{-3} \end{bmatrix}. \tag{3.12}$$

So it is positive definite in the solution domain which implies that the objective function (3.11) is convex.

Applying the Lagrange multiplier method, the cost function is written as

$$f(\lambda_L, \sigma_{b,1}, \ldots, \sigma_{b,L}) = \sum_{l=1}^{L}\frac{1}{\lambda_{b,l}^2\sigma_{b,l}} + \lambda_L\left(\sum_{l=l}^{L}\sigma_{b,l} - P_T\right), \tag{3.13}$$

where $\lambda_L \geq 0$ is the Lagrange multiplier associated with the power constraint.

The cost function is minimized when the derivatives of $f(\lambda_L, \sigma_{b,1}, \ldots, \sigma_{b,L})$ over $\sigma_{b,l}, l = 1,\ldots,L$, are all equal to zero. Thus we have

$$\frac{\partial f}{\partial \sigma_{b,l}} = -\frac{1}{\lambda_{b,l}^2\sigma_{b,l}^2} + \lambda_L = 0, l = 1,\ldots,L. \tag{3.14}$$

Solving (3.14) and then determining λ_L from the equality $\sum_{l=1}^{L}\sigma_{b,l} = P_T$, we

obtain the result as

$$\sigma_{b,l} = \frac{P_T}{\lambda_{b,l} \sum_{j=1}^{L} 1/\lambda_{b,j}}, l = 1, \ldots, L. \tag{3.15}$$

The last step is to verify that the diagonal elements of $\mathbf{\Sigma}_b^{-1}$ are arranged in the inverse order of those of $\mathbf{\Lambda}_b^{-2}$, so that the equality in (3.8) holds. According to (3.15), the diagonal elements of $\mathbf{\Sigma}_b^{-1}$ are arranged in decreasing order, while those of $\mathbf{\Lambda}_b^{-2}$ are in increasing order.

We conclude that the optimal transmit covariance matrix $\mathbf{Q}$ can be expressed as

$$\mathbf{Q}_{opt} = \mathbf{V}_b \mathbf{\Sigma}_b \mathbf{V}_b^H, \tag{3.16}$$

where $\mathbf{\Sigma}_b$ is diagonal with the diagonal elements given by (3.15).

We finally obtain the lower bound by substituting (3.16) into (3.4) as follow:

$$\text{var}_{MU}(\boldsymbol{\omega}_R) = \frac{6N_0}{IN^3 P_T} \left(\sum_{l=1}^{L} \frac{1}{\lambda_{b,l}} \right)^2, \tag{3.17}$$

where $\lambda_{b,l}, l = 1, \ldots, L$ are the singular values of $\mathbf{H}_b$.

3.2.3 Optimal Precoder

The derived performance bound can be achieved when an optimal precoder is adopted. As shown in Fig. 3.2, the input signal $\mathbf{x}(t)$ to the precoder matrix which is derived from the CSIT are K_x uncorrelated data streams each allocated with equal power P_T/K_x. The output of the precoder is $\mathbf{s}(t)$, which is expressed as $\mathbf{s}(t) = \mathbf{F}\mathbf{x}(t)$. With this model, the transmit covariance matrix $\mathbf{Q}$ has the following expression

$$\mathbf{Q} = \text{E}_{\mathbf{x}}[\mathbf{F}\mathbf{x}\mathbf{x}^H \mathbf{F}^H] = \frac{P_T}{K_x} \mathbf{F}\mathbf{F}^H. \tag{3.18}$$

The optimal $\mathbf{Q}_{opt}$ has been derived in (3.16), hence the optimal precoder $\mathbf{F}_{opt}$ can be obtained by taking square root of $\frac{K_x}{P_T} \mathbf{Q}_{opt}$, i.e. $\mathbf{F}_{opt} = \sqrt{\frac{K_x}{P_T}} \mathbf{Q}_{opt}^{1/2}$.
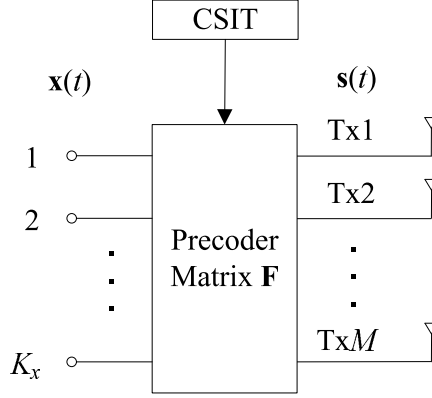
Fig. 3.2: Precoder model

3.3 Practical Precoder Design

The optimal precoder can achieve the performance bound, however, to obtain the matrix $\mathbf{H}_b$ which is required at the transmitter may not be practically possible. Instead, it is possible to make the receiver estimate the channel matrix $\mathbf{H}$ and introduce a feedback channel from the receiver to the transmitter [23]. In this subsection, we propose a practical precoder design based on the available CSIT which will be demonstrated to have its performance close to the optimal precoder.

We postulate the objective function (3.5) using the following

$$
\begin{aligned}
\min_{\mathbf{Q}} \quad & \operatorname{tr}\left((\frac{1}{N}\mathbf{H}\mathbf{Q}\mathbf{H}^H)^{\dagger} \right) \\
\text{subject to} \quad & \operatorname{tr}\left(\mathbf{Q}\right) = P_T \\
& \mathbf{Q} \succeq \mathbf{0}
\end{aligned}
\tag{3.19}
$$

and its relevance to the optimal precoder will be demonstrated afterwards. The solution to (3.19) can be similarly obtained using the method in the previous section. Let the truncated SVD of $\mathbf{H}$ be given by $\mathbf{H} = \mathbf{U}_h \mathbf{\Lambda}_h \mathbf{V}_h^H$, where $\mathbf{U}_h$ and $\mathbf{V}_h$ are $N \times L$ and $M \times L$ matrices with the property $\mathbf{U}_h^H \mathbf{U}_h = \mathbf{I}_L$ and $\mathbf{V}_h^H \mathbf{V}_h = \mathbf{I}_L$, respectively, and $\mathbf{\Lambda}_h = \operatorname{diag}\{\lambda_{h,1}, \ldots, \lambda_{h,L}\}$ is a $L \times L$ diagonal matrix with its diagonal elements being the singular values of $\mathbf{H}$ permutated in decreasing order. After simplifications, the objective function can be rewritten as $N\operatorname{tr}\left(\mathbf{\Lambda}_h^{-2}\mathbf{\Sigma}_h^{-1}\right)$ where $\mathbf{\Sigma}_h = \mathbf{V}_h^H \mathbf{Q} \mathbf{V}_h$, which is similar to (3.7). In order to obtain the solution, $\mathbf{\Sigma}_h$ should be a diagonal matrix. Denoting $\mathbf{\Sigma}_h = \operatorname{diag}\{\sigma_{h,1}, \ldots, \sigma_{h,L}\}$ and using

Lagrange method, the solution for the transmit covariance matrix when $\mathbf{H}$ is used is given by

$$\begin{cases} \mathbf{Q}_{prac} = \mathbf{V}_h \boldsymbol{\Sigma}_h \mathbf{V}_h^H \\ \sigma_{h,l} = \frac{P_T}{\lambda_{h,l} \sum_{j=1}^{L} 1/\lambda_{h,j}}, l = 1, \ldots, L. \end{cases} \tag{3.20}$$

From this result, we can see that the diagonal elements of $\boldsymbol{\Sigma}_h^{-1}$ are arranged in decreasing order, which is opposite to $\boldsymbol{\Lambda}_h^{-2}$. Similar with the optimal precoder, the practical precoder $\mathbf{F}_{prac}$ can be obtained by taking the square root of $\frac{K_x}{P_T}\mathbf{Q}_{prac}$, i.e. $\mathbf{F}_{prac} = \sqrt{\frac{K_x}{P_T}}\mathbf{Q}_{prac}^{1/2}$.

We shall show the impact on the estimated error variance when $\mathbf{H}$ is used instead of $\mathbf{H}_b$. Since $\mathbf{H} = \mathbf{C}_R(\boldsymbol{\Omega}_R)\mathbf{H}_b$, by substituting this into the matrix trace in (3.19), we have

$$\begin{aligned} &\operatorname{tr}\left(\left(\frac{1}{N}\mathbf{C}_R(\boldsymbol{\Omega}_R)\mathbf{H}_b\mathbf{Q}\mathbf{H}_b^H\mathbf{C}_R(\boldsymbol{\Omega}_R)^H\right)^{\dagger}\right) \\ =\ &\operatorname{tr}\left(\left(\frac{1}{N}\mathbf{C}_R(\boldsymbol{\Omega}_R)^H\mathbf{C}_R(\boldsymbol{\Omega}_R)\right)^{-1}\left(\mathbf{H}_b\mathbf{Q}\mathbf{H}_b^H\right)^{-1}\right) \\ =\ &\operatorname{tr}\left(\mathbf{R}_c^{-1}\left(\mathbf{H}_b\mathbf{Q}\mathbf{H}_b^H\right)^{-1}\right), \end{aligned} \tag{3.21}$$

where $\mathbf{R}_c = \frac{1}{N}\mathbf{C}_R(\boldsymbol{\Omega}_R)^H\mathbf{C}_R(\boldsymbol{\Omega}_R)$. For ULA, the steering vector has the form given in (3.1), so the entries of $\mathbf{R}_c$ can be expressed as

$$(\mathbf{R}_c)_{i,k} = \begin{cases} 1, & i = k \\ \frac{1}{N}\sum_{n=1}^{N}\exp\left(-j(n-1)(\omega_{R,i} - \omega_{R,k})\right), & i \neq k \end{cases}. \tag{3.22}$$

It can be seen that when the AoAs are sufficiently separated, the off-diagonal elements of $\mathbf{R}_c$ are much smaller than the diagonal elements when N is large. Under this condition, $\mathbf{R}_c$ can be approximated to an identity matrix since the off-diagonal elements are small numbers. This explains that the trace obtained in (3.19) approaches that given in (3.5) if all AoAs are reasonably separated. Our simulation results will later verify this.

3.4 Simulation of the Optimal and Practical Precoders

The performance of the proposed algorithm is evaluated in a synthetically generated channel. The channel is assumed to have two propagation paths, and the AoAs of the two paths are separated by an angle θ_d whose values vary in the following simulation. The transmitter and receiver are each equipped with a ULA with antenna elements separated by $d_h = \lambda_s/2$. The number of transmit antennas is six, while the number of receive antennas varies in the simulation. We define $\theta_{3\text{dB}}$ as the 3 dB beamwidth of the receiver array whose value is given by $\theta_{3\text{dB}} = 0.891\frac{\lambda_s}{Nd_h}$ when $N \leq 30$ [3]. The input to the precoder consists of two independent pseudo-noise (PN) sequences. At the receiver, the number of samples used for the MUSIC algorithm is 1000. The impact on the receive power due to the channel gain is removed through proper normalization. The signal-to-noise ratio (SNR) is defined as the ratio of the transmission power and the noise power at the receiver. As channel has been normalized, the SNR below can be treated as transmitter or receiver SNR.

The whole simulation consists of two parts. The first part discusses the conditions under which the precoder strategies approach the theoretical bound given in (3.17), while the second part studies the performance of the precoders in the high-resolution scenarios, i.e. when $\theta_d \leq 0.5\theta_{3\text{dB}}$.

3.4.1 Asymptotic Performance of Precoder Strategies

Since the theoretical bound shown in (3.17) is an asymptotic error variance, this part of simulation demonstrates the conditions for the precoding strategies to approach the bound. We perform two simulations to study the AoA estimate errors of two precoding strategies and compare them with the bound.

Firstly, the performances are studied when the number of receive antennas N changes. The separation angle θ_d is maintained at $2\theta_{3\text{dB}}$, so that the effect of closely separated signals which degrades the performance of the MUSIC algorithm can be eliminated. The AoAs of the two paths are set at $90°$ and $90° + \theta_d$, while the corresponding AoDs are set at $130°$ and $30°$, respectively. The amplitudes of the instantaneous complex path gains used before normalization are 0.8 and 0.4. In Fig. 3.3, the performance curves obtained by using the optimal and practical
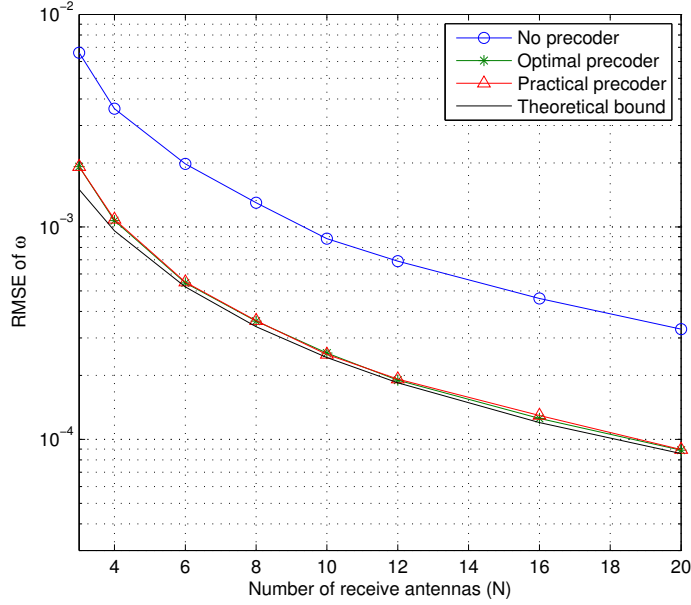
Fig. 3.3: Comparison of performance bound and the performances of precoders as a function of the number of receive antennas (SNR=20dB, $\theta_d = 2\theta_{3\text{dB}}$)

precoders are compared with the achievable performance bound, as a function of N and with SNR set at 20 dB. The root mean square error (RMSE) of ω is used as the performance metric, where $\omega = \pi \cos \Omega$ and Ω is the AoA in degree. We see that the results of precoders get closer to the bound when N increases. When N is sufficiently large, the two curves converge, indicating that the AoA error variances have approached the theoretical limit. In the same figure, the system without precoder is also shown and is found to perform significantly worse.

Secondly, we compare the bound and the two precoder strategies while changing the value of θ_d from $0.1\theta_{3\text{dB}}$ to $2\theta_{3\text{dB}}$. The SNR is again set at 20 dB. The number of receive antennas is set to be sufficiently large, and in our case we choose $N = 12$. From Fig. 3.4, we can see that as θ_d increases, the two precoder strategies approach the bound asymptotically. Specifically, when $\theta_d \geq 2\theta_{3\text{dB}}$, the MUSIC algorithm with a precoder can achieve the bound. This figure also shows the impact of estimation error when practical precoder is used instead of optimal precoder. The two precoders get closer when θ_d increases. When $\theta_d > 0.6\theta_{3\text{dB}}$, the performance of the practical precoder is already very close to that of the optimal precoder. This observation provides a proof of the correctness of the theoretical
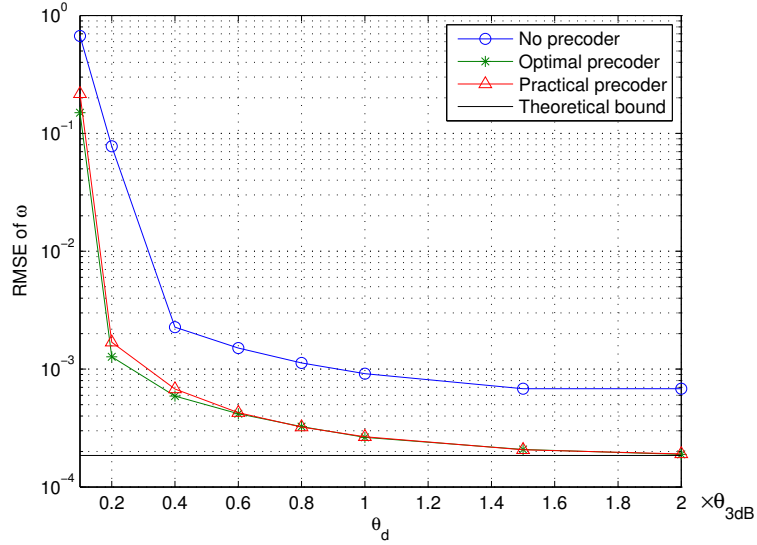
Fig. 3.4: Comparison of the three AoA estimation strategies as a function of the angle of separation θ_d (N=12, SNR=20dB)

explanation in Section 3.3. On the other hand, when θ_d is small, e.g. $\theta_d = 0.2\theta_{3\text{dB}}$, although the performance of practical precoder degrades, it still shows significant improvement over the system without precoder.

3.4.2 Performance Evaluation in the High-Resolution Scenario

In this part, we study the performances of the two precoders in the high-resolution scenario (i.e. $\theta_d \leq 0.5\theta_{3dB}$) which requires the use of the MUSIC algorithm. In our simulation, we choose $\theta_d = 0.5\theta_{3dB}$, and the following two asymptotic schemes are studied.

The first scheme is to increase the number of antennas N while maintaining the SNR at 20 dB. The AoDs and path gains are the same as those in the first part of the simulation. The result is shown in Fig. 3.5. In such a scenario, the performances of the MUSIC algorithm with and without precoder are degraded compared with Fig. 3.3. Even though, the estimation with a precoder exhibits significantly better performance than the estimation without precoder. For example, the system with 8 antennas and a practical precoder has nearly the same performance as the one with 20 antennas but without a precoder.
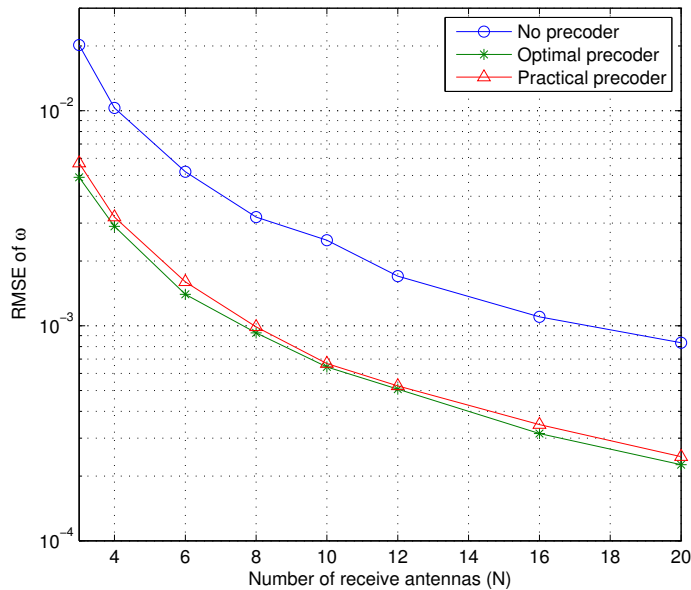
Fig. 3.5: Performances of precoders as a function of the number of receive antennas in the high-resolution scenario (SNR=20dB, $\theta_d = 0.5\theta_{3\text{dB}}$)

The second scheme studies the performances while increasing the SNR and maintaining $N = 12$. The RMSEs of ω are computed and shown in Fig. 3.6(a) when the SNR changes from -10 dB to 20 dB. Compared with when no precoder is used, the two AoA estimation algorithms with precoders show significant improvement in performance. To achieve the same RMSE, the improvement is about 10 dB in SNR. The RMSEs of AoA estimation in degrees which is more intuitive in angle estimation is shown in Fig. 3.6(b).

3.5 Applying Precoder to AoA-Based Localization Algorithm

The precoder design here can be applied to any scenarios that utilize the AoA information to improve its performance. In our work, we apply it to localization by using an existing known location estimation algorithm as an example. In the literature, various AoA-based localization techniques have been proposed. We choose the scheme proposed in [20], since it works in a MIMO system and is

44
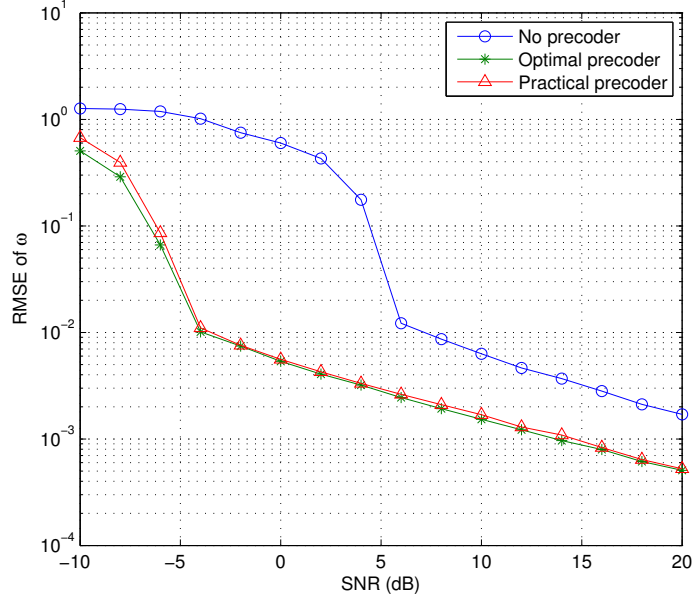
(a) RMSE of ω versus SNR
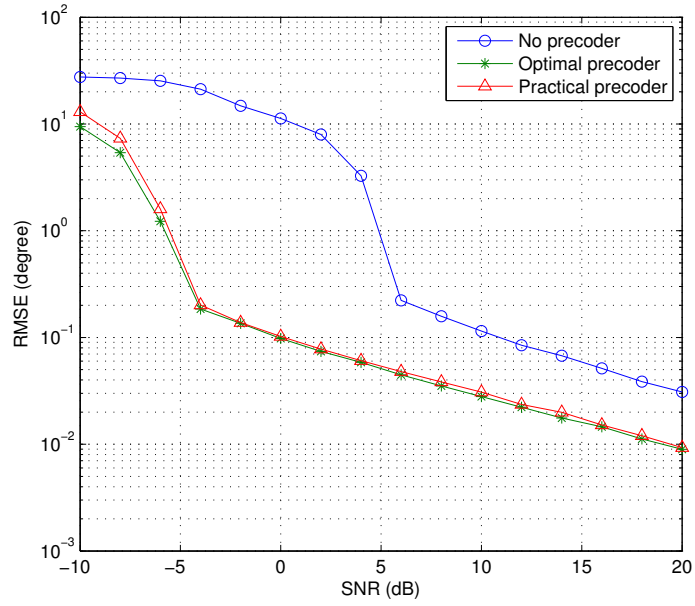
(b) RMSE of AoAs in degree versus SNR

Fig. 3.6: *Comparison of the performances of the three AoA estimation strategies over SNR* $(N = 12,\ \theta_d = 0.5\theta_{3\mathrm{dB}})$

45

robust enough to overcome the NLOS problem in localization.

The localization scheme in [20] leverages on the bidirectional estimation of AoA and time-of-arrival (ToA) of the paths between the mobile terminal (MT) and fixed terminal (FT) which undergo one-bound scattering. The MT initiates the localization process by transmitting a beacon signal. The FT that receives the signal first estimates the ToAs of all the paths using an existing algorithm such as those proposed in [123–125], followed by estimating the AoAs using the MUSIC algorithm. The signal used for AoA estimation is assumed to be precoded. After obtaining the parameters of the channel from the MT to the FT (referred to as forward link hereafter), the ToAs and AoAs of the channel from the FT to the MT (referred to as reverse link hereafter) are subsequently estimated using the same principle. As in the channel model described in Section 3.2, each path is characterized by three parameters: AoD from the MT, AoA to the FT and ToA. If the system operates in the time-division-duplex mode, the channels of the forward link and the reverse link are symmetric, so the AoAs of the reverse link correspond to the AoDs of the forward link. All the estimated parameters are sent to the information processing center. After rejecting the multiple-bound paths [20], the location is determined using the LS algorithm.

An example is depicted in Fig. 3.7, which shows the principle of finding the possible location of the MT through a one-bound path. The FT with known location (x_f, y_f) has the measured AoA $\Omega_{R,l}$ and ToA t_l for the lth forward link path, while the MT with unknown location (x_m, y_m) has the measured AoA $\Omega_{T,l}$ and ToA τ_l for the reverse link of the same path. The path length can be expressed as the product of the speed of wave propagation c and the ToA: $d_{f,l} = ct_l$ and $d_{r,l} = c\tau_l$. Under the constraints of the path length and the AoAs of the forward and reverse links, the location of the MT can be uniquely determined if we have knowledge about the location of the scatterer $S_l(x_{s,l}, y_{s,l})$. From Fig. 3.7, the actual location of S lies along the line that initiates from the FT with the angle $\Omega_{R,l}$. It was shown in [20], all possible MT locations will form a straight line which is shown in Fig. 3.7. If we have the knowledge of two propagation paths originating from the MT, the position of the MT can be determined as the intersection point of the two lines of possible MT locations.

As in Fig. 3.7, in order to find the equation for the line of possible MT locations, we first identify the locations of two endpoints of the line which are
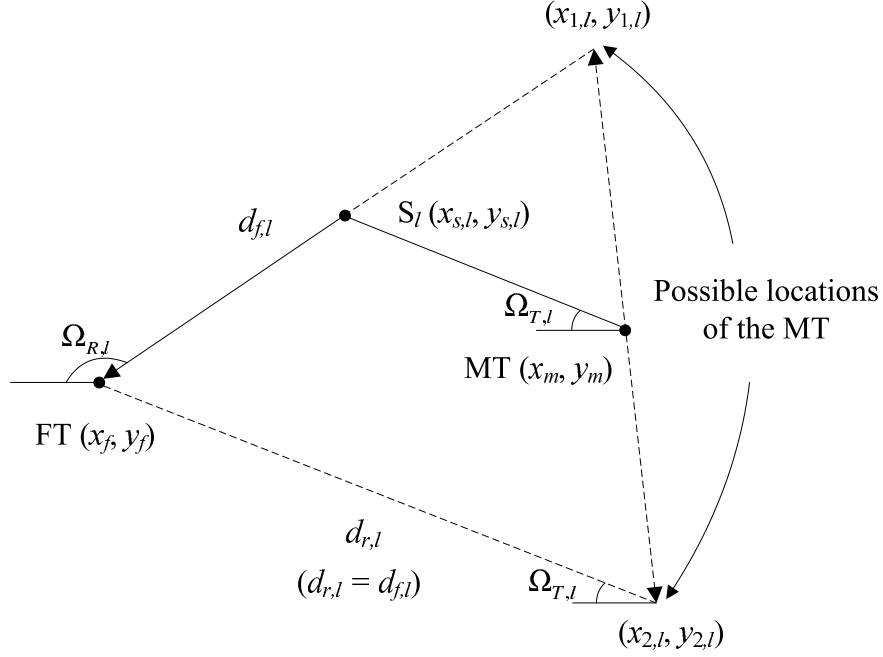
Fig. 3.7: *Possible locations of the MT derived from the parameters of a one-bound path*

given by

$$x_{1,l} = x_f - d_{f,l}\cos\Omega_{R,l}, \quad y_{1,l} = y_f + d_{f,l}\sin\Omega_{R,l},$$
$$x_{2,l} = x_f + d_{r,l}\cos\Omega_{T,l}, \quad y_{2,l} = y_f - d_{r,l}\sin\Omega_{T,l}. \tag{3.23}$$

Then using simple derivations, the equation of the line can be written as

$$y_m = a_l x_m + b_l, \tag{3.24}$$

where

$$a_l = -\frac{d_{f,l}\sin\Omega_{R,l} + d_{r,l}\sin\Omega_{T,l}}{d_{f,l}\cos\Omega_{R,l} + d_{r,l}\cos\Omega_{T,l}},$$
$$b_l = y_f - ax_f + \frac{d_{f,l}d_{r,l}(\sin\Omega_{R,l}\cos\Omega_{T,l} - \cos\Omega_{R,l}\sin\Omega_{T,l})}{d_{f,l}\cos\Omega_{R,l} + d_{r,l}\cos\Omega_{T,l}}.$$

Define the number of FTs as N_f, and the number of paths corresponding to the nth FT as L_n, $n = 1, \ldots, N_f$. With each path corresponding to a line of possible MT locations, there are totally $\sum_{n=1}^{N_f} L_n$ lines. Regarding the

mathematical expression, the coefficients in (3.24) are changed to $a_{l,n}$ and $b_{l,n}$, $l = 1, \ldots, L_n, n = 1, \ldots, N_f$, for the nth FT and the lth path correspondingly. All the lines can be written in the matrix form as

$$\mathbf{A} \begin{bmatrix} x_m \\ y_m \end{bmatrix} = \mathbf{b}, \tag{3.25}$$

where

$$\mathbf{A} = \begin{bmatrix} a_{1,1} & \ldots & a_{L_1,1} & \ldots & a_{1,N_f} & \ldots & a_{L_{N_f},N_f} \\ -1 & \ldots & -1 & \ldots & -1 & \ldots & -1 \end{bmatrix}^T,$$

$$\mathbf{b} = -[b_{1,1} \; \ldots \, b_{L_1,1} \; \ldots \; b_{1,N_f} \; \ldots \; b_{L_{N_f},N_f}]^T.$$

Therefore, the LS solution for (3.25) is given by

$$\begin{bmatrix} x_m \\ y_m \end{bmatrix} = (\mathbf{A}^T \mathbf{A})^{-1} \mathbf{A}^T \mathbf{b}. \tag{3.26}$$

3.6 Simulation of Localization with Precoder

In this section, we will study the performance of the localization algorithm when the use of precoder is possible. The MUSIC algorithm with practical precoder is used to perform AoA estimation, and the algorithm described in Section 3.5 is adopted for location estimation.

The localization scenario is depicted in Fig. 3.8. The MT is located at $(20, 10)$ and its coordinates are the parameters under estimation. Two FTs labeled as FT_1 and FT_2 are located at $(5, 10)$ and $(30, 15)$, respectively. There are three paths between the MT and each FT, two of which are one-bound paths and the third is a two-bound path in dotted line. The scatterers between FT_1 and the MT are placed at $(16, 13)$, $(15, 8)$ for the two one-bound paths and at $(7, 12)$, $(13, 4)$ for the two-bound path, while those between FT_2 and the MT are placed at $(24, 14)$, $(23, 9)$ for the two one-bound paths and at $(27, 16)$, $(25, 2)$ for the two-bound path. The AoAs, AoDs, ToAs and path lengths are calculated according the geometric relationship. The path gains are inverse proportional to the path length, and for each scattering of signal, a fixed coefficient (less than 1) is multiplied. Each of the devices is equipped with a ULA with six antennas separated by half a wavelength.
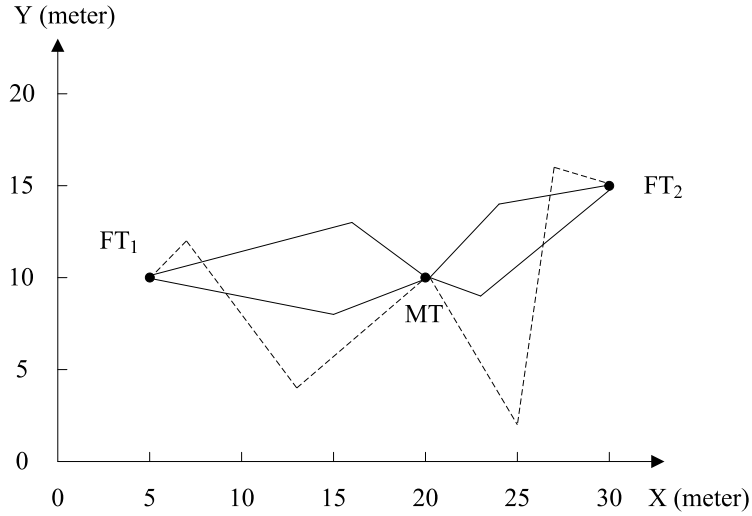
Fig. 3.8: Scenario for the simulation of localization

In the simulation, we compare the accuracy of location estimation with and without practical precoder. According to the geometry described above, the channel matrices between MT and two FTs are computed. In each Monte-Carlo simulation, the AoAs of forward link and reverse link between MT and FT_1 as well as the AoAs of links between MT and FT_2 are all estimated using the MUSIC algorithm, for both with and without precoder. Regarding the ToAs, we assume the errors follow Gaussian distributions with zero mean and have the same variance, and they are generated randomly. All the required channel parameters are then used to determine the location of MT according to the principles described in Section 3.5.

The location errors depend on two parameters, i.e. the SNR (determine the error of AoA estimation, and defined in the same way as in Section 3.4) and the standard derivation of distance measurements σ_d (represent the error of ToA estimation). The RMSE of the location estimation as a function of the SNR is shown in Fig. 3.9, with $\sigma_d = 0$ in the first figure and $\sigma_d = 1$ meter in the second figure. When $\sigma_d = 0$, i.e. the ToA estimation is ideal, we observe performance improvement at both low and high SNRs in Fig. 3.9(a). The largest improvement appears when the SNR ranges from -8 to -2 dB, and the RMSE of location is improved by over 90%, from a few meters (without precoder) to a few centimeters (with precoder). As the SNR increases, the difference becomes less. When SNR=0

49

(a) σ_d=0
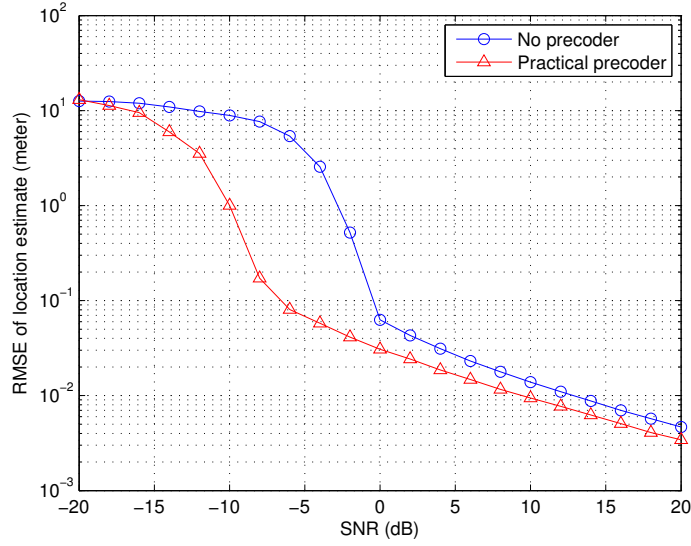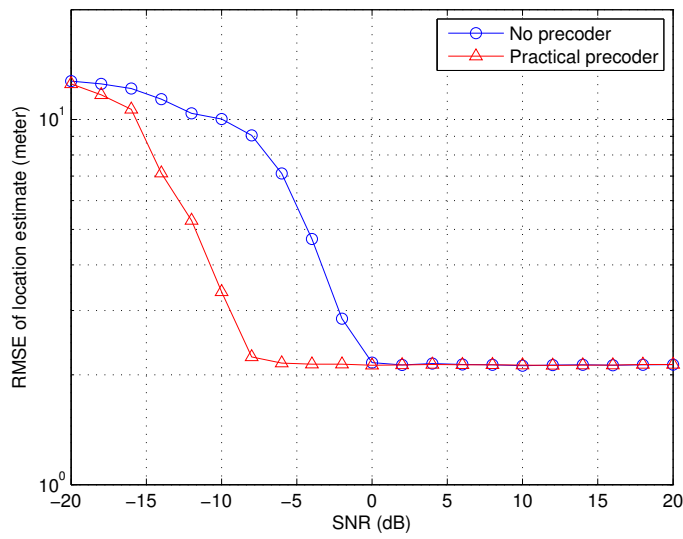
(b) σ_d=1 meter

Fig. 3.9: RMSE of location estimate as a function of SNR when the standard derivation of distance measurements $\sigma_d = 0$ and $\sigma_d = 1$ meter

50
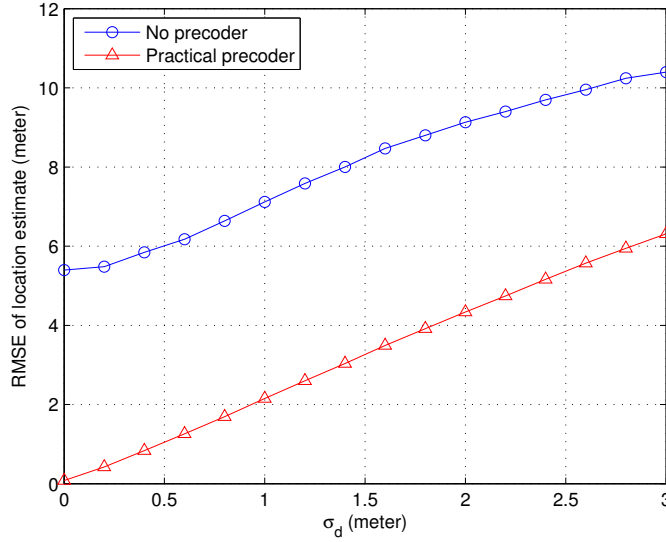
Fig. 3.10: RMSE of location estimate as a function of the standard derivation of distance measurements σ_d when SNR=-6 dB

dB or higher, the precoder results in $25 - 50\%$ improvement compared with the system without precoder. When $\sigma_d = 1$ meter, as shown in Fig. 3.9(b) the improvement at low SNR is still significant, e.g. $50 - 75\%$ improvement when the SNR ranges from -12 to -4 dB. However, it disappears at high SNR. The reason is that the AoA estimation errors with and without precoder are both in the order of 0.1 degree or even lower after 0 dB, and the distance error becomes the dominant factor on localization compared with the AoA estimation error. When the SNR is set at -6 dB and the value of σ_d changed from 0 to 3 meters, we get Fig. 3.10 where significant improvement can be observed.

3.7 Conclusion

In this chapter, we have derived a new asymptotic error variance bound when the transmitted signal can be pre-processed while the MUSIC algorithm is used to estimate the AoAs. We further propose the optimal design of a precoder to achieve the bound asymptotically, and a practical precoder design which is realizable in practice. The performance of the optimal precoder is demonstrated to be able to approach the bound asymptotically through simulation. On the other hand, the

practical precoder is shown to perform close to the optimal precoder even in the high-resolution scenario. The two precoder schemes can considerably improve the performance as compared with the case when no precoder is used, i.e., without any transmit signal design. When the precoder is applied to any AoA-based localization algorithm, the accuracy of location estimation is improved.

Let us remark that our proposed approach is different from [126, III.A] in terms of motivation, formulation and solutions. Our work is motivated by enhancing the performance of the MUSIC algorithm, and minimizing the asymptotic AoA estimation error is the design criterion. On the other hand, the design objective of the precoder in [126, III.A] is to minimize the minimum mean square error (MMSE) of the received symbol. The two different design criteria lead to two different cost functions, and therefore provide two different optimal precoders.

Chapter 4

Improving the Accuracy of ToA Estimation in MIMO Systems

In this chapter, with the objective to minimize the Cramer-Rao lower bound (CRLB) of the time-of-arrival (ToA) estimator, we propose a method to improve the accuracy of ToA estimation through pre-processing the transmitted signal in multiple-input multiple-output (MIMO) systems. We consider two cases: (1) transmit beamforming is adopted when the channel state information at the transmitter (CSIT) is available, and (2) space-time block code (STBC) is utilized as the transmit diversity technique for the case of unavailable CSIT. Under the assumption that the channel state information at the receiver (CSIR) is always available in both cases, we employ receive beamforming at the receiver. We demonstrate through simulation that the performance of the ToA estimator is enhanced with the availability of CSIT, and improved further with the increase in the number of antennas. Under the condition of erroneous CSIT, improvement can still be observed as compared with the case with unavailable CSIT when the signal-to-noise ratio (SNR) is below a threshold.
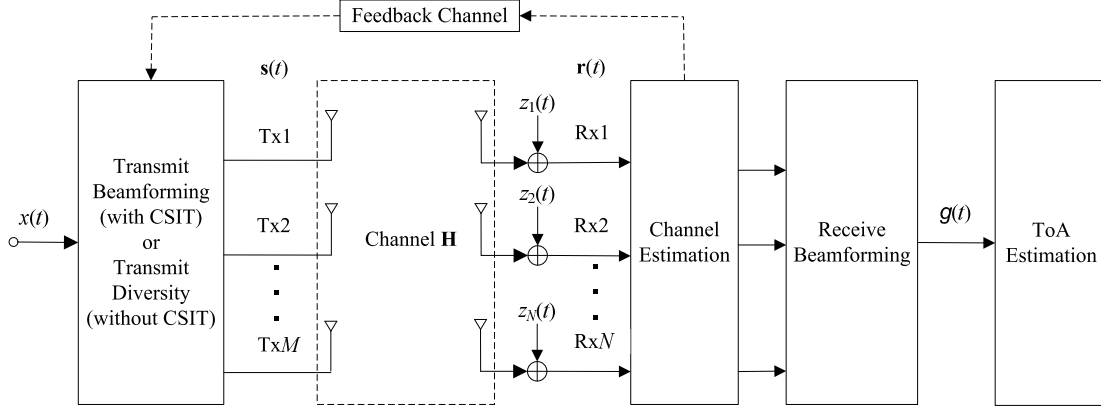
Fig. 4.1: System structure

4.1 Cramer-Rao Lower Bound for ToA Estimation

The system model with a single-path channel is depicted in Fig. 4.1. The transmitter and receiver are each equipped with an antenna array of M and N elements, respectively. The receiver is assumed to estimate the channel periodically, hence CSIR is always known. The beamforming vector at the receiver, $\mathbf{w}_R$, is designed according to CSIR. CSIT may or may not be available. If a feedback channel from the receiver to the transmitter is introduced [23], i.e. the CSIT is made available, transmit beamforming can be applied and the beamforming vector $\mathbf{w}_T$ is computed according to the principle presented in Section 4.2.1. On the other hand, if the CSIT is not available, the transmit diversity technique via STBC is adopted.

Define $x(t)$ as the input signal which consists of modulated pulses

$$x(t) = \sum_{i=-\infty}^{\infty} \sqrt{E_s} b_i a(t - iT_s) \tag{4.1}$$

where E_s is the signal power, $b_i \in \{-1, +1\}$ is the transmitted data symbol, T_s is the symbol duration and $a(t)$ is the pulse with unit energy and time-limited to T_s. The received signal at the receive antenna array can be expressed as

$$\mathbf{r}(t) = \mathbf{h} x(t - \tau) + \mathbf{z}(t) \tag{4.2}$$

54

where $\mathbf{z}(t) = [z_1(t), z_2(t), ..., z_N(t)]^T$ is the additive white Gaussian noise with power spectral density N_0, and τ is the ToA of the path. When CSIT is available, we have $\mathbf{h} = \mathbf{H}\mathbf{w}_T$ where $\mathbf{H}$ is the channel matrix. When the CSIT is not available and transmit diversity technique via STBC is adopted, the channel model can still be expressed using the form of (4.2), and the details will be presented in Section 4.2.2. The output of the receive beamforming vector is expressed as

$$g(t) = \mathbf{w}_R^H \mathbf{h} x(t - \tau) + \mathbf{w}_R^H \mathbf{z}(t). \tag{4.3}$$

The beamforming vector $\mathbf{w}_R$ should be normalized so that it does not introduce any power gain. Therefore, $\mathbf{w}_R^H \mathbf{z}(t)$ can be replaced by a single random variable $n(t)$ which follows Gaussian distribution with zero mean and variance N_0. We also define $\zeta = \mathbf{w}_R^H \mathbf{h}$. The above equation can be simplified to

$$g(t) = \zeta x(t - \tau) + n(t) \tag{4.4}$$

Define $\boldsymbol{\Theta} = [\tau\ \zeta]$ as the parameter vector to be estimated. We set the observation interval at the receiver as $[0, T]$, where $T = IT_s$ and I is an integer denoting the number of observed symbols. Then the maximum likelihood (ML) estimate of $\boldsymbol{\Theta}$ is given by

$$\hat{\boldsymbol{\Theta}}_{ML} = \arg\max_{\boldsymbol{\Theta}} \left\{ \frac{\zeta}{N_0} \int_0^T g(t) x(t - \tau) dt - \frac{\zeta^2}{2N_0} \int_0^T [x(t - \tau)]^2 dt \right\} \tag{4.5}$$

With the above ML estimate function, the Fisher information matrix (FIM) can be expressed as follows

$$\mathbf{J}_{\boldsymbol{\Theta}} = \begin{bmatrix} J_{\tau\tau} & J_{\tau\zeta} \\ J_{\zeta\tau} & J_{\zeta\zeta} \end{bmatrix} \tag{4.6}$$

where

$$J_{\tau\tau} = \frac{\zeta^2}{N_0} \int_0^T [x'(t - \tau)]^2 dt,$$
$$J_{\tau\zeta} = J_{\zeta\tau} = -\frac{\zeta}{N_0} \int_0^T x(t - \tau) x'(t - \tau) dt,$$
$$J_{\zeta\zeta} = \frac{1}{N_0} \int_0^T [x(t - \tau)]^2 dt, \tag{4.7}$$

and $x'(t)$ is the first-order derivative of $x(t)$. In order to simplify the above equations, we define

$$\Xi = \int_0^T [x(t-\tau)]^2 dt,$$

$$\tilde{\Xi} = \int_0^T [x'(t-\tau)]^2 dt,$$

$$\hat{\Xi} = \int_0^T x(t-\tau)x'(t-\tau) dt. \tag{4.8}$$

The CRLB of the ToA estimator is the first element of the inverse of the FIM, which is

$$\text{CRLB}_\tau = [\mathbf{J}_\Theta^{-1}]_{11} = \frac{N_0 \Xi}{\zeta^2(\Xi\tilde{\Xi} - \hat{\Xi}^2)}. \tag{4.9}$$

$\mathbf{H}$ can be obtained by performing channel estimation, so the parameter ζ can be made known before the estimation of τ. Under this situation, the CRLB is reduced to

$$\text{CRLB}_\tau = \frac{N_0}{\zeta^2\tilde{\Xi}}. \tag{4.10}$$

For the transmitted signal that has the form shown in (4.1), it has been shown that $\tilde{\Xi}$ can be expressed as follows [127]

$$\tilde{\Xi} = 4\pi^2 E_s \beta_a^2 \tag{4.11}$$

where β_a is the effective bandwidth of $a(t)$ defined as

$$\beta_a^2 = \frac{\int_{-\infty}^{\infty} f^2 A^2(f) df}{\int_{-\infty}^{\infty} A^2(f) df} \tag{4.12}$$

where $A(f)$ is the Fourier transform of $a(t)$. Substituting (4.11) into (4.10), we have

$$\text{CRLB}_\tau = \frac{N_0}{4\pi^2 \beta_a^2 \zeta^2 E_s}, \tag{4.13}$$

where $\zeta^2 E_s/N_0$ is the SNR at the receiver.

4.2 MIMO Beamforming and Diversity for ToA Estimation

We use the CRLB derived in (4.13) as the objective function, and design appropriate transmit signal and receive techniques to minimize it. It is obvious that minimizing (4.13) is equivalent to maximizing the receive SNR. This matches to the objective in communication system design which aims to optimize the receive SNR in the MIMO link, and obviously some of the known results can be applied. In the following, we will present the strategies when the CSIT is available and not available, respectively. The tightness of this CRLB will be explained in the simulation.

4.2.1 When CSIT Is Available

Theorem 2. *Let the singular value decomposition (SVD) of* $\mathbf{H}$ *be denoted by* $\mathbf{H} = \mathbf{u}_h \lambda_h \mathbf{v}_h^H$, *where* $\mathbf{u}_h$ *and* $\mathbf{v}_h$ *are* $N \times 1$ *and* $M \times 1$ *vectors with the property* $\mathbf{u}_h^H \mathbf{u}_h = 1$ *and* $\mathbf{v}_h^H \mathbf{v}_h = 1$, *respectively, and* λ_h *is the singular value of* $\mathbf{H}$. *Then the beamforming vectors that maximize the receive SNR are* $\mathbf{w}_R = \mathbf{u}_h$ *and* $\mathbf{w}_T = \mathbf{v}_h$, *respectively.*

Proof. See [121]. $\qquad\square$

Substituting the optimal beamforming vectors into the CRLB, we have

$$
\begin{aligned}
CRLB_\tau &= \frac{N_0}{4\pi^2 \beta_a^2 E_s \left\| \mathbf{w}_R^H \mathbf{H} \mathbf{w}_T \right\|^2} \\
&= \frac{N_0}{4\pi^2 \beta_a^2 E_s \lambda_h^2}
\end{aligned}
\tag{4.14}
$$

4.2.2 When CSIT Is Not Available

When CSIT is not available, optimal design through the processing of signal at the transmitter is not possible. However, we shall examine the use of STBC to achieve the diversity gain without reducing the spectral efficiency. On the other hand, the receive SNR can be maximized at the receiver by maximum ratio combining (MRC). Hence, the strategy employed here is to apply the STBC at the transmitter, then independently decode the signals at each receive antenna, and apply the MRC to combine the decoded signals from all receive antennas.

The STBCs for different transmit antenna numbers are listed in [24]. In this work, we use the case when the number of transmit antennas is two (also known as Alamouti code [128]) as an example to derive the corresponding CRLB.

Denote the transmitted signals at time t and $t + T_s$ as $x(t)$ and $x(t + T_s)$, respectively. Then the signals at the two transmit antennas are designed as

$$
\mathbf{s}(t) = \sqrt{\frac{1}{2}} \begin{bmatrix} x(t) \\ x(t + T_s) \end{bmatrix},
$$
$$
\mathbf{s}(t + T_s) = \sqrt{\frac{1}{2}} \begin{bmatrix} x^*(t + T_s) \\ x^*(t) \end{bmatrix}. \tag{4.15}
$$

After transmission through the channel, the signals at the nth receive antenna before decoding are

$$
\tilde{r}_n(t) = \sqrt{\frac{1}{2}} \left(h_{n1} x(t - \tau) + h_{n2} x(t + T_s - \tau) \right) + \tilde{z}_n(t),
$$
$$
\tilde{r}_n(t + T_s) = \sqrt{\frac{1}{2}} \left(-h_{n1} x^*(t + T_s - \tau) + h_{n2} x^*(t - \tau) \right) + \tilde{z}_n(t + T_s), \tag{4.16}
$$

where h_{n1} and h_{n2} are the entries of the nth row of the channel matrix $\mathbf{H}$, and $\tilde{z}_n(t)$ and $\tilde{z}_n(t + T_s)$ are i.i.d. complex Gaussian noise components each of which has zero mean and variance N_0. At the nth antenna, the decoding process is expressed in mathematical form as follows

$$
\begin{bmatrix} r_n(t) \\ r_n(t + T_s) \end{bmatrix} = \frac{1}{\sqrt{|h_{n1}|^2 + |h_{n2}|^2}} \begin{bmatrix} h_{n1}^* & h_{n2} \\ h_{n2}^* & -h_{n1} \end{bmatrix} \begin{bmatrix} \tilde{r}_n(t) \\ \tilde{r}_n^*(t + T_s) \end{bmatrix}
$$
$$
= \begin{bmatrix} \sqrt{\frac{|h_{n1}|^2 + |h_{n2}|^2}{2}} x(t - \tau) + z_n(t) \\ \sqrt{\frac{|h_{n1}|^2 + |h_{n2}|^2}{2}} x(t + T_s - \tau) + z_n(t + T_s) \end{bmatrix} \tag{4.17}
$$

where $r_n(t)$ and $r_n(t + T_s)$ are the signals at time t and $t + T_s$ after decoding, respectively, and $z_n(t)$ and $z_n(t + T_s)$ are i.i.d. complex Gaussian noise components each of which has zero mean and variance N_0.

It is obvious that the signal vector at the receive antenna array after decoding

can be expressed using the following form which is consistent with (4.2)

$$\mathbf{r}(t) = \begin{bmatrix} \sqrt{\frac{|h_{11}|^2 + |h_{12}|^2}{2}} \\ \vdots \\ \sqrt{\frac{|h_{N1}|^2 + |h_{N2}|^2}{2}} \end{bmatrix} x(t - \tau) + \mathbf{z}(t) \qquad (4.18)$$

According to the principle of MRC and with the model in (4.18), the receive beamforming vector should be

$$\mathbf{w}_R = \frac{1}{\|\mathbf{H}\|_F} \left[\sqrt{|h_{11}|^2 + |h_{12}|^2}, \cdots, \sqrt{|h_{N1}|^2 + |h_{N2}|^2} \right]^T. \qquad (4.19)$$

where $\|\cdot\|_F$ is the Frobenius norm. After applying the receive beamforming, we have

$$g(t) = \frac{\|\mathbf{H}\|_F}{\sqrt{2}} x(t - \tau) + n(t) \qquad (4.20)$$

Substituting it into (4.13), the CRLB is finally expressed as follows

$$CRLB_\tau = \frac{N_0}{2\pi^2 \beta_a^2 E_s \|\mathbf{H}\|_F^2}$$
$$= \frac{N_0}{2\pi^2 \beta_a^2 E_s \lambda_h^2} \qquad (4.21)$$

When the transmit antenna number is larger than two, the corresponding CRLBs can be also derived similarly.

4.3   Simulation and Performance Analysis

In this section, the performances of the above strategies are evaluated in a synthetically generated channel. The signal $a(t)$ consists of modulated pulses whose pulse shape is a Gaussian doublet as follows

$$a(t) = \begin{cases} B \left(1 - \frac{4\pi(t - 1.25\xi_a)^2}{\xi_a^2}\right) \exp\left(\frac{-2\pi(t - 1.25\xi_a)^2}{\xi_a^2}\right), & 0 \leq t < T_s \\ 0, & \text{otherwise} \end{cases} \qquad (4.22)$$

where B is used to adjust the pulse energy, and ξ_a determines the pulse width. We choose proper value for B so that the pulse has unit energy. In our work,
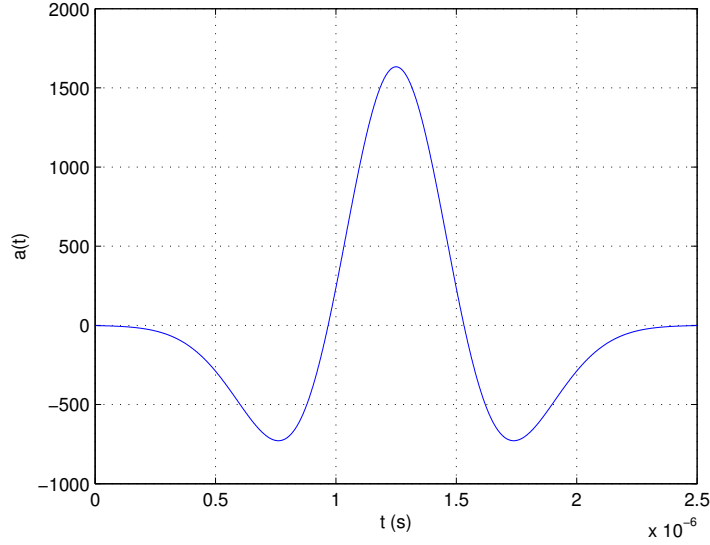
Fig. 4.2: Gaussian doublet used in the simulation

the symbol duration T_s is 2.5 μs, and therefore we choose $\xi_a = 1$ μs so that the pulse values at $t = 0$ and $t = 2.5$ μs are very close to 0. The pulse shape with the chosen parameters is shown in Fig. 4.2. The number of transmitted symbols during observation is $I = 20$. The transmitter and receiver are each equipped with an uniform linear array, and the distance between two adjacent antennas is $d_h = \lambda_s/2$ where λ_s is the wavelength. The channel has a single path whose path gain takes the value of 1. The angle-of-departure (AoD) and AoA of the path are 50° and 130°, respectively. The noise power at each receive antenna is the same, and the SNR is defined as the ratio between the transmission power and the noise power at each receive antenna. We use the root mean square error (RMSE) in ns as the metric to evaluate the performance of the ToA estimator.

In our simulation, we assume perfect CSIR, but the feedback error due to unreliable transmission and feedback delay when obtaining the CSIT is taken into account. The error is defined as follows. We denote the CSIT as $\mathbf{H}_f = \mathbf{H} + \mathbf{E}_f$ where $\mathbf{E}_f$ is the error matrix due to feedback channel comprising i.i.d. complex Gaussian variables with zero mean and variance $\sigma_f^2 \xi^2$. As in [19], $\xi^2 = \|\mathbf{H}\|_F^2 /(MN)$ is defined as the channel normalization factor. σ_f^2 is the quality of the feedback information, for instance, $\sigma_f^2 = 0.1$ indicates 10% error.

In the first part of simulation, we compare the three strategies, namely MIMO
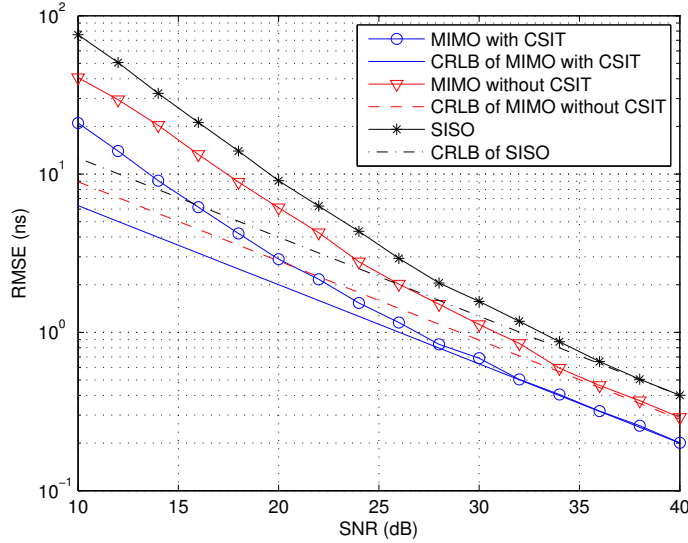
Fig. 4.3: RMSE of ToA estimation versus SNR for the cases of MIMO with CSIT, MIMO without CSIT and SISO (σ_f^2=0)

with perfect CSIT (i.e. $\sigma_f^2 = 0$), MIMO without CSIT and single-input single-output (SISO). The CRLBs of the three cases are also computed. The transmit array and receive array each consists of two elements. From Fig. 4.3, we can see that all three strategies approach the CRLBs asymptotically as a function of the SNR, which indicates that the CRLB is a tight bound at high SNR in our application scenario. Compared with MIMO without CSIT, adopting the CSIT knowledge results in about 3-4 dB performance improvement in SNR. Furthermore, in order to achieve the same performance, the SISO case requires about 6 dB more on the SNR compared with the case of MIMO with CSIT.

The second part evaluates the performance of our techniques while changing the antenna number, which is shown in Fig. 4.4. The two strategies, i.e. MIMO with CSIT and MIMO without CSIT, are simulated. The CSIT is also assumed to be perfect (i.e. $\sigma_f^2 = 0$). For MIMO without CSIT, corresponding STBCs in [24] are adopted when the antenna numbers are 3×3 and 4×4. From the figure, we can see that the performance is improved with increasing the number of antennas. Also, the performance difference between the two strategies is more intuitive. For instance, in order to achieve the same performance, the case of MIMO without CSIT requires a 4×4 array pair, while the case of MIMO with CSIT only needs
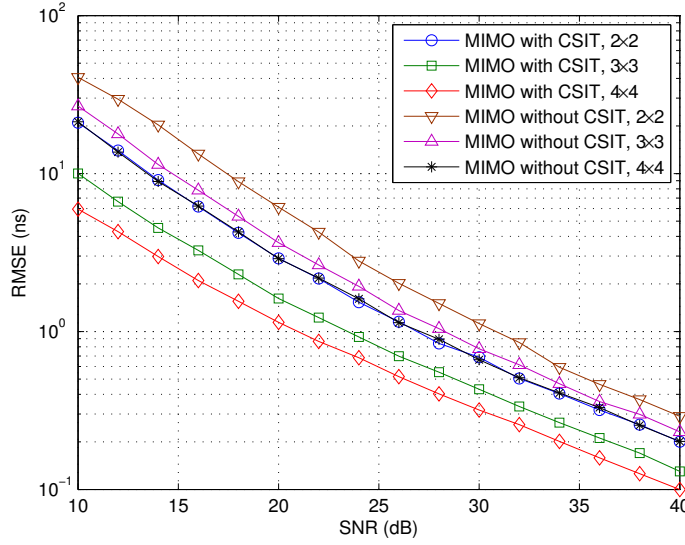
Fig. 4.4: RMSE of ToA estimation versus SNR for the cases of MIMO with and without CSIT while changing the antenna number ($\sigma_f^2=0$)

a 2×2 array pair.

The third part of simulation demonstrates the performance of the case of MIMO with erroneous CSIT. The transmit array and receive array each consists of two elements. We still assume perfect CSIR, but we introduce the error in CSIT due to feedback channel delay and noise. We change the value of σ_f^2, and the results are shown in Fig. 4.5. In general, channel estimation errors result in an error floor in the performance curve of ToA estimation. From the figure, we can see that the performance of MIMO with CSIT is almost not affected with 5% error. However, the performance is downgraded at high SNR when the error increases to 10%, especially when SNR is higher than 38 dB where the errorneous CSIT results in a worse performance compared with the case when no CSIT is used. If the feedback error is 15%, it is better not to use the CSIT when the SNR is higher than 24 dB.

4.4 Conclusion

By means of minimizing the CRLB of the ToA estimator, we propose a method to improve the accuracy of ToA estimation in two scenarios where the
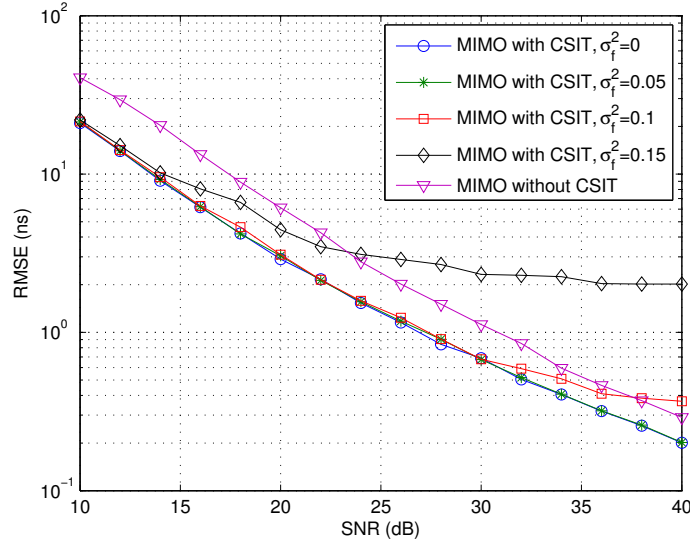
Fig. 4.5: RMSE of ToA estimation versus SNR for the case of MIMO with erroneous CSIT

CSIT are available and not available, respectively. The transmit and receive beam-forming is adopted when the CSIT is available, while the transmit diversity via STBC and receive beamforming are utilized when the CSIT is not available. The performance is enhanced with the availability of CSIT and the increase in the number of antennas. Even with erroneous CSIT, improvement can be observed compared with the case of unavailable CSIT when the SNR is below a threshold.

Chapter 5

MAP-Based Channel Estimation for SIMO and MIMO Systems

This chapter takes the conventional approach to improve the localization accuracy through a more accurate joint parameters estimation techniques, which include both temporal and spatial domain channel parameters. Quantifying the localization accuracy is not the focus of this chapter. The focus is to study the accuracy of the parameter estimation which will impact the performance of any localization algorithm used. A maximum a posterior (MAP) based channel estimation algorithm is proposed to estimate both the temporal and spatial domain channel parameters for single-input multiple-output (SIMO) systems transmitting over an extended Saleh-Valenzuela (SV) channel. The proposed algorithm leverages on prior knowledge of statistical channel information of signal clusters and rays within a cluster, and uses the expectation-maximization (EM) algorithm to resolve the high dimensional optimization problem into iteratively solving the multiple 3-dimensional (3-D) optimizations. The successive interference cancellation (SIC) method is applied in the initialization stage to obtain the initial guess to the EM algorithm. Simulations are carried out in two typical indoor scenarios following the extended SV model. The proposed algorithm is shown to outperform the maximum likelihood (ML) based algorithm reported for SIMO systems. Finally, we discuss how the algorithm can be extended and applied to multiple-input multiple-output (MIMO) systems.
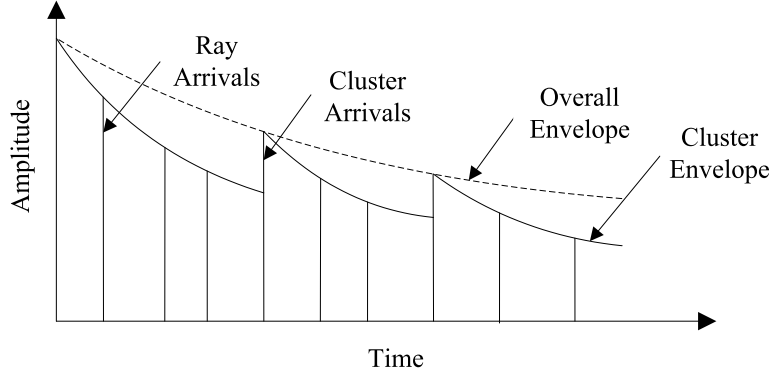
Fig. 5.1: Cluster and ray arrivals in the temporal domain of the extended SV model

5.1 Channel and Signal Model

5.1.1 Overview of the Extended Saleh-Valenzuela Model

The extended SV model [129] results from space-time channel measurements over indoor propagation environment for MIMO/SIMO systems. It is an extension to the SV time-of-arrival (ToA) model [130] by incorporating the spatial information. The model is based on the observation that all multipath rays arrive in clusters. The channel impulse response (CIR) $h(\tau, \theta)$, where τ and θ are the ToA and the angle-of-arrival (AoA) respectively, is given by

$$h(\tau, \theta) = \sum_{l=1}^{L_c} \sum_{k=1}^{K_l} \alpha_{kl} \delta(\tau - T_l - \tau_{kl}) \delta(\theta - \Theta_{R,l} - \varphi_{R,kl}) \tag{5.1}$$

where L_c and K_l are the number of clusters and the number of rays within the lth cluster, respectively. α_{kl} is the complex path gain of the kth ray in the lth cluster and follows the complex normal distribution with mean 0 and variance σ_{kl}^2. The total delay of each ray is the sum of T_l (the delay of the lth cluster) and τ_{kl} (the delay of the kth ray in the lth cluster). Similarly, the AoA of each ray is the sum of $\Theta_{R,l}$ (the mean AoA of the lth cluster) and $\varphi_{R,kl}$ (the AoA of the kth ray in the lth cluster relative to $\Theta_{R,l}$).

In the temporal domain, the complex path gain of clusters and rays within a cluster attenuate exponentially by two different time constants. The variance σ_{kl}^2 is given by

$$\sigma_{kl}^2 = \sigma_{11}^2 \exp(-T_l/\Gamma) \exp(-\tau_{kl}/\gamma) \tag{5.2}$$

where σ_{11}^2 is the variance of the complex path gain of the first ray within the first-arriving cluster. The variance is a function of the distance between the transmitter and receiver. The ToAs of clusters, as well as the ToAs for the rays in each cluster, are given by two independent Poisson processes of different rates. The cluster arrival rate Φ refers to the intercluster arrival times, and the ray arrival rate ϕ refers to the intracluster arrival times. The distributions are given by

$$p(T_l|T_{l-1}) = \Phi \exp(-\Phi(T_l - T_{l-1})), \quad T_{l-1} < T_l \tag{5.3}$$

$$p(\tau_{kl}|\tau_{k-1,l}) = \phi \exp(-\phi(\tau_{kl} - \tau_{k-1,l})), \quad \tau_{k-1,l} < \tau_{kl} \tag{5.4}$$

The two distributions are assumed to be independent of each other. In addition, T_1 and τ_{1l} ($l = 1, \ldots, K_1$) are both assumed to be zero. In the spatial domain, the mean AoA for each cluster is uniformly distributed over $[0, 2\pi)$. For rays within a cluster, the deviation in the AoA with respect to the respective mean arrival angle is assumed to follow a Laplacian distribution with standard deviation σ.

$$p(\varphi_{R,kl}) = \frac{1}{\sqrt{2}\sigma} \exp\left(-\left|\frac{\sqrt{2}\varphi_{R,kl}}{\sigma}\right|\right) \tag{5.5}$$

As assumed in [129], the time and angle distributions are independent of each other.

The above distributions and model parameters are derived by experimental measurements in [129]. It is implied that the extended SV model could represent the signal propagation situations in many types of buildings according to their experiments conducted in buildings with varying construction. Therefore, in our application, this model is adopted to develop our algorithm, and the model parameters which depends on the building construction can be obtained by field measurements at the time when a localization system is set up inside a building.

5.1.2 Signal Model

The transmitted signal $s(t)$ consists of infinite rectangular pulses modulated by a pseudo-noise (PN) sequence as described in [82]. $s(t) = \sqrt{E_s} \sum_{i=-\infty}^{\infty} b_i a(t - iT_s)$, where E_s is the signal energy per bit, T_s denotes the symbol duration, and $b_i \in \{-1, +1\}$. Here we adopt a rectangular pulse with unit energy and time-limited to T_s for $a(t)$.
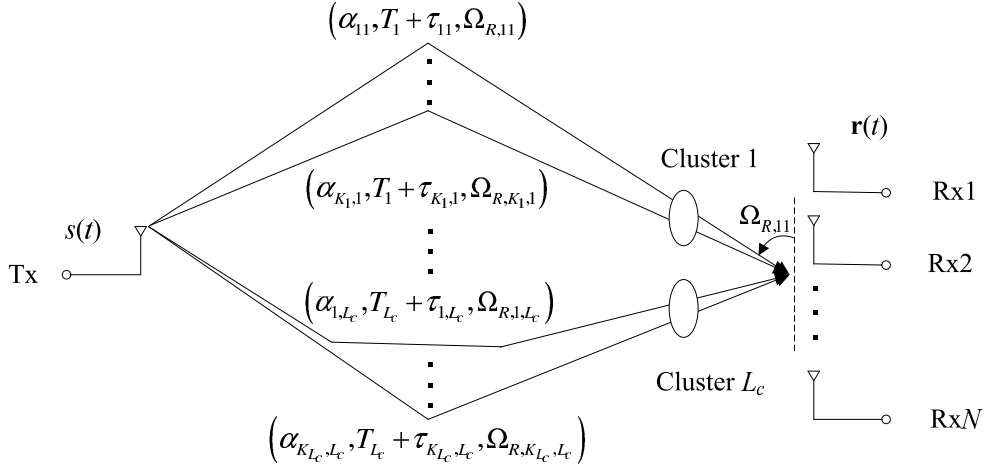
Fig. 5.2: *Clustered multipath propagation in SIMO channel*

The clustered multipath propagation of a SIMO system in a mobile radio environment is shown in Fig. 5.2. The paths are classified into L_c clusters, and each ray contains three parameters, i.e. complex path gain, ToA and AoA. For simplicity, we assume that the receiver is equipped with a uniform linear array (ULA), however, the proposed algorithm is applicable for any arbitrary array shape. The array consists of N antennas spaced apart by $d_h = \lambda_s/2$, where λ_s is the wavelength. Thus the array steering vector can be expressed as $\mathbf{c}(\Omega) = [c_1(\Omega), \ldots, c_N(\Omega)]^T$, where $c_n(\Omega) = \exp[j2\pi(n-1)d_h \cos\Omega/\lambda_s]$, $n = 1, \ldots, N$ and Ω is the direction of the incoming or exit wave. Since the CIR has the expression shown in (5.1), the received signal vector $\mathbf{r}(t) = [r_1(t), \ldots, r_N(t)]^T$ at the output of the antenna array can be expressed as

$$\mathbf{r}(t) = \sum_{l=1}^{L_c} \sum_{k=1}^{K_l} \alpha_{kl} \mathbf{c}(\Omega_{R,kl}) s(t - T_l - \tau_{kl}) + \mathbf{z}(t) \tag{5.6}$$

where $\Omega_{R,kl} = \Theta_{R,l} + \varphi_{R,kl}$ is the AoA of the kth ray within the lth cluster, $\mathbf{z}(t)$ is white Gaussian noise vector with mean zero and power spectral density N_0.

By defining

$$\mathbf{u}(t; \boldsymbol{\theta}_{kl}) = \alpha_{kl} \mathbf{c}(\Omega_{R,kl}) s(t - T_l - \tau_{kl}) \tag{5.7}$$

and

$$\mathbf{u}(t; \boldsymbol{\theta}) = \sum_{l=1}^{L_c} \sum_{k=1}^{K_l} \mathbf{u}(t; \boldsymbol{\theta}_{kl}) \tag{5.8}$$

68

where $\boldsymbol{\theta} = [\boldsymbol{\theta}_{11}, \ldots, \boldsymbol{\theta}_{K_1,1}, \ldots, \boldsymbol{\theta}_{1,L_c}, \ldots, \boldsymbol{\theta}_{K_{L_c},L_c}]$ is the parameter vector of all paths, $\boldsymbol{\theta}_l = [\boldsymbol{\theta}_{1,l}, \ldots, \boldsymbol{\theta}_{K_l,l}]$ is the parameter vector of the rays in the lth cluster, and $\boldsymbol{\theta}_{kl} = [\alpha_{kl}, T_l + \tau_{kl}, \Omega_{R,kl}]$ is the parameter vector of the kth ray in the lth cluster, then $\mathbf{r}(t)$ can be expressed in a more compact form as

$$
\begin{aligned}
\mathbf{r}(t) &= \mathbf{u}(t; \boldsymbol{\theta}) + \mathbf{z}(t) \\
&= \sum_{l=1}^{L_c} \sum_{k=1}^{K_l} \mathbf{u}(t; \boldsymbol{\theta}_{kl}) + \mathbf{z}(t)
\end{aligned}
\tag{5.9}
$$

5.2   MAP-based Estimation Algorithm

Our objective is to develop a MAP-based channel estimation algorithm of superimposed signals. In order to reduce the computational complexity so that the algorithm is realizable, we apply the EM algorithm. We assume that we have prior knowledge of the parameters in the extended SV model, i.e., the values of $\Phi, \phi, \Gamma, \gamma$ and σ in (5.2) to (5.5) are known.

5.2.1   MAP Estimation

The problem is how to estimate the parameter vector $\boldsymbol{\theta}$, given a serial of observations of the received signal $\mathbf{r}(t)$, sampled at the time instants $t_1, \ldots, t_I$, respectively, where I is the total number of samples. We assume that the channel does not change over the whole sample period. Using the MAP estimation, we aim to find the value of $\boldsymbol{\theta}$ which gives the largest value to the a posteriori distribution $p(\boldsymbol{\theta}|\mathbf{r}(t_1), \ldots, \mathbf{r}(t_I))$. According to Bayes theorem, the a posteriori distribution can be expressed as

$$
p(\boldsymbol{\theta}|\mathbf{r}(t_1), \ldots, \mathbf{r}(t_I)) = \frac{p(\mathbf{r}(t_1), \ldots, \mathbf{r}(t_I)|\boldsymbol{\theta})p(\boldsymbol{\theta})}{p(\mathbf{r}(t_1), \ldots, \mathbf{r}(t_I))}
\tag{5.10}
$$

where $p(\boldsymbol{\theta})$ is the probability of $\boldsymbol{\theta}$, $p(\mathbf{r}(t_1), \ldots, \mathbf{r}(t_I))$ is the probability of the observation $(\mathbf{r}(t_1), \ldots, \mathbf{r}(t_I))$, and $p(\mathbf{r}(t_1), \ldots, \mathbf{r}(t_I)|\boldsymbol{\theta})$ is the a priori probability given by

$$
p(\mathbf{r}(t_1), \ldots, \mathbf{r}(t_I)|\boldsymbol{\theta}) = \prod_{i=1}^{I} \frac{1}{(\pi N_0)^{N/2}} \exp\left(-\frac{\|\mathbf{r}(t_i) - \mathbf{u}(t_i; \boldsymbol{\theta})\|^2}{N_0}\right)
\tag{5.11}
$$

Since $p(\mathbf{r}(t_1), \ldots, \mathbf{r}(t_I))$ is a constant, it can be dropped in the maximization problem. By substituting (5.11) into (5.10), taking the natural logarithm and ignoring the constants which does not affect the optimization, the estimation can be shown to be equivalent to

$$\hat{\boldsymbol{\theta}}_{MAP} = \arg\max_{\boldsymbol{\theta}} \left\{ \sum_{i=1}^{I} \left[2\Re\{\mathbf{r}^H(t_i)\mathbf{u}(t_i; \boldsymbol{\theta})\} - \|\mathbf{u}(t_i; \boldsymbol{\theta})\|^2 \right] + N_0 \ln p(\boldsymbol{\theta}) \right\} \quad (5.12)$$

The maximization problem given in (5.12) is a $3\sum_{l=1}^{L_c} K_l$-D nonlinear optimization problem. It has very high computation complexity and hence is not suitable for real-time applications. Besides, it is difficult to obtain the expression for $p(\boldsymbol{\theta})$. Thus, we need a method to simplify this problem.

5.2.2 The EM Algorithm

The EM algorithm has been first derived in [131], and it has been applied to estimate channel parameters of superimposed signals in [79]. In our work, we apply the EM algorithm with the aim to reduce the computational complexity of the maximization problem given in (5.12). The $(3\sum_{l=1}^{L_c} K_l)$-D nonlinear optimization problem is decoupled into $(\sum_{l=1}^{L_c} K_l)$ 3-D optimization problems and solved iteratively.

The concepts of "incomplete data" and "complete data" are the basis of the EM algorithm. The received signal $\mathbf{r}(t)$ is identified as the incomplete data. As is mentioned in [82], the set of received signals transmitted through all the paths constitute the complete data, which is expressed as

$$\mathbf{w}_{kl}(t) = \mathbf{u}(t; \boldsymbol{\theta}_{kl}) + \sqrt{\beta_{kl}}\mathbf{z}(t), \quad (k = 1, \ldots, K_l; l = 1, \ldots, L_c) \quad (5.13)$$

where the non-negative parameter β_{kl} satisfies the constraint $\sum_{l=1}^{L_c} \sum_{k=1}^{K_l} \beta_{kl} = 1$. As suggested in [82], β_{kl} is assigned with the value of 1 to simplify the analysis. Our simulation results presented shortly show that such an approximation can still result in reasonable good estimate. Therefore, the incomplete date and complete date are related according to the relationship

$$\mathbf{r}(t) = \sum_{l=1}^{L_c} \sum_{k=1}^{K_l} \mathbf{w}_{kl}(t) \quad (5.14)$$
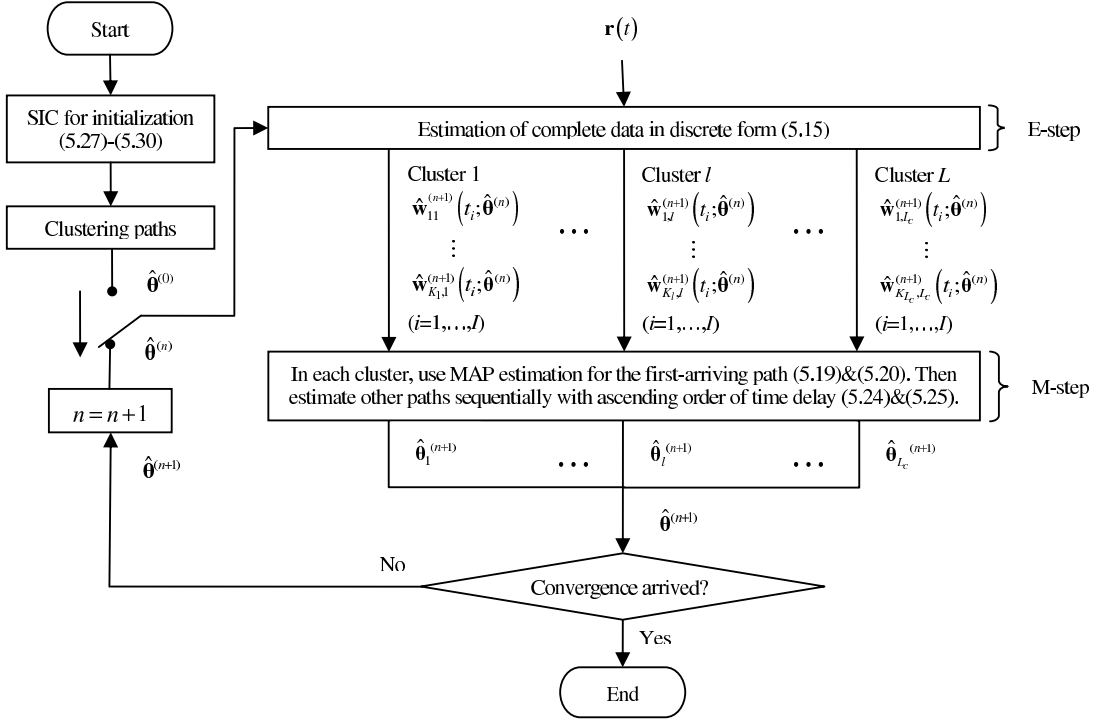
Fig. 5.3: Flow chart of the algorithm

The basic idea behind the EM algorithm is that we first estimate the complete data (unknown underlying variables) using the incomplete data (the samples) and the current estimate of the parameters through the expectation step (E-step), and then using this inferred data to find the new estimate of the parameters through the maximization step (M-step) [132]. This process repeats iteratively, until the values of the parameters converge to a stable solution. The flow of the algorithm is shown in Fig. 5.3.

Estimation of Complete Data

This step is also called the E-step. The estimate of the complete data $\mathbf{w}_{kl}(t)$ in discrete form is represented by $\hat{\mathbf{w}}_{kl}(t_i), i = 1, \ldots, I$, and is based on the observations of the incomplete data $\mathbf{r}(t)$ and the current estimate of $\boldsymbol{\theta}$. The discrete

complete data of the nth iteration cycle is given by

$$\hat{\mathbf{w}}_{kl}^{(n)}\left(t_i; \hat{\boldsymbol{\theta}}^{(n-1)}\right) = E_{\hat{\boldsymbol{\theta}}^{(n-1)}}\left[\mathbf{w}_{kl}(t_i)|\mathbf{r}(t_i)\right]$$

$$= \mathbf{u}\left(t_i; \hat{\boldsymbol{\theta}}_{kl}^{(n-1)}\right) + \beta_{kl}\left[\mathbf{r}(t_i) - \sum_{l'=1}^{L_c}\sum_{k'=1}^{K_l}\mathbf{u}\left(t_i; \hat{\boldsymbol{\theta}}_{k'l'}^{(n-1)}\right)\right]$$

$$(i = 1, \ldots, I; k = 1, \ldots, K_l; l = 1, \ldots, L_c) \qquad (5.15)$$

where $\hat{\boldsymbol{\theta}}^{(n-1)}$ is the estimate of $\boldsymbol{\theta}$ after the $(n-1)$th iteration cycle. The last step of (5.15) comes from [79].

MAP Estimation of a Single Path

This step is referred to as the M-step. In the nth iteration cycle, after we have obtained the complete data in the first step, we use it to find the optimum estimation of parameters. We aim to find the value which maximizes the a posteriori distribution using (5.12), which is

$$\left(\hat{\boldsymbol{\theta}}_{kl}^{(n)}\right)_{MAP}$$

$$= \arg\max_{\boldsymbol{\theta}_{kl}}\left\{\sum_{i=1}^{I}\left[2\Re\left\{\hat{\mathbf{w}}_{kl}^{(n)}(t_i)^H\mathbf{u}(t_i; \boldsymbol{\theta}_{kl})\right\} - \|\mathbf{u}(t_i; \boldsymbol{\theta}_{kl})\|^2\right] + \beta_{kl}N_0\ln p(\boldsymbol{\theta}_{kl})\right\},$$

$$(k = 1, \ldots, K_l; l = 1, \ldots, L_c) \qquad (5.16)$$

To obtain the expression of $p(\boldsymbol{\theta}_{kl})$, we need to consider two different cases.

1. $k = 1$: In this case, we estimate the parameter vector for the first-arriving ray in each cluster. We have

$$p(\boldsymbol{\theta}_{1l}) = p(\alpha_{1l}, T_l, \Omega_{R,1l}) = p(\alpha_{1l}|T_l)p(T_l)p(\Omega_{R,1l}) \qquad (5.17)$$

According to the extended SV model, the distributions of α_{1l} and T_l conditioned on T_l and T_{l-1}, respectively, are known. However, since T_1 is zero as assumed in the model, the time delay can be estimated sequentially in ascending order - T_{l-1} which has been estimated in the current iteration cycle will be used to estimate T_l. We further assume that we do not have any prior information on $\Omega_{R,1l}$ and treat it as being uniformly distributed over

72

$[0, 2\pi)$. We therefore are able to express $p(\boldsymbol{\theta}_{1l})$ in the nth iteration cycle as

$$p(\boldsymbol{\theta}_{1l})^{(n)} = \frac{\Phi}{2\pi^2\sigma_{11}^2} \exp\left(-\Phi(T_l - \hat{T}_{l-1}^{(n)}) + \frac{T_l}{\Gamma} - \frac{|\alpha_{1l}|^2}{\sigma_{11}^2 \exp(-T_l/\Gamma)}\right), T_l > \hat{T}_{l-1}^{(n)}$$

(5.18)

where $\hat{T}_{l-1}^{(n)}$ is the estimate of T_{l-1} in the current nth iteration cycle.

Substituting (5.18) into (5.16), we get the expression for $\left(\hat{\boldsymbol{\theta}}_{1l}^{(n)}\right)_{MAP}$. The optimum value for α_{1l} can be derived in a closed form as a function of T_l and $\Omega_{R,1l}$ by equating the first-order derivative of (5.16) with respect to α_{1l} to 0. This results in (5.20). Substituting the result into (5.16), we obtain (5.19), which is a 2-D search problem to find the optimum value of ToA and AoA. The estimate of the parameters of the nth iteration cycle is given by

$$\left(\widehat{T_l, \Omega_{R,1l}}^{(n)}\right)_{MAP}$$
$$= \arg\max_{(T_l, \Omega_{R,1l})}\left\{\frac{\left|f\left(T_l, \Omega_{R,1l}; \hat{\mathbf{w}}_{1l}^{(n)}\right)\right|^2}{IE_s \|\mathbf{c}(\Omega_{R,1l})\|^2 + N_0 \exp(T_l/\Gamma)/\sigma_{11}^2} + \left(\frac{1}{\Gamma} - \Phi\right)N_0 T_l\right\}, T_l > \hat{T}_{l-1}^{(n)}$$

(5.19)

$$(\hat{\alpha}_{1l}^{(n)})_{MAP} = \frac{f\left(\widehat{T_l, \Omega_{R,1l}}^{(n)}; \hat{\mathbf{w}}_{1l}^{(n)}\right)}{IE_s \left\|\mathbf{c}(\hat{\Omega}_{R,1l}^{(n)})\right\|^2 + N_0 \exp(\hat{T}_l^{(n)}/\Gamma)/\sigma_{11}^2}$$

(5.20)

where

$$f(T, \Omega; \mathbf{w}) = \sum_{i=1}^{I} \mathbf{c}^H(\Omega)\mathbf{w}(t_i)s(t_i - T)$$

(5.21)

2. $k \neq 1$: Similarly, we can write

$$p(\boldsymbol{\theta}_{kl}) = p(\alpha_{kl}, \tau_{kl}, \Omega_{R,kl}) = p(\alpha_{kl}|\tau_{kl})p(\tau_{kl})p(\Omega_{R,kl})$$

(5.22)

Here, we know the distributions of α_{kl} and τ_{kl} conditioned on τ_{kl} and $\tau_{k-1,l}$, respectively. After the first-arriving path in each cluster (i.e. $k = 1$) is estimated, the rays within the cluster are then estimated sequentially with ascending order of time delay. When estimating $\boldsymbol{\theta}_{kl}$, the parameters T_l, $\tau_{k-1,l}$ and $\Omega_{R,1l}$ are known constants. Furthermore, we are able to compute the distribution of $\Omega_{R,kl}$ conditioned on $\Omega_{R,1l}$, as shown in (5.23), based on the fact that it is the sum of a uniformly distributed variable over $[0, 2\pi)$ and a

Laplacian distributed variable. This allows us to take advantage of the fact that rays in the same cluster should show small deviation in AoA, rather than estimating the AoA of each ray independently.

$$p(\Omega_{R,kl}|\Omega_{R,1l}) = \frac{\sigma + \sqrt{2}|\Omega_{R,kl} - \Omega_{R,1l}|}{2\sqrt{2}\sigma^2} \exp\left(-\frac{\sqrt{2}|\Omega_{R,kl} - \Omega_{R,1l}|}{\sigma}\right) \quad (5.23)$$

Using (5.23), the expression of $p(\boldsymbol{\theta}_{kl})$ in the nth iteration cycle can be derived in the similar way as before. Through similar derivations, the estimate of the parameters in the nth iteration cycle is given by

$$\left(\widehat{\tau_{kl}, \Omega_{R,kl}}^{(n)}\right)_{MAP}$$

$$= \arg \max_{(\tau_{kl}, \Omega_{R,kl})} \left\{ \frac{\left|f\left(\tau_{kl}, \Omega_{R,kl}; \hat{\mathbf{w}}_{kl}^{(n)}\right)\right|^2}{IE_s\|\mathbf{c}(\Omega_{R,kl})\|^2 + N_0 \exp(\hat{T}_l^{(n)}/\Gamma)\exp(\tau_{kl}/\gamma)/\sigma_{11}^2} + \left(\frac{1}{\gamma} - \phi\right)N_0\tau_{kl} \right.$$

$$\left. + N_0 \ln\left(\sigma + \sqrt{2}|\Omega_{R,kl} - \hat{\Omega}_{R,1l}^{(n)}|\right) - \frac{\sqrt{2}N_0|\Omega_{R,kl} - \hat{\Omega}_{R,1l}^{(n)}|}{\sigma} \right\}, \quad \tau_{kl} > \hat{\tau}_{k-1,l}^{(n)}$$

$$(5.24)$$

$$(\hat{\alpha}_{kl}^{(n)})_{MAP} = \frac{f\left(\widehat{\tau_{kl}, \Omega_{R,kl}}^{(n)}; \hat{\mathbf{w}}_{kl}^{(n)}\right)}{IE_s\left\|\mathbf{c}(\hat{\Omega}_{R,kl}^{(n)})\right\|^2 + N_0 \exp(\hat{T}_l^{(n)}/\Gamma)\exp(\hat{\tau}_{kl}^{(n)}/\gamma)/\sigma_{11}^2} \quad (5.25)$$

where

$$f(\tau, \Omega; \mathbf{w}) = \sum_{i=1}^{I} \mathbf{c}^H(\Omega)\mathbf{w}(t_i)s(t_i - \hat{T}_l - \tau) \quad (5.26)$$

and $\hat{T}_l^{(n)}$, $\hat{\tau}_{k-1,l}^{(n)}$ and $\hat{\Omega}_{R,1l}^{(n)}$ are the estimate of T_l, $\tau_{k-1,l}$ and $\Omega_{R,1l}$ in the current nth iteration cycle, respectively.

5.3 Initialization Issue

The convergence speed of the EM algorithm depends heavily on the initial value due to the non-convex optimization. In our method, we use the SIC technique described in [133] for initialization purpose. The total number of paths is $L = \sum_{l=1}^{L_c} K_l$. The estimate of the parameter vectors during the initialization process is represented by $\hat{\boldsymbol{\theta}}^{(0)} = [\hat{\boldsymbol{\theta}}_1^{(0)}, \dots, \hat{\boldsymbol{\theta}}_L^{(0)}]$, where $\hat{\boldsymbol{\theta}}_l^{(0)} = [\hat{\alpha}_l^{(0)}, \hat{\tau}_l^{(0)}, \hat{\Omega}_{R,l}^{(0)}], l =$

$1, \ldots, L$. First, the components of $\hat{\boldsymbol{\theta}}^{(0)}$ are all initialized to zero, i.e. $\hat{\boldsymbol{\theta}}^{(0)} = [0, \ldots, 0]$. Then all paths are estimated successively. Before the initialization of the lth path, the parameters for the previous $(l-1)$ paths have been obtained and the estimates of remaining paths are still equal to 0, i.e. $\hat{\boldsymbol{\theta}}^{(0)} = [\hat{\boldsymbol{\theta}}_1^{(0)}, \ldots, \hat{\boldsymbol{\theta}}_{l-1}^{(0)}, 0, \ldots, 0]$. When estimating the lth path, the interference caused by the previously estimated paths are calculated and subtracted from the received signal as shown in (5.27), and the parameters are calculated according to (5.28)-(5.30). During the initialization process, the concept "cluster" is not used. Below is the derivation of SIC.

For $l = 1, \ldots, L$, we initialize the parameter vector of the lth path as below.

$$\mathbf{r}^{(l)}(t_i) = \mathbf{r}(t_i) - \sum_{l'=1}^{l-1} \mathbf{u}\left(t_i; \hat{\boldsymbol{\theta}}_{l'}^{(0)}\right); \quad i = 1, \ldots, I \tag{5.27}$$

$$\hat{\tau}_l^{(0)} = \arg\max_{\tau_l} \left\{ \sum_{n=1}^{N} \left| \sum_{i=1}^{I} s(t_i - \tau_l) r_n^{(l)}(t_i) \right|^2 \right\} \tag{5.28}$$

$$\hat{\Omega}_{R,l}^{(0)} = \arg\max_{\Omega_{R,l}} \left\{ \left| \sum_{i=1}^{I} s(t_i - \hat{\tau}_l^{(0)}) \mathbf{c}^H(\Omega_{R,l}) \mathbf{r}^{(l)}(t_i) \right|^2 \right\} \tag{5.29}$$

$$\hat{\alpha}_l^{(0)} = \frac{\sum_{i=1}^{I} s(t_i - \hat{\tau}_l^{(0)}) \mathbf{c}^H(\hat{\Omega}_{R,l}^{(0)}) \mathbf{r}^{(l)}(t_i)}{IE_s \left\| \mathbf{c}^H(\hat{\Omega}_{R,l}^{(0)}) \right\|^2} \tag{5.30}$$

The output of the SIC initialization is a parameter vector containing the parameters for all paths. However, the paths are not yet grouped into clusters. We propose a simple method to solve this problem. As in [129], the clusters are identified in the ToA/AoA domain, i.e. the rays in the same cluster have similar ToAs and AoAs. Each path can be represented by a point with ToA and AoA as the coordinate on the 2-D plane. The paths within the same cluster must be close to each other. Thus, we first assign ToA and AoA with proper weights respectively, and then compute the weighted Euclidean distance of any pair of two paths. The paths with distances below a predefined threshold are classified into a cluster.

Table 5.1: Setting of parameters of the extended SV model

Parameters	First scenario	Second scenario
Γ (ns)	34	78
γ (ns)	29	82
$1/\Phi$ (ns)	17	17
$1/\phi$ (ns)	5	7
σ (degree)	26	22

5.4   Simulation and Performance Analysis

The performance of the proposed algorithm is evaluated in synthetically generated propagation channels. The receiver is an ULA with eleven elements separated by half wavelength. The modulated PN sequence consists of 1024 rectangular pulses with duration $T_s = 1$ ns. The discretization steps of our algorithm are 0.4 ns and 0.2° for the ToA and AoA, respectively. The performance is evaluated over 60 randomly generated channels according to the extended SV model, and we examine the average performance. In order to simplify the analysis, all the channels are normalized. Each channel consists of 3 clusters, and the clusters have $[4, 3, 3]$ rays respectively. The AoA of each ray is distributed on $[0, \pi)$. We evaluate the performance in two scenarios each of which corresponds to a group of parameters of the extended SV model, similar to that in [129]. The first scenario is similar with the Clyde Building in [129] which is constructed mostly of reinforced concrete and cinder block with all internal walls composed of cinder block, while the second scenario is similar with Crabtree Building in [129] which is built with steel girders with internal walls constructed by gypsum board over a steel frame. The second building represents a scenario with a more complex geometry, i.e. more doorways, walls, or rooms between transmitter and receiver. Table 5.1 summarizes the parameters of the model used in the two scenarios.

We compute the root mean square error (RMSE) of complex path gain, ToA and AoA respectively, with the SNR changing from -12 to 20 dB for two scenarios using the two algorithms, i.e. MAP-based and ML-based estimation. The results are presented in Figs. 5.4 to 5.6. The error in estimating the complex path gain is computed from $(|\alpha| - |\hat{\alpha}|)/|\alpha|$, where $\hat{\alpha}$ is the estimate of α. It is shown that our algorithm outperforms the ML-based algorithm, especially when the SNR is low, for the same RMSE performance we can achieve in about 3 to 6

dB improvement for complex path gain, 2 to 4 dB improvement for ToA and 1 to 2 dB improvement for AoA respectively. This improvement diminishes as SNR increases. This observation coincides with (5.19), (5.20), (5.24) and (5.25), where the prior distributions have little contributions when $N_0 \ll E_s$.

For AoA, the improvement of the MAP algorithm compared with ML is not significant. The reason is that we have made some approximations when determining the distribution of $\Omega_{R,1l}$ and $\Omega_{R,kl}$ by using (5.23). The distributions in the angle domain are not entirely exploited. We observe that the performances in the two scenarios are different, indicating that the performance is dependent on the type of environment.

The performance of ToA tends to be stable when the SNR is higher than 6 dB, while for AoA, it changes much more slowly when SNR is higher than 12 dB. In our proposed algorithm, accuracy is also constrained by the discretization steps for ToA and AoA in addition to SNR, hence, the RMSE performance does not improve further with further improvement in SNR. The convergence rate of our algorithm is shown in Figs. 5.7 to 5.9 when the SNR is 20 dB. In general, it converges fast, but it may have fluctuations on some occasions. The optimization problem has multiple parameters, so for a single parameter, the interim result may be closer to the real value than the final result when it converges. But the final result is optimum when considering the multiple parameters as a whole. For instance, the RMSE of complex path gain for the first scenario is the smallest at 18 iterations as shown in Fig. 5.7. However, the RMSE of AoA still does not achieve its minimum yet. Thus, when considering all the three parameters, the objective function obtains the optimality after convergence.

5.5 Extension to MIMO Systems

In this section, the previously derived algorithm is extended to MIMO systems. A numerical example is provided to show the validity of the extension.
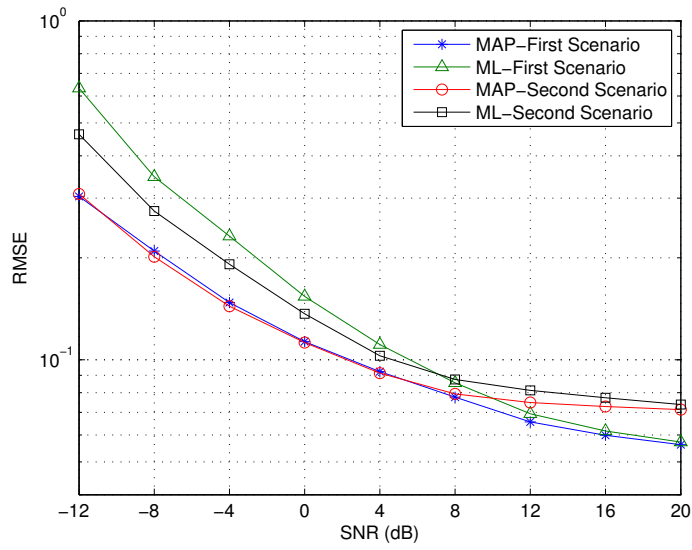
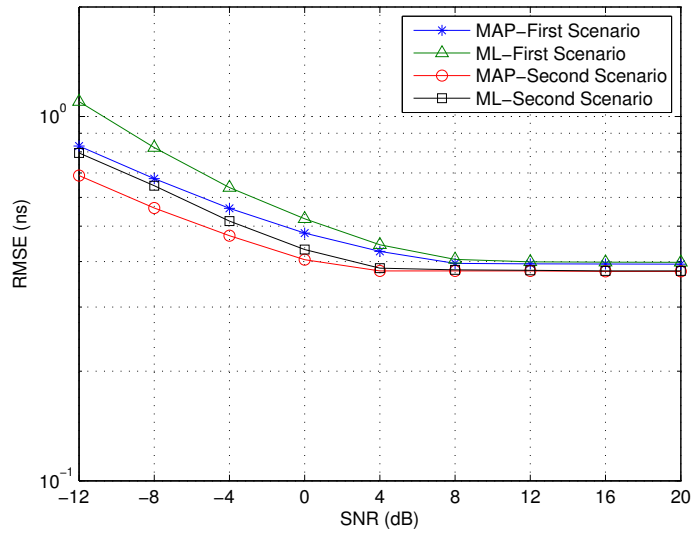Fig. 5.4: RMSE of complex path gain
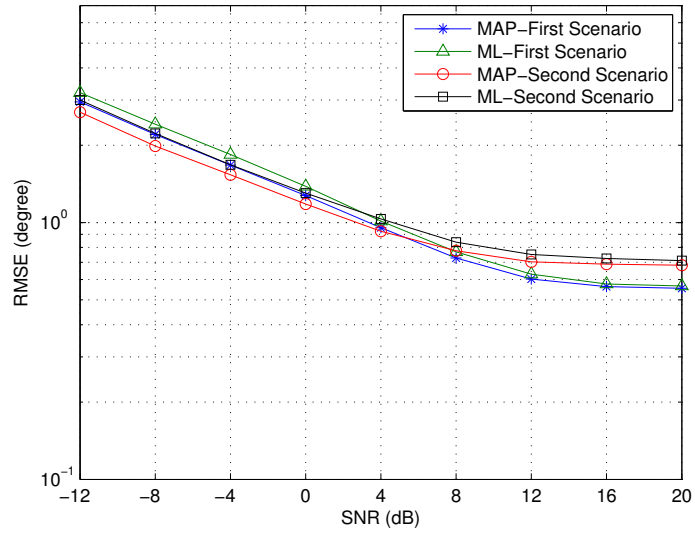

Fig. 5.5: RMSE of ToA

78

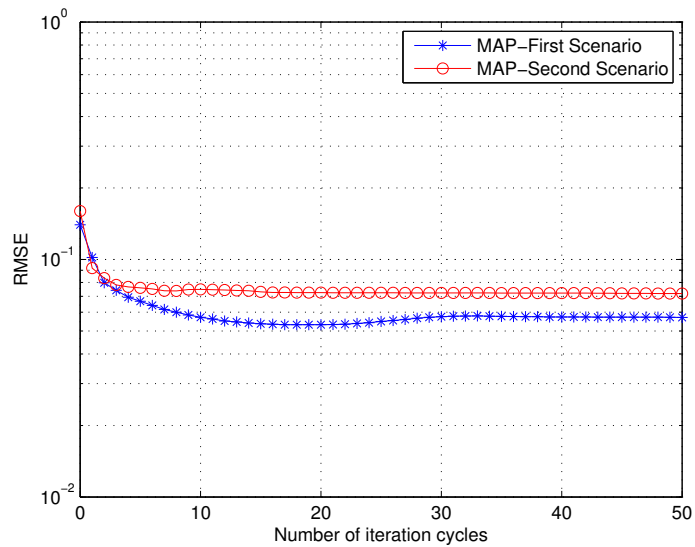*Fig. 5.6: RMSE of AoA*

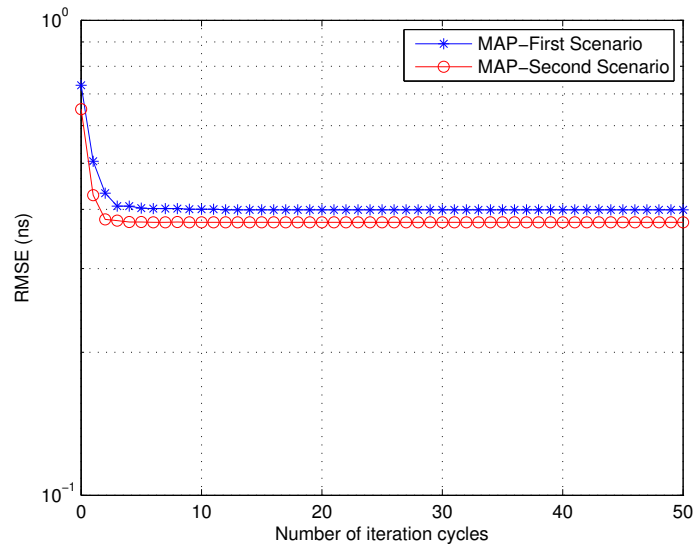*Fig. 5.7: RMSE of complex path gain versus number of iteration cycles, SNR=20 dB*

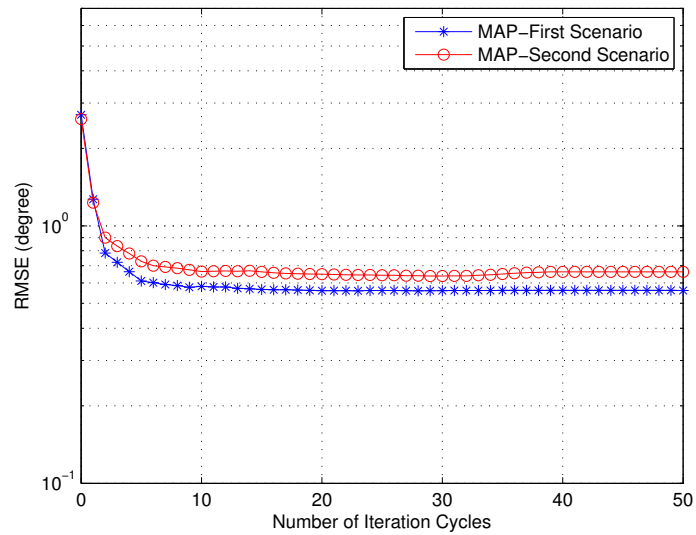Fig. 5.8: RMSE of ToA versus number of iteration cycles, SNR=20 dB

Fig. 5.9: RMSE of AoA versus number of iteration cycles, SNR=20 dB

5.5.1 Theoretical Derivation

To include the angle-of-departure (AoD) information at the transmitter, the extended SV model is modified to [134]

$$h(t, \theta_T, \theta_R) = \sum_{l=1}^{L_c} \sum_{k=1}^{K_l} \alpha_{kl} \delta(t - T_l - \tau_{kl}) \delta(\theta_T - \Theta_{T,l} - \varphi_{T,kl}) \delta(\theta_R - \Theta_{R,l} - \varphi_{R,kl}) \quad (5.31)$$

where θ_T and θ_R are the transmit and receive angles, $\Theta_{T,l}$ and $\Theta_{R,l}$ are the mean transmit and receive angles of the lth cluster, and $\varphi_{T,kl}$ and $\varphi_{R,kl}$ are the transmit and receive angles of the kth ray in the lth cluster, relative to the respective mean angles in each cluster. The other parameters are the same as those defined in (5.1). The distributions of complex path gains, ToAs and AoAs, are the same with those presented in (5.2)-(5.5). For AoDs, the mean angles of clusters, $\Theta_{T,l}$, are uniformly distributed over $[0, 2\pi)$, while the angle of the ray with respect to its respective mean angle of cluster also follows Laplacian distribution with standard derivation σ, which is the same as the distribution of AoAs.

Let the transmitter be equipped with a ULA of M antennas, the signal transmitted should consists of M PN sequences in order to exploit the diversity and distinguish the AoDs of paths. Thus the expression of the received signal (5.6) is modified to

$$\mathbf{r}(t) = \sum_{l=1}^{L_c} \sum_{k=1}^{K_l} \alpha_{kl} \mathbf{c}_R(\Omega_{R,kl}) \mathbf{c}_T^T(\Omega_{T,kl}) \mathbf{s}(t - T_l - \tau_{kl}) + \mathbf{z}(t) \quad (5.32)$$

where $\Omega_{T,kl} = \Theta_{T,l} + \varphi_{T,kl}$ and $\Omega_{R,kl} = \Theta_{R,l} + \varphi_{R,kl}$ are the AoD and AoA of the kth ray within the lth cluster respectively, $\mathbf{c}_T(\cdot)$ and $\mathbf{c}_R(\cdot)$ are the transmit and receive array manifold respectively, and $\mathbf{s}(t)$ is the transmitted signal.

The parameter vector under estimation also includes the AoDs which is $\boldsymbol{\theta} = [\boldsymbol{\theta}_{11}, \ldots, \boldsymbol{\theta}_{K_1,1}, \ldots, \boldsymbol{\theta}_{1,L_c}, \ldots, \boldsymbol{\theta}_{K_{L_c}, L_c}]$ where $\boldsymbol{\theta}_{kl} = [\alpha_{kl}, T_l + \tau_{kl}, \Omega_{T,kl}, \Omega_{R,kl}]$. For the EM algorithm, the E-step and M-step are modified as follow.

For E-step, we re-define $\mathbf{u}(t; \boldsymbol{\theta}_{kl}) = \alpha_{kl} \mathbf{c}_R(\Omega_{R,kl}) \mathbf{c}_T^T(\Omega_{T,kl}) \mathbf{s}(t - T_l - \tau_{kl})$. Substituting it into (5.15), the formula for computing the complete data is obtained.

For M-step, the MAP estimation of a single path is performed for two different cases. When $k = 1$, i.e. estimating the first-arriving ray in each cluster, $p(\boldsymbol{\theta}_{1l})$ needs to include the distribution of AoD denoted by $p(\Omega_{T,1l})$ which is assumed to

follow an uniform distribution over $[0, 2\pi)$, the same as that for AoA denoted by $p(\Omega_{R,1l})$. Using the same principle in computing (5.19) and (5.20), a 3-D search problem is obtained to find the MAP solution of ToA, AoA and AoD, and the complex path gain is also computed in close-form. The estimate of the parameters after the nth iteration is

$$
\begin{aligned}
\left(T_l, \widehat{\Omega_{T,1l}, \Omega_{R,1l}}^{(n)} \right)_{MAP} & \\
= \arg \max_{(T_l, \Omega_{T,1l}, \Omega_{R,1l})} & \left\{ \frac{\left| f\left(T_l, \Omega_{T,1l}, \Omega_{R,1l}; \hat{\mathbf{w}}_{1l}^{(n)} \right) \right|^2}{\sum_{i=1}^{I} \left\| \mathbf{c}_R(\Omega_{R,1l}) \mathbf{c}_T^T(\Omega_{T,1l}) \mathbf{s}(t_i - T_l) \right\|^2 + N_0 \exp(T_l/\Gamma)/\sigma_{11}^2} \right. \\
& \left. + \left(\frac{1}{\Gamma} - \Phi \right) N_0 T_l \right\}, \quad T_l > \hat{T}_{l-1}^{(n)}
\end{aligned}
\tag{5.33}
$$

$$
(\hat{\alpha}_{1l}^{(n)})_{MAP} = \frac{f\left(T_l, \widehat{\Omega_{T,1l}, \Omega_{R,1l}}^{(n)}; \hat{\mathbf{w}}_{1l}^{(n)} \right)}{\sum_{i=1}^{I} \left\| \mathbf{c}_R\left(\hat{\Omega}_{R,1l}^{(n)} \right) \mathbf{c}_T^T\left(\hat{\Omega}_{T,1l}^{(n)} \right) \mathbf{s}\left(t_i - \hat{T}_l^{(n)} \right) \right\|^2 + N_0 \exp(\hat{T}_l^{(n)}/\Gamma)/\sigma_{11}^2}
\tag{5.34}
$$

where

$$
f(T, \Omega_T, \Omega_R; \mathbf{w}) = \sum_{i=1}^{I} \mathbf{w}^T(t_i) \mathbf{c}_R^*(\Omega_R) \mathbf{c}_T^H(\Omega_T) \mathbf{s}(t_i - T)
\tag{5.35}
$$

When $k \neq 1$, i.e. estimating other rays of each cluster, $p(\boldsymbol{\theta}_{kl})$ needs to include the distribution of AoD which has the same distribution as AoA shown in (5.23). Similarly, the MAP solution consists of a 3-D search problem and a closed-form expression for complex path gain. The estimates of the parameters after the nth

iteration are given by

$$
\left(\tau_{kl}, \widehat{\Omega_{T,kl}, \Omega_{R,kl}}^{(n)}\right)_{MAP}
$$

$$
= \arg \max_{(\tau_{kl}, \Omega_{T,kl}, \Omega_{R,kl})} \left\{ N_0 \ln\left[\left(\sigma + \sqrt{2}\left|\Omega_{T,kl} - \hat{\Omega}_{T,1l}^{(n)}\right|\right)\left(\sigma + \sqrt{2}\left|\Omega_{R,kl} - \hat{\Omega}_{R,1l}^{(n)}\right|\right)\right]\right.
$$

$$
+ \frac{\left|f\left(\tau_{kl}, \Omega_{T,kl}, \Omega_{R,kl}; \hat{\mathbf{w}}_{kl}^{(n)}\right)\right|^2}{\sum_{i=1}^{I}\left\|\mathbf{c}_R(\Omega_{R,kl})\mathbf{c}_T^T(\Omega_{T,kl})\mathbf{s}(t_i - \hat{T}_l^{(n)} - \tau_{kl})\right\|^2 + N_0 \exp(\hat{T}_l^{(n)}/\Gamma)\exp(\tau_{kl}/\gamma)/\sigma_{11}^2}
$$

$$
\left. + \left(\frac{1}{\gamma} - \phi\right)N_0\tau_{kl} - \frac{\sqrt{2}N_0\left(\left|\Omega_{T,kl} - \hat{\Omega}_{T,1l}^{(n)}\right| + \left|\Omega_{R,kl} - \hat{\Omega}_{R,1l}^{(n)}\right|\right)}{\sigma}\right\}, \quad \tau_{kl} > \hat{\tau}_{k-1,l}^{(n)} \quad (5.36)
$$

$$
(\hat{\alpha}_{kl}^{(n)})_{MAP}
$$

$$
= \frac{f\left(\tau_{kl}, \widehat{\Omega_{T,kl}, \Omega_{R,kl}}^{(n)}; \hat{\mathbf{w}}_{kl}^{(n)}\right)}{\sum_{i=1}^{I}\left\|\mathbf{c}_R\left(\hat{\Omega}_{R,kl}^{(n)}\right)\mathbf{c}_T^T\left(\hat{\Omega}_{T,kl}^{(n)}\right)\mathbf{s}\left(t_i - \hat{T}_l^{(n)} - \hat{\tau}_{kl}^{(n)}\right)\right\|^2 + N_0 \exp(\hat{T}_l^{(n)}/\Gamma)\exp(\hat{\tau}_{kl}^{(n)}/\gamma)/\sigma_{11}^2}
$$

$$
(5.37)
$$

where

$$
f(\tau, \Omega_T, \Omega_R; \mathbf{w}) = \sum_{i=1}^{I}\mathbf{w}^T(t_i)\mathbf{c}_R^*(\Omega_R)\mathbf{c}_T^H(\Omega_T)\mathbf{s}(t_i - \hat{T}_l - \tau) \qquad (5.38)
$$

At the initialization phase, $s(t)$ in (5.28) is replaced by the vector $\mathbf{s}(t)$. A 2-D search for both AoA and AoD is derived to replace (5.29), which is

$$
(\widehat{\Omega_{T,l}, \Omega_{R,l}}) = \arg \max_{(\Omega_{T,l}, \Omega_{R,l})} \left\{\left|\sum_{i=1}^{I}\mathbf{s}^T(t_i - \hat{\tau}_l)\mathbf{c}_T^*(\Omega_{T,l})\mathbf{c}_R^H(\Omega_{R,l})\mathbf{r}^{(l)}(t_i)\right|^2\right\} \quad (5.39)
$$

The expression in (5.30) needs to be changed accordingly. After initialization, the paths are grouped into clusters. Unlike in SIMO systems where clusters are identified in the joint ToA/AoA domain, the joint AoD/AoD domain has a better resolution to identify clusters for MIMO systems [135, 136]. Thus, the paths are grouped into clusters according to the respective AoDs and AoAs.

From the above derivation, we can see that the extension of the proposed algorithm is straightforward and not much different with the original one except that the metrics used in clustering are different in the initialization phase and a higher dimensional search problem is involved in finding the optimal solution. The first issue does not affect the final result, since in the following iterations of

Table 5.2: The real values and estimates of the channel parameters

		Cluster 1 (4 paths)				Cluster 2 (3 paths)			Cluster 3 (3 paths)		
		1	2	3	4	1	2	3	1	2	3
Path gain	Real	0.98	0.82	0.91	0.77	0.67	0.30	0.38	0.51	0.55	0.05
	Estimate	0.97	0.86	0.91	0.73	0.67	0.31	0.41	0.50	0.56	0.07
ToA (ns)	Real	0	4.8	6.2	7.3	57.3	65.7	69	71.3	75.3	77.5
	Estimate	0	5.3	5.4	6.4	57.0	65.5	68.5	70.7	75.4	78.5
AoD (°)	Real	-53.9	-72.1	-44.5	-69.7	0.2	9.3	28.0	76.6	59.1	33.7
	Estimate	-54.0	-69.7	-44.4	-72.1	0.2	9.0	28.4	74.6	59.4	28.1
AoA (°)	Real	-79.5	-69.5	-36.3	-69.7	18.2	-13.2	36.0	50.7	40.1	44.6
	Estimate	-79.9	-69.7	-36.2	-69.5	18.3	-13.4	36.6	50.8	40.1	50.3

EM algorithm the parameters can be adjusted to fit the corresponding clusters. This has been shown in Section 5.4 that finally the algorithm converges. For the second issue, a numerical example of estimation in a randomly generated channel is provided in the next subsection to demonstrate that the optimal solution can be found even with higher dimensional search. The evaluation of average performance is not provided here to avoid repetition with the simulation of the algorithm for SIMO systems.

5.5.2 Numerical Example

The validity of the algorithm in MIMO systems is shown in this numerical example. The transmitter and receiver are each equipped with a ULA with 11 elements separated by half a wavelength. The modulated PN sequence consists of 1024 rectangular pulses with duration $T_s = 1$ ns. The discretization steps of our algorithm are 0.4 ns for ToA and 0.2° for both AoD and AoA. A channel is randomly generated according to the extended SV model for MIMO systems with the parameters listed in Table 5.1 for the first scenario. In order to simplify the analysis, the channel is normalized. The channel consists of 3 clusters, and the clusters have $[4, 3, 3]$ rays respectively. The AoD and AoA of each ray are both distributed over $[0, \pi)$. The MAP estimation is performed when the SNR is 10 dB. Table II lists the real values and the estimates of all the parameters for all paths. From the table, we can see that the MAP algorithm can distinguish all the paths and achieves high accuracy.

5.6   Conclusion

In this chapter, we propose a MAP-based algorithm for channel parameter estimation of superimposed signals. The extended SV model provides us the prior knowledge on the statistical distributions of these parameters, which is exploited in the proposed MAP-based algorithm to achieve a more accurate estimate. In order to reduce the computational complexity of our proposed algorithm, EM algorithm is applied. Our simulation results show that the proposed algorithm outperforms the ML-based algorithm especially at low SNR. In general, the algorithm exhibits fast convergence. Finally, the algorithm is extended to MIMO systems.

Chapter 6

AoA-Assisted Extended Kalman Filter Tracking

When the location of a MT needs to be continuously monitored, a simple tracking algorithm can be used to reduce the frequency in performing regular localization and estimation latency. In this chapter, we propose a novel mobile terminal (MT) tracking approach performed at the fixed terminal (FT). The method involves three steps: motion-dependent parameters estimation, extended Kalman filter (EKF) based tracking and accuracy enhancement through additional partial location information. An algorithm based on the space-time correlation of the received signal is first used to estimate the radial velocity (both the speed and direction) of the MT. The EKF-based tracking method is next adopted to estimate the current location of the MT by using the estimated parameters and the previous location estimate. Finally, the MUSIC (MUtiple SIgnal Classification) algorithm is applied to obtain additional high-resolution angle-of-arrival (HR-AoA) estimate and we show how this partial location information can be fused with the tracking results to further improve the tracking accuracy. The performances of the algorithms are studied through simulations.
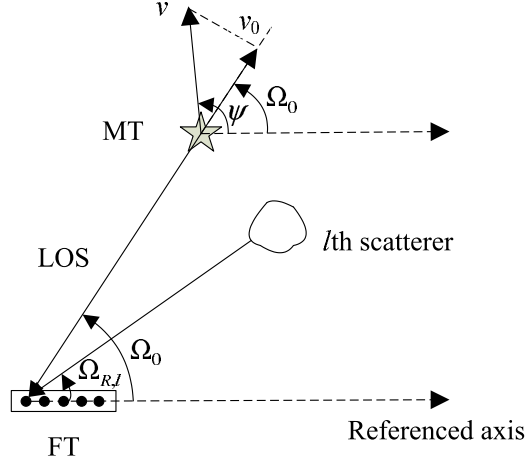
Fig. 6.1: The signal model

6.1 Estimation of Motion-dependent Parameters

At the FT, the radial velocity of the MT, which includes both the speed and the direction, are estimated by using the space-time correlation of the received signal.

6.1.1 Signal Model

As depicted in Fig. 6.1, the FT is equipped with an antenna array, and without loss in generality, we assume an uniform linear array (ULA) with N elements whose direction is used as the referenced axis (labeled as x-axis). A MT transmits beacon signals periodically and moves at the speed v in the direction ψ with respect to the referenced axis. The channel between the MT and the FT is assumed to undergo Rician fading with a deterministic line-of-sight (LOS) component and a random diffuse component. Ω_0 is the LOS direction along the FT and the MT, and $\Omega_{R,l}$ is the direction of the lth incoming wave in the diffuse component. We define the radial velocity of the MT as the projection of the velocity along the LOS direction. Therefore the speed of the radial velocity is $v_0 = v\cos(\Omega_0 - \psi)$ which is also known as the range rate [13], and its direction is equal to the LOS direction Ω_0. The maximum Doppler frequency of the received signal is given by $f_D = vf_c/c$, where f_c is the carrier frequency and c is the speed of light, while the Doppler frequency caused by v_0 is given by $f_0 = v_0 f_c/c$.

When the MT transmits an unmodulated carrier, the lowpass complex envelope received at the nth antenna of the FT can be expressed as

$$r_n(t) = u_n(t) + z_n(t), \tag{6.1}$$

where $z_n(t)$ is the complex white Gaussian noise with zero mean and power spectral density N_0. The signal $u_n(t)$ includes diffuse and LOS components,

$$u_n(t) = \sqrt{\frac{KP_R}{K+1}} \exp\left\{j2\pi(n-1)d_h\cos\Omega_0/\lambda_s - j2\pi f_D t\cos(\Omega_0 - \psi)\right\}$$

$$+ \sqrt{\frac{P_R}{K+1}}q_n(t),$$

$$= \sqrt{\frac{KP_R}{K+1}} \exp\left\{j2\pi(n-1)d_h\cos\Omega_0\lambda_s - j2\pi f_0 t\right\} + \sqrt{\frac{P_R}{K+1}}q_n(t), \tag{6.2}$$

where P_R is the total received signal power at the receiver, and K is the Rician factor defined as the ratio of the LOS power and the diffuse power. The unit power signal $q_n(t)$ represents the diffuse component which is

$$q_n(t) = \lim_{L\to\infty} \frac{1}{\sqrt{L}} \sum_{l=1}^{L} \alpha_l \exp\left\{j2\pi(n-1)d_h\cos\Omega_{R,l}\lambda_s - j2\pi f_D t\cos(\Omega_{R,l} - \psi)\right\}, \tag{6.3}$$

where L is the total number of the incoming waves, the complex path gains α_l are independent and identically distributed (i.i.d.) random variables with finite variances. α_l should satisfy $\lim_{L\to\infty} L^{-1}\sum_{l=1}^{L} \mathrm{E}_{\alpha_l}[|\alpha_l|^2] = 1$, so as to fulfill the unit power constraint on $q_n(t)$.

6.1.2 Space-Time Correlation Based Radial Velocity Estimation

Define the space-time correlation of the received signals between the nth and mth antenna elements as $C_r(n-m,\tau)$, and it can be calculated by

$$C_r(n-m,\tau) = \mathrm{E}[r_n(t)r_m^*(t+\tau)] = \mathrm{E}[u_n(t)u_m^*(t+\tau)]. \tag{6.4}$$

The latter equation holds due to the independence property between the signal and noise as well as between the noises at different antennas. Substituting (6.2) into (6.4), we have

$$
C_r(n - m, \tau) = \frac{KP_R}{K + 1} \exp \left\{ j\mu_0 + j\eta \cos \Omega_0 \right\}
$$
$$
+ \frac{P_R}{K + 1} \lim_{L \to \infty} \frac{1}{L} \sum_{l=1}^{L} \mathrm{E}_{\alpha_l}[|\alpha_l|^2] \exp \left\{ j\mu \cos(\Omega_{R,l} - \psi) + j\eta \cos \Omega_{R,l} \right\}
$$
$$(6.5)$$

where $\mu = 2\pi f_D \tau$, $\mu_0 = 2\pi f_0 \tau$ and $\eta = 2\pi(n - m)d_h/\lambda_s$. According to the derivation in [137], (6.5) can be expressed in integral form which is more convenient for further analysis

$$
C_r(n - m, \tau) = \frac{KP_R}{K + 1} \exp \left\{ j\mu_0 + j\eta \cos \Omega_0 \right\}
$$
$$
+ \frac{P_R}{K + 1} \int_0^{2\pi} p(\theta) \exp \left\{ j\mu \cos(\theta - \psi) + j\eta \cos \theta \right\} d\theta, \qquad (6.6)
$$

where $p(\theta)$ is the angle distribution of the waves in the diffuse component seen at the FT receiver.

The proposed algorithm is different with those using similar correlation model such as [102] in the following two aspects. Firstly, the estimation in [102] is performed at the MT. Hence, its derivation is based on a correlation model without the variable ψ, because the angle between the antenna array at the receiver (i.e. the MT) and the moving direction of the MT is fixed. Secondly, we proposed a joint estimation of motion parameters v_0 and Ω_0.

Among the various angle distributions available in the literature, the von-Mises distribution has been widely used for estimating the channel parameters [102]. The distribution has the following form

$$
p(\theta) = \frac{\exp \left\{ \kappa \cos(\theta - \Omega_R) \right\}}{2\pi I_0(\kappa)}, \quad \theta \in [0, 2\pi), \qquad (6.7)
$$

where $I_0(\cdot)$ is the zeroth-order modified Bessel function of the first kind, Ω_R is the mean direction of the diffuse component, and the parameter κ controls the angle spread. When κ approaches to zero, the distribution converts to uniform distribution. On the other hand, when κ is medium and large, the von-Mises distribution

can be approximated by a Gaussian distribution with mean Ω_R and variance $1/\kappa$ [138]. In the following derivation, we assume that κ is sufficiently large such that the von-Mises distribution can be approximated by Gaussian distribution, and under this condition, it is reasonable to assume $\Omega_R = \Omega_0$ [139]. However, simulations will demonstrate that as long as the Rician factor K is not small, the value of κ has very limited effect on the estimation accuracy.

Substituting the Gaussian distribution with mean Ω_R and variance $1/\kappa$ into (6.6), and using the same approximation as in [140], the space-time correlation is finally expressed as

$$
C_r(n-m,\tau) \approx \exp\left\{j\mu_0 + j\eta\cos\Omega_0\right\} \left\{ \frac{KP_R}{K+1} \right.
$$
$$
\left. + \frac{P_R}{K+1}\exp\left[-\frac{(\mu\sin(\Omega_0-\psi)+\eta\sin\Omega_0)^2}{2\kappa} \right] \right\}. \tag{6.8}
$$

Evaluating $C_r(n-m,\tau)$ involves the knowledge on the channel parameters K and κ. Nevertheless, our estimation only requires the phase information and hence the complexity is low. Taking the phase angle of $C_r(n-m,\tau)$, we have

$$
\angle C_r(n-m,\tau) \approx \mu_0 + \eta\cos\Omega_0 = 2\pi f_c\tau v_0/c + 2\pi(n-m)d_h\cos\Omega_0/\lambda_s. \tag{6.9}
$$

By setting $n = m$ and $\tau = 0, n - m = 1$ respectively, the estimate of v_0 and Ω_0 can be finally obtained by

$$
\hat{v}_0 \approx \frac{c\angle\widehat{C_r(0,\tau)}}{2\pi f_c\tau},
$$
$$
\hat{\Omega}_0 \approx \arccos\frac{\lambda_s\angle\widehat{C_r(1,0)}}{2\pi d_h}, \tag{6.10}
$$

where $\widehat{C_r(0,\tau)}$ and $\widehat{C_r(1,0)}$ are the estimates of $C_r(0,\tau)$ and $C_r(1,0)$, respectively.

6.2 Extended Kalman Filter Based Tracking

We here present the EKF-based tracking algorithm which estimates the current location based on the estimated motion-dependent parameters and the previous location estimate. The following state transition and measurement model

are used in accordance with the framework of EKF.

We adopt the nearly-constant-velocity model [12], where the velocity of the target is assumed to be nearly constant over a period T_K between two consecutive tracking time instants. The acceleration is so small that it is treated as an additive white Gaussian noise added to the velocity. The state vector $\boldsymbol{\vartheta} = [x_m, v_x, y_m, v_y]^T$ consists of the location at (x_m, y_m) and velocity (v_x, v_y). Denoting the true state at the kth time instant as $\boldsymbol{\vartheta}^{(k)}$, the EKF assumes that it is evolved from the previous true state $\boldsymbol{\vartheta}^{(k-1)}$ using the following state transition model

$$\boldsymbol{\vartheta}^{(k)} = \mathbf{D}\boldsymbol{\vartheta}^{(k-1)} + \mathbf{G}\boldsymbol{\varpi}^{(k)}, \tag{6.11}$$

where

$$\mathbf{D} = \begin{bmatrix} 1 & T_K & 0 & 0 \\ 0 & 1 & 0 & 0 \\ 0 & 0 & 1 & T_K \\ 0 & 0 & 0 & 1 \end{bmatrix}, \quad \mathbf{G} = \begin{bmatrix} T_K^2/2 & 0 \\ T_K & 0 \\ 0 & T_K^2/2 \\ 0 & T_K \end{bmatrix},$$

$\boldsymbol{\varpi} = [\varpi_x, \varpi_y]^T$ is the additive white Gaussian noise representing the 2-D noisy accelerations. ϖ_x and ϖ_y are i.i.d. random variables with zero mean and finite variances.

The measurement vector includes the estimates of the speed $\hat{v}_0$ and the direction $\hat{\Omega}_0$ of the radial velocity. The measurement at the kth time instant is associated with the true state at the kth time instant $\boldsymbol{\vartheta}^{(k)}$ via the following measurement model

$$\begin{bmatrix} \hat{v}_0 \\ \hat{\Omega}_0 \end{bmatrix}^{(k)} = \chi\left(\boldsymbol{\vartheta}^{(k)}\right) + \boldsymbol{\iota}^{(k)}. \tag{6.12}$$

The vector $\boldsymbol{\iota} = [\iota_v, \iota_\Omega]^T$ is the measurement noise, and ι_v and ι_Ω are i.i.d. random variables with zero mean and finite variances. $\chi(\boldsymbol{\vartheta})$ is the function used to compute the real value of $[v_0, \Omega_0]^T$ from $\boldsymbol{\vartheta}$,

$$\chi(\boldsymbol{\vartheta}) = \left[\frac{(x_m - x_f)v_x + (y_m - y_f)v_y}{\sqrt{(x_m - x_f)^2 + (y_m - y_f)^2}}, \arctan\frac{y_m - y_f}{x_m - x_f} \right]^T, \tag{6.13}$$

where (x_f, y_f) is the location of the FT that performs the tracking.

The EKF estimation process is implemented as follow. We first calculate the

predicted state at the current time instant $\hat{\boldsymbol{\vartheta}}^{(k|k-1)}$ using the relationship $\hat{\boldsymbol{\vartheta}}^{(k|k-1)} = \mathbf{D}\hat{\boldsymbol{\vartheta}}^{(k-1|k-1)}$ in the prediction step, based on the EKF output at the previous time instant, i.e. $\hat{\boldsymbol{\vartheta}}^{(k-1|k-1)}$. A standard update process is next applied to find the updated state estimate $\hat{\boldsymbol{\vartheta}}^{(k|k)}$, i.e. the EKF output at the current time instant.

The initial state vector is required before carrying out the tracking process. The initial guess of the MT location can be estimated at the FT using a localization algorithm, such as those presented in [1, 2, 141], while the velocity information can be obtained at the MT (accelerometers and magnetometers have been available on many kinds of MTs, even hand-hold devices [10]) and transmitted to the FT. After initialization, the MT starts to periodically transmit beacon signals, and the FT performs the measurement and EKF-based estimation as described above using the received signal to track the trajectory of the MT. The computation burden is thus transferred to the FT after initialization phase, so the consumption of energy and resources at the MT can be maintained at a low level.

6.3 Angle-of-Arrival Assisted Performance Enhancement

When the location of the MT is tracked using the above EKF-based algorithm, the estimation errors will be accumulated as the tracking proceeds. We propose a fusion algorithm to overcome this problem by utilizing additional partial location information which can be made available. For example, if the FT is equipped with an antenna array, it is possible to perform HR-AoA estimate using subspace-based algorithms [4] (MUSIC [29], ESPRIT [39] and etc.), and incorporate this additional information in the tracking process to improve accuracy. Since re-calibration by complete location information requires extensive resource, using such partial location information at the FT to assist in tracking is a good tradeoff. The FT that performs the enhancement needs not necessarily be the one which performs EFK. The final processing can be made at the information fusion center.

The motivation of the enhancement algorithm is illustrated in Fig. 6.2. The EKF-based tracking results in an uncertain region due to the noisy measurements and the uncertain region gets larger over time if no re-calibration by the MT is performed. The fusion of HR-AoA estimate with EKF estimates is a way to improve the accuracy. It is performed from time to time during the tracking
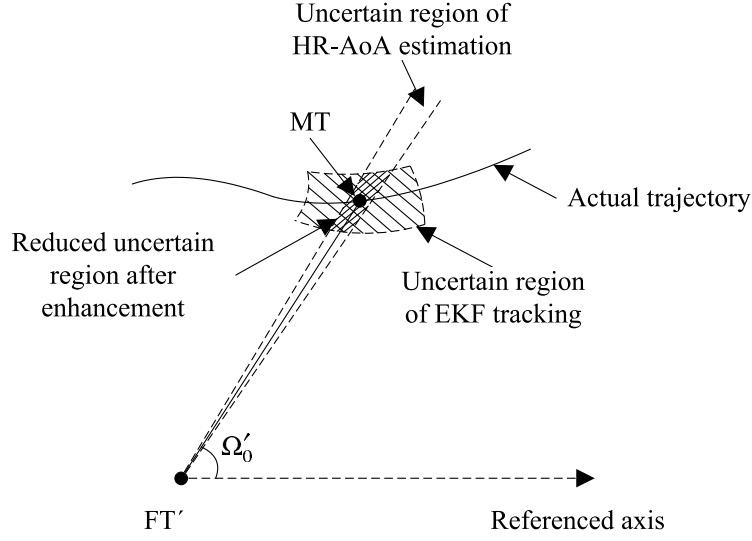
Fig. 6.2: Motivation of HR-AoA assisted performance enhancement

process by FTs. The frequency of performing such enhancement depends on the rate that errors are accumulated and the available computational resources.

The performance enhancement is at the expense of additional complexity, which results from the HR-AoA estimation and fusion of HR-AoA estimate and tracking result. However, we expect the complexity not to increase much, because the computations are both 1-dimensional search in the solution domain. Furthermore, as will shown in the simulation later, the frequency of performing such enhancement can be reduced under some conditions while the performance is only slightly downgraded, which means less additional complexity is needed to achieve required accuracy.

6.3.1 MUSIC-Based Algorithm for HR-AoA Estimation

In this subsection, we propose a MUSIC-based estimation algorithm to obtain the HR-AoA estimate. As shown in Fig. 6.3, the actual location of the MT at a specific time instant is denoted as (x_m, y_m). We denote FT′ which is located at (x'_f, y'_f) and equipped with a ULA with N elements to perform HR-AoA estimation. The actual angle-of-arrival (AoA) observed by FT′ is denoted by Ω'_0 and its high-resolution estimate is $\hat{\Omega}'_0$. If the same FT performs both the enhancement and tracking, (x'_f, y'_f) is equal to (x_f, y_f), and Ω'_0 is equal to Ω_0.

94

When the MT transmits an unmodulated carrier, denote the received signal vector at FT$'$ as $\mathbf{r}'(t)$ and the spatial correlation matrix of the received signal as $\mathbf{C}_{r'} = \mathrm{E}[\mathbf{r}'(t)\mathbf{r}'^H(t)]$. Using the correlation model described in Section 6.1, the element of $\mathbf{C}_{r'}$ at the nth row and mth column can be expressed as

$$(\mathbf{C}_{r'})_{n,m} \approx \exp\left\{j2\pi(n-m)d_h\cos\Omega_0'/\lambda_s\right\}\left\{\frac{K'P_R'}{K'+1}\right.$$
$$\left.+\frac{P_R'}{K'+1}\exp\left[-\frac{(2\pi(n-m)d_h\sin\Omega_0')^2}{2\kappa'\lambda_s}\right]\right\}, \text{if } n \neq m, \qquad (6.14)$$

where P_R', K' and κ' are the channel parameters corresponding to FT$'$. If $n = m$, we have $(\mathbf{C}_{r'})_{n,m} \approx P_R' + N_0'$, where N_0' is the power of the white Gaussian noise at FT$'$. Similarly, we also use the phase angles of elements of the spatial correlation matrix for further analysis. We define a matrix $\mathbf{R}_{r'} = \exp(j\angle\mathbf{C}_{r'})$ whose element at the nth row and mth column is

$$\mathbf{R}_{r'}(n,m) \approx \exp\{j2\pi(n-m)d_h\cos\Omega_0'/\lambda_s\}. \qquad (6.15)$$

Therefore, it can be decomposed as $\mathbf{R}_{r'} \approx \mathbf{u}_r\mathbf{u}_r^H$, and the vector $\mathbf{u}_r$ has the expression $\mathbf{u}_r = [1, \exp(j2\pi d_h\cos\Omega_0'/\lambda_s), \ldots, \exp(j2\pi(N-1)d_h\cos\Omega_0'/\lambda_s)]^T$. If we do the eigenvalue decomposition on $\mathbf{R}_{r'}$, the eigenvector which corresponds to the largest eigenvalue can be used as the signal subspace, and other eigenvectors correspond to the noise subspace. Therefore, it is straightforward to apply the MUSIC algorithm to obtain the estimate $\hat{\Omega}_0'$.

As a summary, the algorithm includes the following steps:

1. Estimate the spatial correlation matrix $\mathbf{C}_{r'}$, and obtain the matrix $\mathbf{R}_{r'}$.

2. Apply the eigenvalue decomposition on $\mathbf{R}_{r'}$, and use the eigenvector which corresponds to the largest eigenvalue to construct the signal subspace.

3. Compute the null spectrum function, and search for the minimum. The corresponding angle is the estimated AoA $\hat{\Omega}_0'$.

6.3.2 Enhancing the EKF Tracking Result with HR-AoA Estimate

After obtaining the HR-AoA estimate, our objective is to fuse it with the EKF tracking result to enhance the tracking performance. The problem here is to find the solution that maximizes the a posterior probability $p(x_m, y_m | \hat{x}_m, \hat{y}_m, \hat{\hat{\Omega}}'_0)$, given the EKF tracking result $(\hat{x}_m, \hat{y}_m)$ and the HR-AoA estimate $\hat{\hat{\Omega}}'_0$. Using the Bayes' theorem, we have

$$p(x_m, y_m | \hat{x}_m, \hat{y}_m, \hat{\hat{\Omega}}'_0) = \frac{p(\hat{x}_m, \hat{y}_m, \hat{\hat{\Omega}}'_0 | x_m, y_m) p(x_m, y_m)}{p(\hat{x}_m, \hat{y}_m, \hat{\hat{\Omega}}'_0)}. \tag{6.16}$$

The component $p(\hat{x}_m, \hat{y}_m, \hat{\hat{\Omega}}'_0)$ does not depend the value of (x_m, y_m), and $f(x_m, y_m)$ can be assumed to be uniform. We further assume $(\hat{x}_m, \hat{y}_m)$ and $\hat{\hat{\Omega}}'_0$ are independent variables, because $(\hat{x}_m, \hat{y}_m)$ is estimated using the EKF tracking while $\hat{\hat{\Omega}}'_0$ is obtained separately by AoA estimation algorithm. Thus the problem is further simplified to maximizing the product $p(\hat{x}_m, \hat{y}_m | x_m, y_m) p(\hat{\hat{\Omega}}'_0 | x_m, y_m)$.

For AoA estimators, the error distribution of the estimate depends on the specific algorithm. Much work has been done to analyze the performances of these algorithms [30, 32]. For instance, the error of the MUSIC estimator is shown to be Gaussian distributed asymptotically with the error variance derived [30]. Hence, we adopt $p(\hat{\hat{\Omega}}'_0 | x_m, y_m)$ following a Gaussian distribution with mean Ω'_0 and variance $\sigma^2_{\Omega'}$.

Since $(\hat{x}_m, \hat{y}_m)$ is estimated from the EKF-based tracking algorithm, its error includes the accumulation of errors in the previous steps, the noisy measurement of the current step, linearization of the observation function, etc. If there has been sufficient large number of steps before the current step, the Central Limit Theorem can be applied here and $(\hat{x}_m, \hat{y}_m)$ can be modeled as bivariate Gaussian variables with mean x_m and y_m and variances $\sigma^2_{\hat{x}}$ and $\sigma^2_{\hat{y}}$ respectively. We further assume $\sigma^2_{\hat{x}} = \sigma^2_{\hat{y}} = \sigma^2_0$.

With the above assumptions, $p(\hat{x}_m, \hat{y}_m, \hat{\hat{\Omega}}'_0 | x_m, y_m)$ can be expressed as

$$p(\hat{x}_m, \hat{y}_m, \hat{\hat{\Omega}}'_0 | x_m, y_m) = \frac{1}{2\pi \sigma_{\Omega'} \sigma^2_0} \exp\left\{ -\frac{(\hat{\hat{\Omega}}'_0 - \Omega'_0)^2}{2\sigma^2_{\Omega'}} - \frac{(\hat{x}_m - x_m)^2 + (\hat{y}_m - y_m)^2}{2\sigma^2_0} \right\}$$
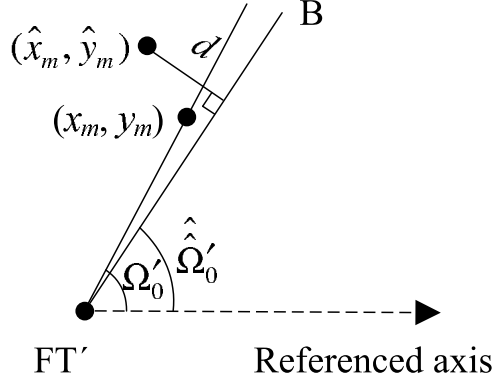
$$\tag{6.17}$$

Fig. 6.3: Fusion of the tracking result and the HR-AoA estimate

Taking its natural logarithm and ignoring the constants which do not affect the solution, the objective function can be expressed as

$$\min_{x_m, y_m} \quad f(x_m, y_m) = \left(\hat{\hat{\Omega}}'_0 - \Omega'_0\right)^2 + A_w \left[(\hat{x}_m - x_m)^2 + (\hat{y}_m - y_m)^2\right], \qquad (6.18)$$

where $A_w = \sigma^2_{\Omega'}/\sigma^2_0$, and $\Omega'_0 = \arctan \frac{y_m - y'_f}{x_m - x'_f}$. This expression can be understood as the weighted sum of angle error and position error, while A_w is the weight.

In practice, $\sigma^2_{\Omega'}$ depends on many factors, such as channel conditions, the algorithm used [32] and the transmitted signal pattern [40], while σ^2_0 relies on the measurements accuracy and may increase over time. Hence, it is very difficult to obtain the accurate value of A_w. We here use a simple method to find an approximate value. Since AoA estimate has high-resolution, the estimated location has a very high possibility lying near the line denoted by Line B in Fig. 6.3 which is originated from FT′ and makes the angle $\hat{\hat{\Omega}}'_0$ with the referenced axis; and this means $(\hat{\hat{\Omega}}'_0 - \Omega'_0)$ is very small. On the other hand, denote the distance between $(\hat{x}_m, \hat{y}_m)$ and Line B as d which is expressed as

$$d = \frac{\left|(\hat{x}_m - x'_f) \tan \hat{\hat{\Omega}}'_0 - \hat{y}_m + y'_f\right|}{\sqrt{1 + (\tan \hat{\hat{\Omega}}'_0)^2}}.$$

If d is small, the tracking estimate $(\hat{x}_m, \hat{y}_m)$ has high probability to be reliable, and vice versa. Based on this intuition, we set $A_w \propto 1/d^2$, so that we de-emphasize the term which is likely to generate cumulative errors.

Next, we present a method to reduce the complexity of the 2-dimensional (2-D) search problem (6.18). Denote the solution of (6.18) as $(\tilde{x}_m, \tilde{y}_m)$, and it should make the first order derivatives of $f(x_m, y_m)$ over x_m and y_m both equal to 0.

$$
\begin{aligned}
\frac{\partial f}{\partial x_m}\bigg|_{x_m=\tilde{x}_m, y_m=\tilde{y}_m} &= \frac{2(\hat{\tilde{\Omega}}'_0 - \tilde{\Omega}'_0)(\tilde{y}_m - y'_f)}{(\tilde{x}_m - x'_f)^2 + (\tilde{y}_m - y'_f)^2} + 2A_w(\tilde{x}_m - \hat{x}) = 0, \\
\frac{\partial f}{\partial y_m}\bigg|_{x_m=\tilde{x}_m, y_m=\tilde{y}_m} &= -\frac{2(\hat{\tilde{\Omega}}'_0 - \tilde{\Omega}'_0)(\tilde{x}_m - x'_f)}{(\tilde{x}_m - x'_f)^2 + (\tilde{y}_m - y'_f)^2} + 2A_w(\tilde{y}_m - \hat{y}) = 0, \quad (6.19)
\end{aligned}
$$

where $\tilde{\Omega}'_0$ is the value of Ω'_0 when substituting $(\tilde{x}_m, \tilde{y}_m)$. Let us first consider a special case where $d = 0$. It is obvious that under this condition, the solution should be $(\tilde{x}_m, \tilde{y}_m) = (\hat{x}_m, \hat{y}_m)$. For the case $d \neq 0$, $(\tilde{x}_m, \tilde{y}_m)$ cannot either lie on the line B or take the value of $(\hat{x}_m, \hat{y}_m)$. Therefore, by performing manipulations on (6.19), we can obtain

$$
\left(\tilde{x}_m - \frac{x'_f + \hat{x}_m}{2}\right)^2 + \left(\tilde{y}_m - \frac{y'_f + \hat{y}_m}{2}\right)^2 = \frac{(x'_f - \hat{x}_m)^2 + (y'_f - \hat{y}_m)^2}{4}. \quad (6.20)
$$

By adding (6.20) as a constraint and also including the special case, we can finally write the objective function as

$$
\begin{aligned}
\min_{x_m, y_m} \quad & f(x_m, y_m) = \left(\hat{\tilde{\Omega}}'_0 - \Omega'_0\right)^2 + A_w\left[(\hat{x}_m - x_m)^2 + (\hat{y}_m - y_m)^2\right] \\
\text{subject to}: \quad & \left(x_m - \frac{x'_f + \hat{x}_m}{2}\right)^2 + \left(y_m - \frac{y'_f + \hat{y}_m}{2}\right)^2 = \frac{(x'_f - \hat{x}_m)^2 + (y'_f - \hat{y}_m)^2}{4}
\end{aligned}
$$

$$(6.21)$$

which is a 1-D search problem with the solution domain being a circle. Obviously, the real location must lie near the line B and $(\hat{x}_m, \hat{y}_m)$. Therefore in practice, searching over the arc near the line B and $(\hat{x}_m, \hat{y}_m)$ is sufficient to find the solution.

## 6.4 Simulation and Performance Analysis

Simulations are carried out to analyze the performances of the proposed approach. In the first part, the space-time correlation based algorithm for motion-dependent parameters estimation is evaluated under different channel conditions. In the second part, the complete tracking process, including motion parameters

estimation, EKF-based tracking and enhancement with HR-AoA, are simulated with the MT moving along a known trajectory. Each FT is equipped with a ULA of 10 elements and consecutive antennas are separated by half wavelength. The signal-to-noise ratio (SNR) is defined as the ratio of received signal power and the noise power, i.e. P_R/N_0, and is set to be 10 dB at all FTs through the whole simulation for a fair comparison. The carrier frequency used is 2.4 GHz. The number of samples for computing the spatial and temporal correlations of the received signal is 32 except when the algorithm is evaluated with different numbers of samples in Section 6.4.1, and samples are taken with the frequency of 500 Hz. In each channel realization, the number of waves in the diffuse component is set to be sufficiently large, and in our simulation, we take $L = 200$. In each channel realization, the AoAs as well as other channel parameters are randomly generated according to corresponding distributions.

6.4.1 Simulation of Parameters Estimation Algorithm

We simulate the performance of the algorithm for motion parameters estimation when K is ranged from 0 dB to 6 dB, and κ is ranged from 1 to 50. Other parameters are fixed at $\Omega_0 = 50°$, $\psi = 0°$ and $v = 1$ m/s. The simulation result is shown in Fig. 6.4, where Fig. 6.4(a) and Fig. 6.4(b) give the root mean square errors (RMSEs) of the speed v_0 and the direction Ω_0 of the radial velocity, respectively. The performance tends to be stable with the increase of κ for a certain value of K, and improves when K increases. In Section 6.1.2, we assume that κ is sufficiently large so that the von-Mises distribution can be approximated by a Gaussian distribution. However, as shown in the figure, the effect of κ on the estimation accuracy is almost negligible as long as the Rician factor K is sufficiently large (≥ 6 dB) even when κ is small. On the other hand, if K is small (≤ 4 dB), the effect of κ is insignificant when it is larger than 3.

Next, we evaluate the performance while changing the MT speed v and the direction Ω_0, while keeping $K = 4$ dB and $\kappa = 3$. The direction of the MT ψ is still $0°$. We change v from 0.1 m/s to 5 m/s, and choose the values of $30°$, $50°$ and $80°$ for Ω_0. The results are presented in Fig. 6.5. The results show that when Ω_0 is fixed, the accuracy of estimating v_0 downgrades with the increase of v, and estimating Ω_0 performs in the opposite way. For a certain value of v, the performances of estimating both v_0 and Ω_0 improve as the radial direction (LOS)
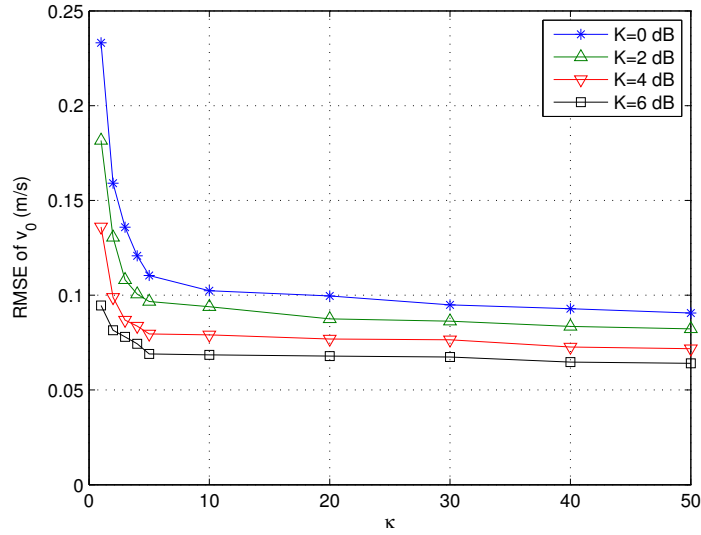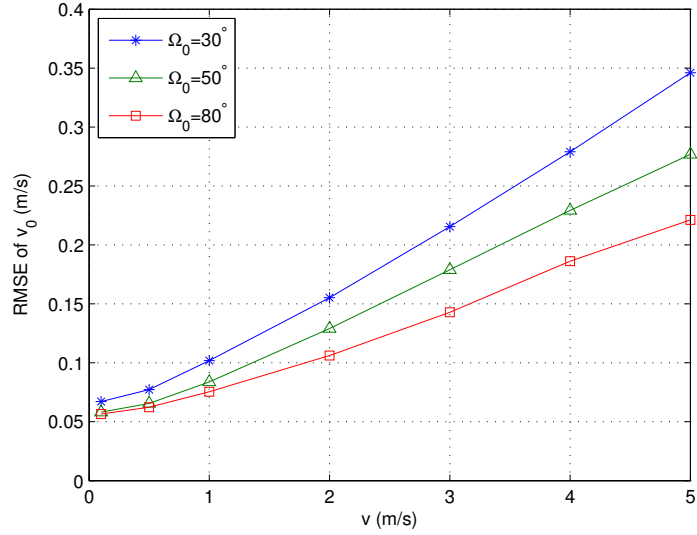
(a) RMSE of estimating v_0 - the speed of the radial velocity
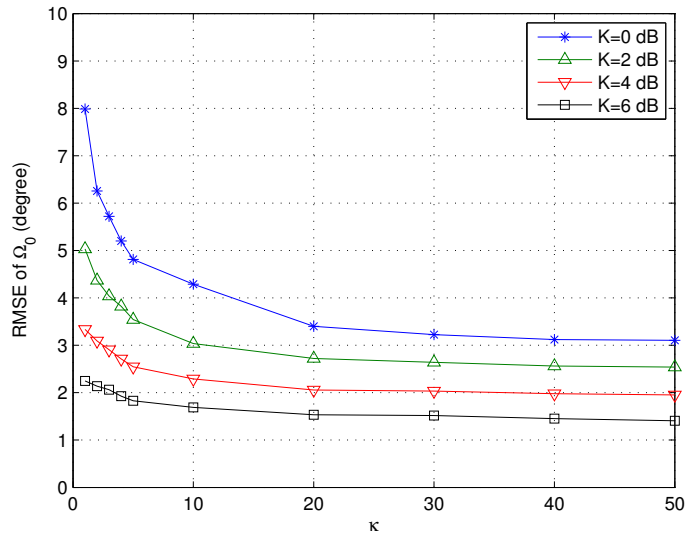
(b) RMSE of estimating Ω_0 - the direction of the radial velocity

Fig. 6.4: The RMSEs of the proposed parameter estimation algorithm while changing the values of K and κ

(a) RMSE of estimating v_0 - the speed of the radial velocity
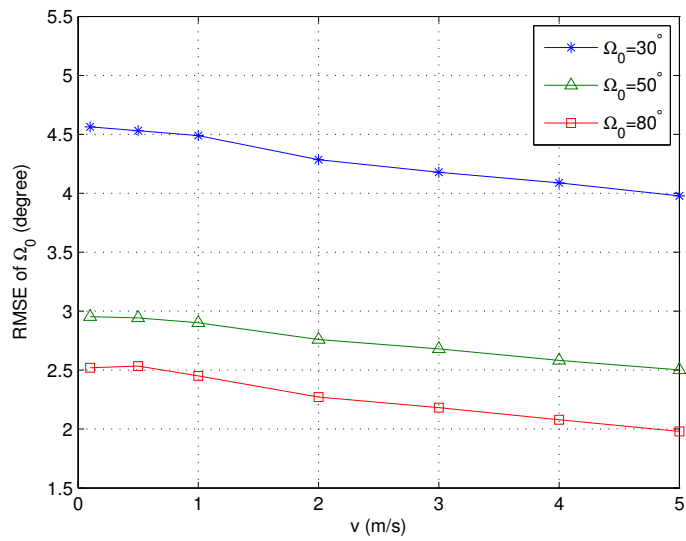

(b) RMSE of estimating Ω_0 - the direction of the radial velocity

Fig. 6.5: The RMSEs of the proposed parameter estimation algorithm while changing the values of v and Ω_0
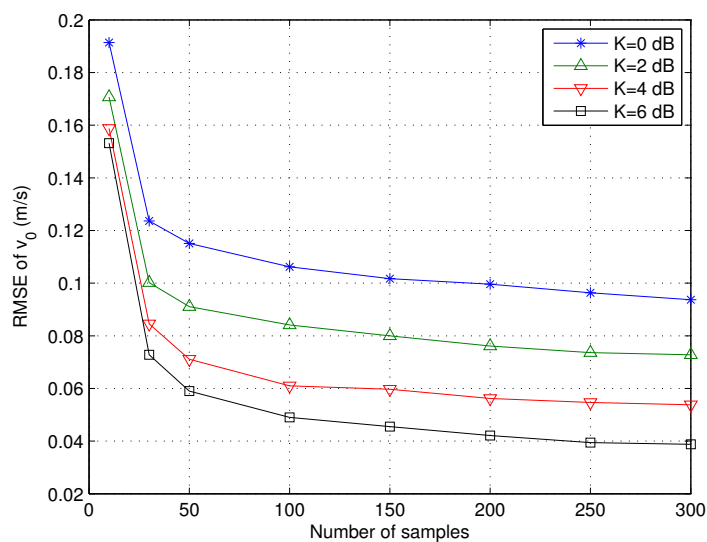
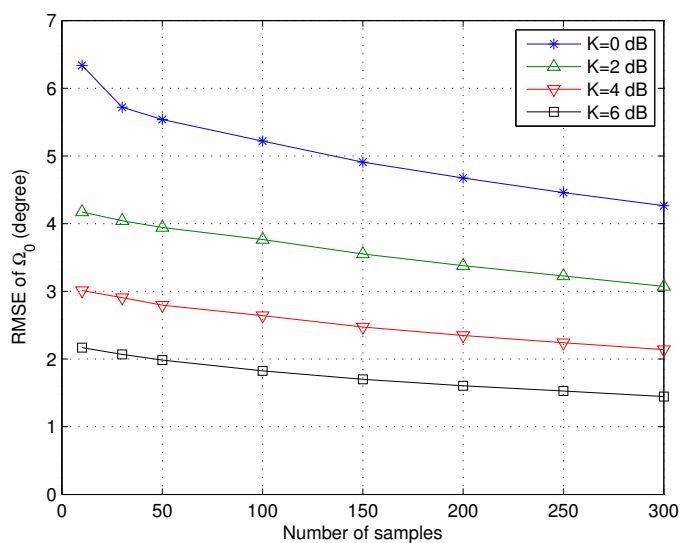(a) RMSE of estimating v_0 - the speed of the radial velocity

(b) RMSE of estimating Ω_0 - the direction of the radial velocity

Fig. 6.6: The RMSEs of the proposed parameter estimation algorithm with different numbers of samples

is closer to the perpendicular direction of FT.

The complexity of the algorithm highly depends on the number of samples required. Therefore, we also simulate its performances while changing the number of samples, which is shown in Fig. 6.6. We set other parameters at $\kappa = 3$, $\Omega_0 = 50°$, $\psi = 0°$ and $v = 1$ m/s. As clearly shown in the figure, the performance is enhanced with more samples. However, when the samples are more than 30, the improvement is not significant. As such, the number of samples can be set to around 30 as the best tradeoff of complexity and accuracy in practice.

6.4.2   Tracking with a Fixed MT Trajectory

We apply the complete three-step tracking approach to a scenario where the MT moves along a fixed trajectory. The field is a 30 m $\times$ 22 m area, in which the X-axis starts at -15 m and ends at 15 m while the Y-axis is from 0 m to 22 m. The MT moves along an U-shape trajectory with length of 46 m, which is denoted by "Actual trajectory" in Fig. 6.7. The trajectory starts at $(-10, 14)$, makes two $90°$-turns at $(10, 14)$ and $(10, 8)$, and ends at $(-10, 8)$. We assume the initial location and velocity of the MT are accurately known by the FT that performs the tracking. With the initial state, the EKF-based tracking is performed at the frequency of 1 Hz. At each time instant, the radial velocity which includes both v_0 and Ω_0 is first estimated using the algorithm described in Section 6.1, and then EKF is adopted to estimate the location. The HR-AoA estimation is performed at a specified frequency, and is fused with the EKF tracking result. We set the two channel parameters $\kappa = 3$ and K to be varied in the following simulation.

We first consider the case where the same FT located at $(0, 0)$ performs both tracking and enhancement. The statistical performances of the proposed approach are demonstrated in Fig. 6.8, where the speed of the MT v changes from 0.5 m/s to 2 m/s. The Rician factor K is set to be 0 dB in Fig. 6.8(a) and 4 dB in Fig. 6.8(b). The RMSE of tracking increases when the MT moves with higher speed. The tracking errors without performance enhancement are around 1.2 m to 3.5 m for different values of v when $K = 0$ dB, and about 0.7 m to 2 m when $K = 4$ dB. The proposed HR-AoA based enhancement method is performed at different frequencies, i.e. 0.1 Hz, 0.2 Hz, 0.5 Hz and 1 Hz, as shown in the figure. It can be clearly seen that the enhancement becomes stronger while enhancement is made more frequently. The improvement is significant for the case of $K = 0$ dB, which
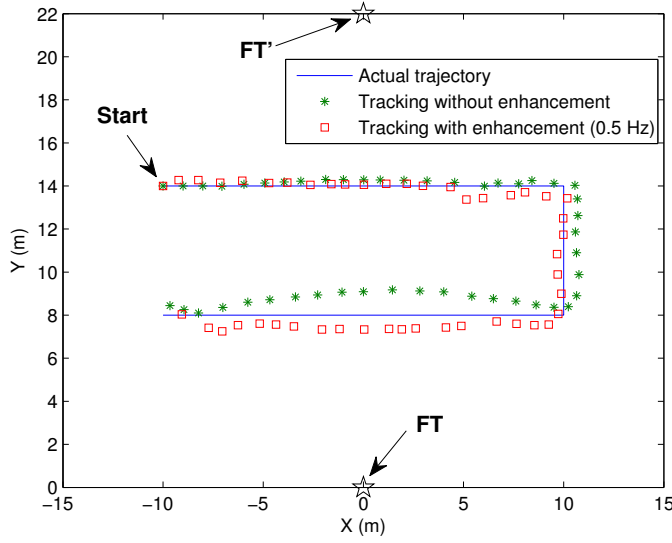
Fig. 6.7: A sample of MT tracking ($K = 4$ dB, $v = 1$ m/s). The EKF tracking is performed by FT located at $(0,0)$, while the HR-AoA enhancement is performed by FT$'$ located at $(0,22)$.

is up to about 45%. When $K = 4$ dB, the enhancement is less significant which is up to about 30%. The reason is that in the presence of stronger LOS (higher K), space-time parameter estimation algorithm gives sufficiently good estimate and hence HR-AoA information contributes less on the overall performance.

Next, we consider the second case where different FTs are used to track the MT and perform the enhancement respectively. We assume the FT that tracks the MT is located at $(0,0)$, while the FT that performs the enhancement is placed at $(0,22)$, and the channel parameters K and κ between the MT and the two FTs are the same. Other settings remain the same as before. The statistical performances shown in Fig. 6.9 demonstrates that the performance enhancement is even more significant than the first case, which is up to 70% for both $K = 0$ dB and $K = 4$ dB. Comparing with the first case, this approach has three advantages. Firstly, the improvement does not vary significant with how frequent enhancement is performed, especially when v is small and medium. Even when the enhancement frequency is as low as 0.1 Hz or 0.2 Hz, the performance improvement is still significant. Secondly, even with higher K, the improvement is still significant, which is different from the first case. Thirdly, the enhanced performance does not change significantly with different values of v when the frequency of enhancement
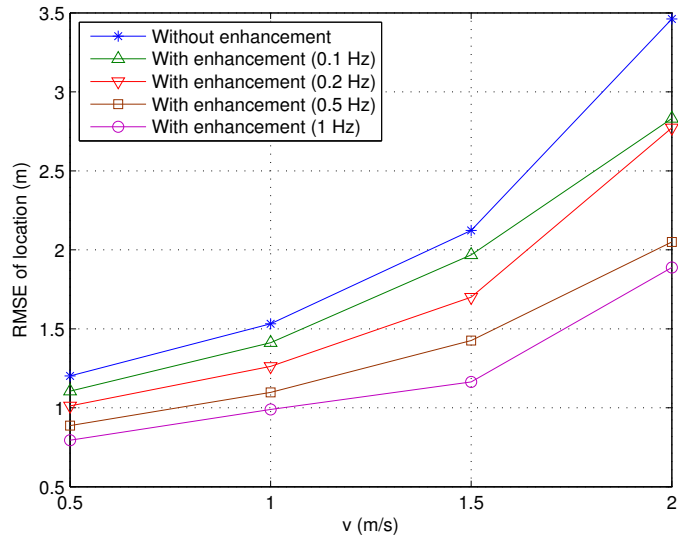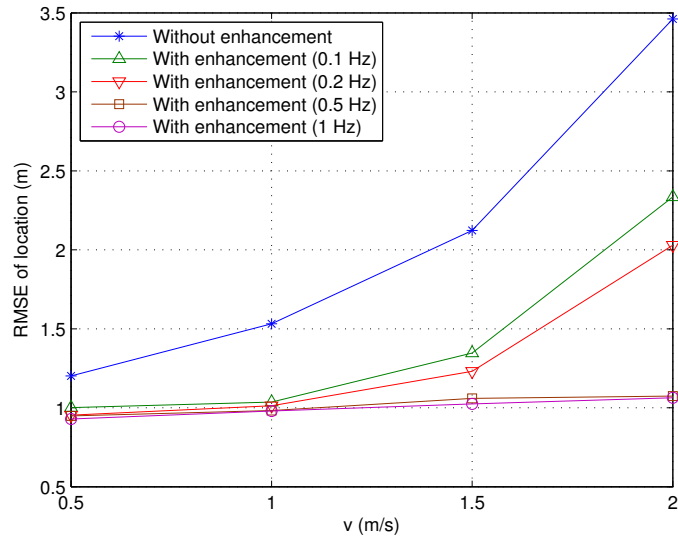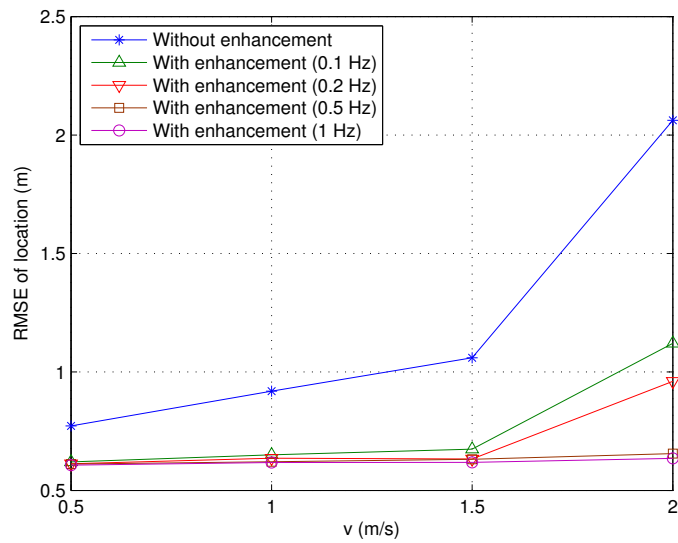
(a) $K = 0$ dB
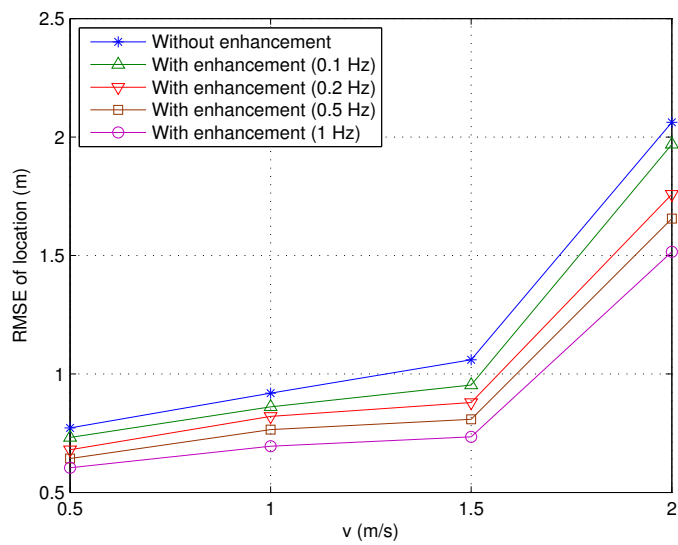
(b) $K = 4$ dB

Fig. 6.8: Performances of EKF-based tracking and HR-AoA enhancement, and the same FT performs both tracking and enhancement
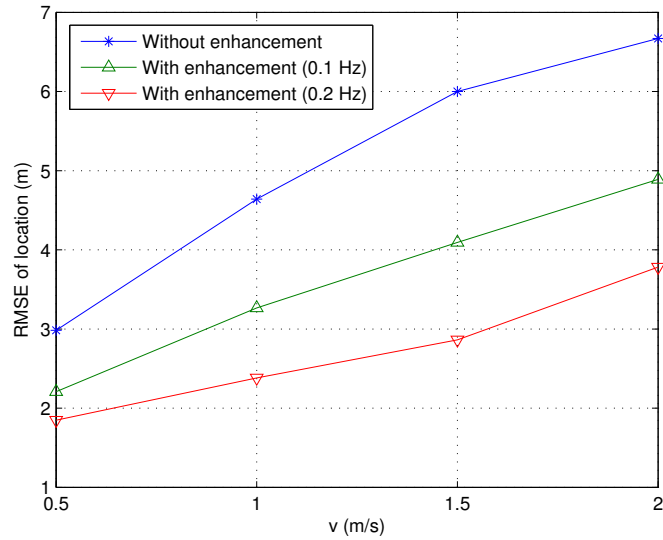
(a) $K = 0$ dB

(b) $K = 4$ dB

Fig. 6.9: Performances of EKF-based tracking and HR-AoA enhancement, and different FTs perform tracking and enhancement respectively

is 0.5 or 1 Hz, where the errors fall into the intervals of 0.9-1.1 m when $K = 0$ dB and 0.6-0.7 m when $K = 4$ dB. Hence, this approach is more suitable for situations with unknown mobility and if the enhancement cannot be done frequently. It introduces cooperation between different FTs and hence the advantages are due to the diversity gain. However, this is at the expense of system complexity to perform data fusion and processing.

The performance of the proposed method is also studied under non-line-of-sight (NLOS) scenario, where the LOS signal is blocked by an object but signals can reach the receiver through reflections and/or diffractions around the object. Examples of such scenarios include when human body blocks the LOS signals or a building obstructs the LOS signal between the MT and cellular tower. Under this condition, the received signal comprises of the diffuse component only, i.e. $K = -\infty$ dB. In our simulation, the EKF-based tracking is done completely without the LOS component. However, in order to obtain HR-AoA estimates for performance enhancement, we assume the MT is able to see the LOS occasionally and the HR-AoA based enhancement can be performed at a frequency of 0.2 Hz or 0.1 Hz. When the LOS is occasionally present, we set $K = 0$ dB. For the case when the same FT performs both tracking and enhancement as shown in Fig. 6.10(a), the tracking without enhancement can achieve accuracy of 3 meters when $v = 0.5$ m/s to 6.7 meters when $v = 2$ m/s. Although the enhancement is performed at low frequencies, it still results in significantly reduction in the error, e.g. the error after enhancement with the frequency of 0.2 Hz is around 2 meters when $v = 0.5$ m/s to 4 meters when $v = 2$ m/s. When different FTs perform the tracking and enhancement respectively as in Fig. 6.10(b), the improvement is even more significant.

6.4.3 Tracking with a Randomly Generated MT Trajectory

The proposed approach is next evaluated in the same scenario, but the MT moves along a trajectory that is randomly generated according to the Gauss-Markov mobility model [142]. The velocity of the MT is assumed to be correlated over time and is modeled as a Gauss-Markov process. Mathematically, in a 2-D

(a)
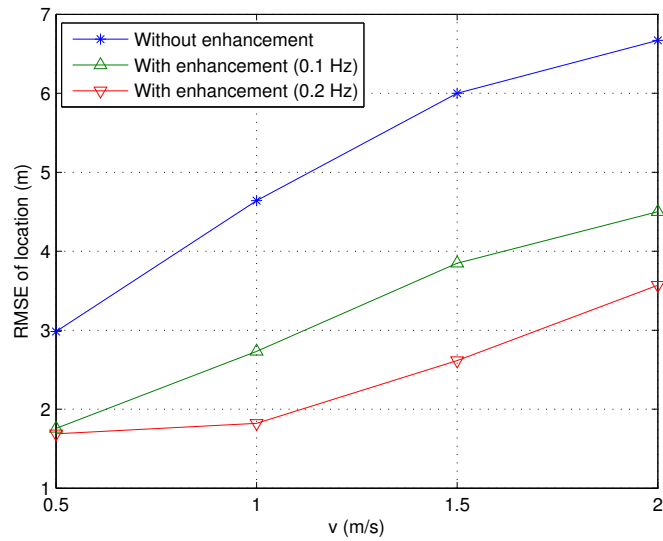
(b)

Fig. 6.10: Performances of EKF-based tracking and HR-AoA enhancement under NLOS condition: (a) the same FT performs both tracking and enhancement; (b) different FTs perform tracking and enhancement respectively.
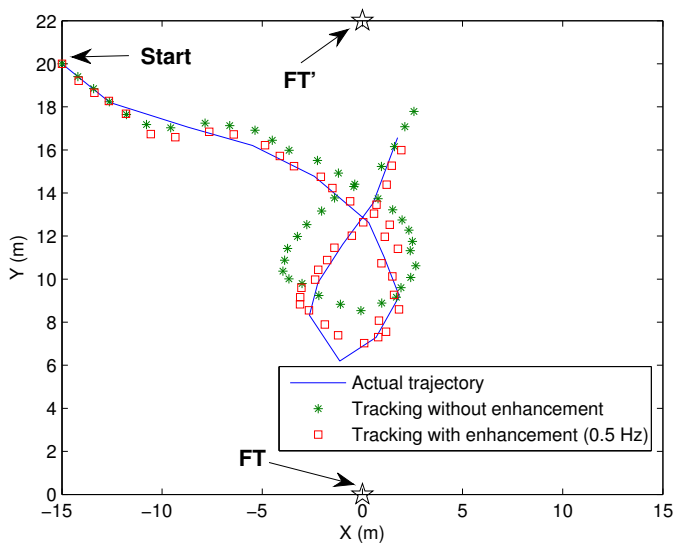
Fig. 6.11: *A sample of MT tracking for the randomly generated trajectory ($K = 4$ dB). The EKF tracking is performed by FT located at $(0, 0)$, while the HR-AoA enhancement is performed by FT$'$ located at $(0, 22)$.*
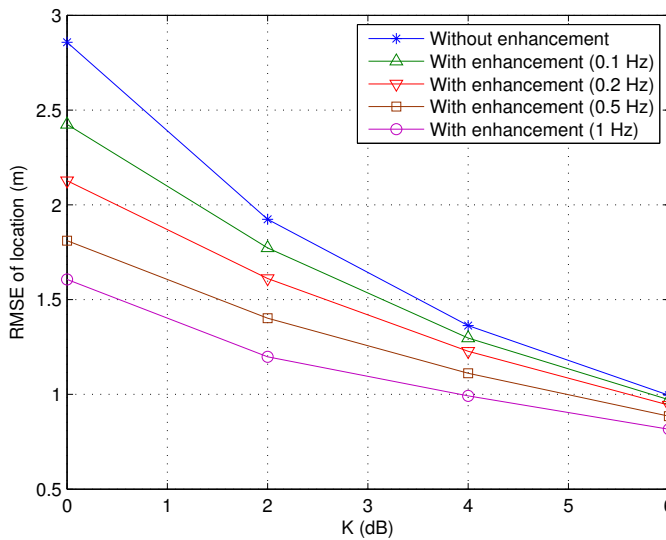

Fig. 6.12: *Performances of EKF-based tracking and HR-AoA enhancement for randomly generated trajectory, and the same FT performs both tracking and enhancement*
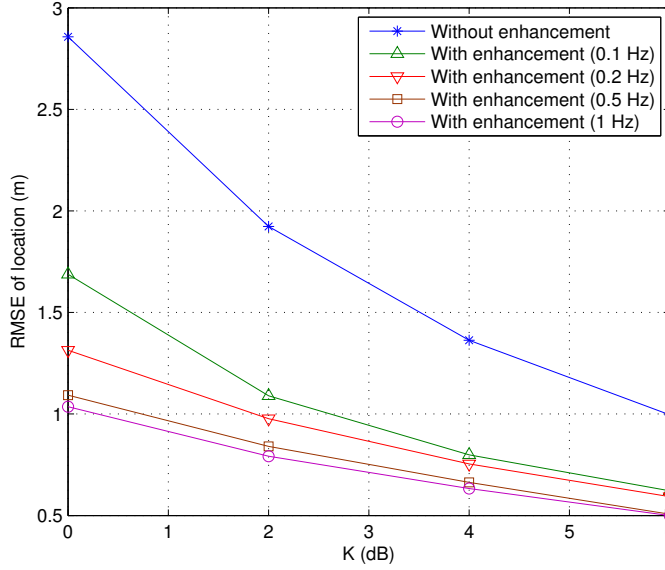
Fig. 6.13: Performances of EKF-based tracking and HR-AoA enhancement for randomly generated trajectory, and different FTs perform tracking and enhancement respectively

plane, the velocity at the time instant t is expressed as

$$
\begin{aligned}
v_x^{(t)} &= \rho v_x^{(t-1)} + (1-\rho)\bar{v}_x + \sqrt{1-\rho^2}\varsigma_x^{(t-1)}, \\
v_y^{(t)} &= \rho v_y^{(t-1)} + (1-\rho)\bar{v}_y + \sqrt{1-\rho^2}\varsigma_y^{(t-1)},
\end{aligned}
\tag{6.22}
$$

where $\rho \in [0,1]$ controls the memory level, $v_x^{(t)}$ and $v_y^{(t)}$ are the velocities on X-axis and Y-axis at time instant t respectively, $v_x^{(t-1)}$ and $v_y^{(t-1)}$ are the velocities at time instant $t-1$, $\bar{v}_x$ and $\bar{v}_y$ are the asymptotic means, and ς_x and ς_y are independent random variables with zeros mean and finite variances. The parameter ρ reflects the randomness of the Gauss-Markov process, and a larger value represents a higher memory level.

In the simulation ,we generate the trajectory by setting $\rho = 0.9$, and the mean speed of the MT $\bar{v} = \sqrt{\bar{v}_x^2 + \bar{v}_y^2} = 1$ m/s, which is labeled as "Actual trajectory" in Fig 6.11. The MT starts moving at (-15, 20), and changes its speed every 3 seconds according to the model (6.22). The whole process lasts for 42 seconds. Other settings stay the same with the previous subsection.

Firstly, we also discuss the case that the same FT located at $(0,0)$ performs both tracking and enhancement. Fig. 6.12 demonstrates the statistical perfor-
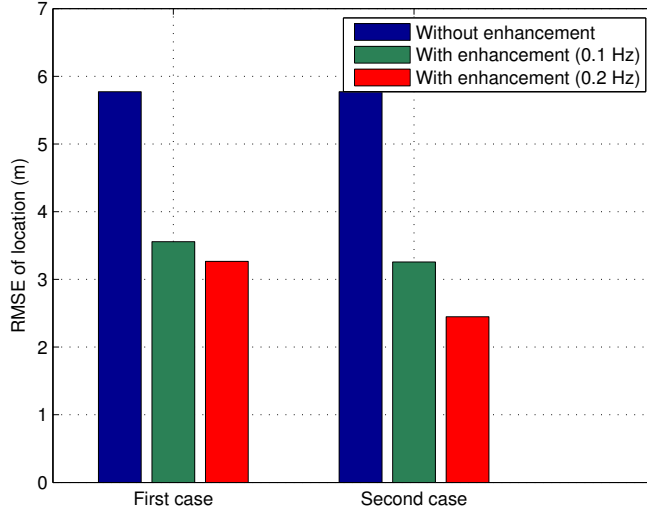
Fig. 6.14: Performances of EKF-based tracking and HR-AoA enhancement for randomly generated trajectory under NLOS condition. First case: the same FT performs both tracking and enhancement; second case: different FTs perform tracking and enhancement respectively.

mance of the proposed approach. The tracking approach without enhancement becomes more accurate with the Rician factor K increasing. When $K = 0$ dB, it is able to achieve an average accuracy of 2.8 meters, while the accuracy is about 1 meter when $K = 6$ dB. Similar with the case with fixed MT trajectory, the HR-AoA enhancement becomes more significant while increasing its frequency, which is up to about 45% for this trajectory.

When different FTs located at $(0,0)$ and $(0,22)$ perform tracking and enhancement respectively, the results are shown in Fig. 6.13 where the HR-AoA enhancement can achieve up to about 60% performance improvement. Compared with the first case, we can observe similar advantages presented at the end of the previous subsection.

Under NLOS condition, the performance of the complete tracking approach is shown in Fig. 6.14. We use the same assumption as in the last section that the MT is able to see the LOS occasionally and the HR-AoA based enhancement can be performed at a frequency of 0.2 Hz or 1 Hz. Whenever the LOS is present, we set $K = 0$ dB. We can see that the error before enhancement is nearly 6 meters. This error is decreased to $2.5 - 3.5$ meters by performing enhancement.

111

6.5 Conclusion

In this chapter, we propose a three-step MT tracking approach performed at the FT. The three-step algorithm consists of motion-dependent parameters estimation based on space-time correlation of the received signal, EKF-based tracking to estimated the location, and HR-AoA based performance enhancement to reduce the accumulative error. The motion parameters estimation algorithm is evaluated while changing the channel parameters, followed by the location estimation with EKF-based tracking. Performance improvement is achieved by incorporating the HR-AoA based enhancement.

Chapter 7

Conclusions and Future Work

Localization and tracking have attracted considerable attention recently. In this thesis, we study the performances of various localization and tracking algorithms developed for multiple-input multiple-output (MIMO) systems. MIMO has emerged as an important technique in the next generation wireless networks. Since MIMO systems are equipped with antenna array at both the transmitter and receiver, it is able to provide the processing capability in an additional dimension - the spatial dimension and make the so called space-time processing possible. In this thesis, we have studied the impact of space-time processing which a MIMO system can provide in terms of enhancement in location estimation accuracy. The space-time processing techniques are applied to either the transmitter or receiver, and channel state information (CSI) is made use of to enhance the location-dependent parameters estimation and localization accuracy. Furthermore, we have also studied remote tracking problem by applying space-time processing and developed a new method for efficient tracking.

7.1   Precoder Design for AoA Estimation

In Chapter 3, we propose precoder design strategies to improve the performance of the angle-of-arrival (AoA) and location estimation. We first derive a new asymptotic performance bound for the MUSIC (MUltiple SIgnal Classification) algorithm which is used as the AoA estimator, when the signal can be preprocessed at the transmitter before transmission. The performance bound can

be achieved asymptotically if we adopt the optimal precoder. However, such an optimal precoder is not practical, since it requires the CSI exclusive of the effect due to the receiver antenna array. We next propose a more feasible approach, which makes use of the feedback CSI estimated at the receiver. We demonstrate that the practical precoder performs close to the optimal precoder which benchmarks the performance through both theoretical analysis and simulations. Both precoders exhibit performance improvement compared with the case when no precoder is used. Furthermore, the practical precoder technique is applied to a known AoA-based localization method, and enhanced location estimation performance is achieved by comparing with the case without precoder through simulations.

Although the proposed precoder schemes can achieve the bound asymptotically, there is still some performance degradation in the high-resolution scenario which make the performances of MUSIC algorithm with and without a precoder diverge from the performance limit, as shown in Fig. 3.4. Thus, there is still room to improve the performance of the algorithm in the high-resolution scenario. A future direction for this work is to study effective techniques for such scenario which are able to approach the bound. The performance degradation is partially due to the high correlation between closely spaced signals in the high-resolution scenario, so an effective method to reduce such correlation is required.

7.2   ToA Estimation in MIMO Systems

The signal pre-processing technique is next applied to time-of-arrival (ToA) estimation, and the work is presented in Chapter 4. We start from deriving the Cramer-Rao lower bound (CRLB) when using the maximum likelihood (ML) estimator, which is later used as the metric. With the objective of minimizing the CRLB, we propose our method to improve the performance of the ToA estimator. When CSI at the transmitter (CSIT) is available, transmit beamforming is adopted as the signal pre-processing technique at the transmitter, while space-time block code (STBC) is utilized as the transmit diversity technique for the case of unavailable CSIT. Since we can assume that the CSI at the receiver (CSIR) is always available as channel estimation is a key component in a receiver, we employ receive beamforming at the receiver. By studying through simulations, we demonstrate that the performance of the ToA estimator is enhanced with the availability

114

of CSIT. It is further enhanced by increasing the number of antennas. Under the condition of erroneous CSIT, improvement can still be observed compared with the case without CSIT when the signal-to-noise ratio (SNR) is below a threshold.

The proposed approach is derived based on a single-path channel. However, multipath components usually present in real environment, especially in the indoor or urban areas. Under such conditions, the performance of the proposed approach will be degraded. Therefore, the ToA estimation problem in MIMO systems in multipath environment is a possible future direction for this work. Such a problem can be implemented based on two criteria. The first one is to enhance the estimation accuracy of the line-of-sight (LOS) path only, because many localization algorithms in the literature only use the LOS component to perform localization. The second criteria is to jointly reduce the errors of LOS and multipath components. This is also useful, because the multipath components have been utilized for localization in [20, 89, 90].

7.3 MAP-Based Joint Channel Parameter Estimation

In Chapter 5, we develop a maximum a posterior (MAP) based joint temporal and spatial parameters estimation algorithm for single-input multiple-output (SIMO) and MIMO systems. We take advantage of prior knowledge of statistical channel information obtained from the extended Saleh-Valenzuela (SV) channel model, and use the space-time processing technique to do joint estimation such that multiple channel parameters can be estimated under the same framework. In order to make the MAP-based approach feasible, we use the expectation-maximization (EM) algorithm to resolve the high dimensional optimization problem into iteratively solving the multiple 3-dimensional (3-D) optimizations. Simulations are carried out in two typical indoor scenarios following the extended SV model. The proposed algorithm is shown to outperform the ML-based algorithm reported for SIMO systems. We also demonstrate that the iterative approach generally converge fast within a few iterations. Finally, we discuss how the algorithm can be extended and applied to MIMO systems, whose feasibility is demonstrated by a numerical example.

The proposed approach is reduced to iteratively solving multiple 3-D opti-

mizations when applying the EM algorithm. We point out that this 3-D optimization problem can be further reduced to three 1-D search problems by applying the SAGE (Space-Alternating Generalized EM) algorithm [143] which has been applied to ML-based parameters estimation in [82]. The future work on this topic will involve studying its feasibility and performance comparison between SAGE-based and EM-based approaches in improving the localization accuracy.

7.4　AoA-Assisted Mobile Terminal Tracking

By applying space-time processing technique to remote tracking problem, we propose an efficient tracking approach which is presented in Chapter 6. The battery lifetime which limits the application of self tracking is resolved by performing the tracking at the fixed terminal (FT) side. The proposed approach involves three steps. First, we develop a space-time correlation based algorithm to estimate the radial velocity (both the speed and direction) of the mobile terminal (MT). With a suitable channel model identified, we show that both the radial speed and direction of a MT can be jointly estimated from the phase of the complex space-time correlation, and has low computational complexity. The extended Kalman filter (EKF) is next adopted to estimate the current location by fusing the measurements and the previous location estimate. Finally, the MUSIC algorithm is applied to obtain additional high-resolution AoA (HR-AoA) estimate and we show how this partial location information can be fused with the tracking results to further improve the tracking accuracy. The space-time correlation based parameter estimation algorithm is first studied through simulation and shows effective performances under different channel conditions and MT speeds. Then, the complete tracking approach is applied to a fixed trajectory and a randomly generated trajectory, respectively. It is shown that with different tracking and enhancing frequencies, the proposed approach exhibits different accuracies.

In the derivation of the approach, we assume that the parameter κ is sufficiently large, such that the von-Mises distribution can be approximated by Gaussian distribution. Under this condition, it is reasonable to assume $\Omega_0 = \Omega_R$. We then demonstrate through simulation that as long as the Rician factor K is not small, the value of κ has very limited effect on the estimation accuracy. However, if we consider the extreme condition when both K and κ are small (e.g. $K \leq 2$

dB and $\kappa \leq 2$), the performance of the motion-dependent parameters estimation algorithm is degraded. A future direction is to study effective method under this condition. Since Ω_0 and Ω_R may not be assumed to be equal, the estimation becomes a joint estimation of both Ω_0 and Ω_R. Another direction is to extend the approach to non-LOS (NLOS) scenario under the aboved mentioned extreme condition. In non-extreme condition, the extension is very straightforward, since Ω_R is equal to the LOS AoA, and the performance has been studied in the simulation of Chapter 6. However, under the above mentioned extreme scenario, we can only obtain the estimate of Ω_R which is different from LOS AoA. Therefore, the EKF part need to be revised so as to mitigate the NLOS effect.

Bibliography

[1] H. Liu, H. Darabi, and P. Banerjee, "Survey of wireless indoor positioning techniques and systems," *IEEE Trans. Syst. Man Cybern.*, vol. 37, no. 6, pp. 1067–1080, 2007.

[2] S. Gezici, Z. Tian, G. B. Giannakis, H. Kobayashi, A. F. Molisch, H. V. Poor, and Z. Sahinoglu, "Localization via ultra-wideband radios: a look at positioning aspects for future sensor networks," *IEEE Signal Processing Mag.*, vol. 22, no. 4, pp. 70–84, 2005.

[3] H. L. V. Trees, *Detection, Estimation and Modulation Theory Part IV: Optimum Array Processing*. New York: Wiley-Interscience, 2002.

[4] H. Krim and M. Viberg, "Two decades of array signal processing research: the parametric approach," *IEEE Signal Process Mag.*, vol. 13, no. 4, pp. 67–94, 1996.

[5] I. Guvenc and C. C. Chong, "A survey on TOA based wireless localization and NLOS mitigation techniques," *IEEE Commun. Surv. Tutorials*, vol. 11, no. 3, pp. 107–124, 2009.

[6] L. Xiong, "A selective model to suppress NLOS signals in angle-of-arrival (AOA) location estimation," in *Proc. PIMRC*, pp. 461–465, 1998.

[7] L. Cong and W. Zhuang, "Non-line-of-sight error mitigation in mobile location," *IEEE Trans. Wireless Commun.*, vol. 4, no. 2, pp. 560–573, 2005.

[8] P. Bahl and V. Padmanabhan, "RADAR: An in-building RF based user location and tracking system," in *Proc. IEEE INFOCOM*, pp. 775–784, 2000.

[9] W. Honkavirta, T. Perala, S. Ali-Loytty, and R. Piche, "A comprehensive survey of WLAN location fingerprinting methods," in *Proc. WPNC*, pp. 243–251, 2009.

[10] Y. Jin, W.-S. Soh, and W.-C. Wong, "Indoor localization with channel impulse response based fingerprint and nonparametric regression," *IEEE Trans. Wireless Commun.*, vol. 9, no. 3, pp. 1120–1127, 2010.

[11] C. Nerguizian, C. Despins, and S. Affes, "Geolocation in mines with an impulse response fingerprinting technique and neural networks," *IEEE Trans. Wireless Commun.*, vol. 5, no. 3, pp. 603–611, 2006.

[12] X. R. Li and V. P. Jilkov, "Survey of maneuvering target tracking. Part I: Dynamic models," *IEEE Trans. Aerosp. Electron. Syst.*, vol. 39, no. 4, pp. 1333–1364, 2003.

[13] X. R. Li and V. P. Jilkov, "Survey of maneuvering target tracking. Part III: Measurement models," *Proc. SPIE, Signal and Data Processing of Small Targets*, vol. 4473, pp. 423–446, 2001.

[14] H.-J. Jang, J. W. Kim, and D.-H. Hwang, "Robust step detection method for pedestrian navigation systems," *Electron. Lett*, vol. 43, no. 14, 2007.

[15] Y. Jin, M. Motani, W.-S. Soh, and J. Zhang, "SparseTrack: Enhancing indoor pedestrian tracking with sparse infrastructure support," in *Proc. IEEE INFOCOM*, pp. 1–9, Mar. 2010.

[16] E. R. Bachmann, X. Yun, and A. Brumfield, "Limitations of attitude estimation algorithms for inertial/magnetic sensor modules," *IEEE Trans. Rob. Autom.*, vol. 14, no. 3, pp. 76–87, 2007.

[17] J. Hummel, M. Figl, C. Kollmann, and H. Bergmann, "Evaluation of a miniature electromagnetic position tracker," *Med. Phys.*, vol. 29, no. 10, pp. 2205–2212, 2002.

[18] U. Hammes, E. Wolsztynski, and A. M. Zoubir, "Robust tracking and geolocation for wireless networks in NLOS environments," *IEEE J. Sel. Top. Sign. Proces.*, vol. 3, no. 5, pp. 889–901, 2009.

[19] A. B. Gershman and N. D. Sidiropoulos, *Space-Time Processing for MIMO Communications.* John Wiley & Sons, 2005.

[20] C. K. Seow and S. Y. Tan, "Non-line-of-sight localization in multipath environments," *IEEE Trans. Mob. Comput.*, vol. 7, no. 5, pp. 647–660, 2008.

[21] M. Biguesh and A. B. Gershman, "Training-based mimo channel estimation: a study of estimator tradeoffs and optimal training signals," *IEEE Trans. Signal Process.*, vol. 54, no. 3, pp. 884–893, 2006.

[22] C. Budianu and L. Tong, "Channel estimation for space-time orthogonal block codes," *IEEE Trans. Signal Process.*, vol. 50, no. 10, pp. 2515–2528, 2002.

[23] M. Vu and A. Paulraj, "MIMO wireless linear precoding," *IEEE Signal Process Mag.*, vol. 24, no. 5, pp. 86–105, 2007.

[24] V. Tarokh, H. Jafarkhani, and A. R. Calderbank, "Space-time codes from orthogonal designs," *IEEE Trans. Inf. Theory*, vol. 45, no. 5, pp. 1456–1467, 1999.

[25] S. L. Marple Jr, *Digital Spectral Analysis.* Prentice-Hall, Englewood Cliffs, New Jersey, 1987.

[26] Q. T. Zhang, "A statistical resolution theory of the beamformer-based spatial spectrum for determining the directions of signals in white noise," *IEEE Trans. Signal Process.*, vol. 43, no. 8, pp. 1867–1873, 1995.

[27] J. Capon, "High-resolution frequency-wavenumber spectrum analysis," *Proc. IEEE*, vol. 57, no. 8, pp. 1408–1418, 1969.

[28] R. T. Lacoss, "Data adaptive spectral analysis methods," *Geophys.*, vol. 36, no. 4, pp. 661–675, 1971.

[29] R. Schmidt, "Multiple emitter location and signal parameter estimation," *IEEE Trans. Antennas Propag.*, vol. 34, no. 3, pp. 276–280, 1986.

[30] P. Stoica and A. Nehorai, "MUSIC, maximum likelihood, and Cramer-Rao bound," *IEEE Trans. Acoust. Speech Signal Process.*, vol. 37, no. 5, pp. 720–741, 1989.

[31] A. L. Swindlehurst and T. Kailath, "A performance analysis of subspace-based methods in the presence of model errors, Part I: The MUSIC algorithm," *IEEE Trans. Signal Process.*, vol. 40, no. 7, pp. 1758–1774, 1992.

[32] F. Li and R. J. Vaccaro, "Unified analysis for DOA estimation algorithms in array signal processing," *Signal Process.*, vol. 25, no. 2, pp. 147–169, 1991.

[33] A. Ferreol, P. Larzabal, and M. Viberg, "On the asymptotic performance analysis of subspace DOA estimation in the presence of modeling errors: case of MUSIC," *IEEE Trans. Signal Process.*, vol. 54, no. 3, pp. 907–920, 2006.

[34] A. Ferreol, P. Larzabal, and M. Viberg, "On the resolution probability of MUSIC in presence of modeling errors," *IEEE Trans. Signal Process.*, vol. 56, no. 5, pp. 1945–1953, 2008.

[35] A. Barabell, "Improving the resolution performance of eigenstructure-based direction-finding algorithms," in *Proc. IEEE ICASSP*, vol. 8, pp. 336–339, 1983.

[36] M. Rubsamen and A. B. Gershman, "Direction-of-arrival estimation for nonuniform sensor arrays: From manifold separation to Fourier domain MUSIC methods," *IEEE Trans. Signal Process.*, vol. 57, no. 2, pp. 588–599, 2009.

[37] M. Pesavento, A. B. Gershman, and M. Haardt, "Unitary root-MUSIC with a real-valued eigendecomposition: A theoretical and experimental performance study," *IEEE Trans. Signal Process.*, vol. 48, no. 5, pp. 1306–1314, 2000.

[38] R. Klukas and M. Fattouche, "Line-of-sight angle of arrival estimation in the outdoor multipath environment," *IEEE Trans. Veh. Technol.*, vol. 47, no. 1, pp. 342–351, 1998.

[39] R. Roy and T. Kailath, "ESPRIT-estimation of signal parameters via rotational invariance techniques," *IEEE Trans. Acoust. Speech Signal Process.*, vol. 37, no. 7, pp. 984–995, 1989.

[40] L. Zhang, Y. H. Chew, and W.-C. Wong, "Transmit precoder design to improve the performance of the MUSIC algorithm," *Signal Process.*, vol. 93, no. 11, pp. 3202–3208, 2013. (available online).

[41] S. A. Zekavat and R. M. Buehrer, *Handbook of Position Location: Theory, Practice, and Advances.* Wiley-IEEE Press, 2012.

[42] C. D. Mcgillem and T. S. Rappaport, "A beacon navigation method for autonomous vehicles," *IEEE Trans. Veh. Technol.*, vol. 38, no. 3, pp. 132–139, 1989.

[43] Y. Iwasaki, N. Kawaguchi, and Y. Inagaki, "Design, implementation and evaluations of a direction based service system for both indoor and outdoor," in *Ubiquitous Computing Systems*, vol. 3598 of *Lecture Notes in Computer Science*, pp. 20–36, 2005.

[44] S. F. A. Shah, S. Srirangarajan, and A. H. Tewfik, "Implementation of a directional beacon-based positioning location algorithm in a signal processing framework," *IEEE Trans. Wireless Commun.*, vol. 9, no. 3, pp. 1044–1053, 2010.

[45] S. F. A. Shah and A. H. Tewfik, "Performance analysis of directional beacon based position location algorithm for UWB systems," in *Proc. IEEE GLOBECOM*, pp. 2409–2413, Nov. 2005.

[46] C. Wong, R. Klukas, and G. Messier, "Using WLAN infrastructure for angle-of-arrival indoor user location," in *Proc. IEEE VTC-Fall*, pp. 1–5, Sept. 2008.

[47] D. Niculescu and B. Nath, "Ad hoc positioning system (APS) using AOA," in *Proc. IEEE INFOCOM*, pp. 1734–1743, 2003.

[48] P. Biswas, H. Aghajan, and Y. Ye, "Integration of angle of arrival information for multimodal sensor network localization using semidefinite programming," in *Proc. 39th Asilomar Conference on Signals, Systems and Computers*, Nov. 2005.

[49] R. Peng and M. L. Sichitiu, "Angle of arrival localization for wireless sensor networks," in *Proc. SECON'06*, pp. 374–382, 2006.

[50] C. H. Knapp and C. G. Carter, "The generalized correlation method for estimation of time delay," *IEEE Trans. Acoust. Speech Signal Process.*, vol. 24, no. 4, pp. 320–327, 1976.

[51] D. Hertz, "Time delay estimation by combining efficient algorithms and generalized cross-correlation methods," *IEEE Trans. Acoust. Speech Signal Process.*, vol. 34, no. 1, pp. 1–7, 1986.

[52] G. Fock, J. Baltersee, P. Schulz-Rittich, and H. Meyr, "Channel tracking for rake receivers in closely spaced multipath environments," *IEEE J. Sel. Area. Comm.*, vol. 19, no. 12, pp. 2420–2431, 2001.

[53] M. D. Hahm, Z. I. Mirovski, and E. L. Titlebaum, "Deconvolution in the presence of Doppler with application to specular multipath parameter estimation," *IEEE Trans. Signal Process.*, vol. 45, no. 9, pp. 2203–2219, 1997.

[54] H. Saarnisaari, "ML time delay estimation in a multipath channel," in *Proc. IEEE ISSTA*, pp. 1007–1011, Sept. 1996.

[55] C. D. Wann and L. K. Chang, "Modified GML algorithm with simulated annealing for estimation of signal arrival time," in *Proc. IEEE TENCON*, pp. 1–4, Oct. 2007.

[56] C. D. Wann and L. K. Chang, "Modified GML algorithm for estimation of signal arrival time in UWB systems," in *Proc. IEEE GLOBECOM*, pp. 1–5, Nov. 2006.

[57] J. Y. Lee and R. A. Scholtz, "Ranging in a dense multipath environment using an UWB radio link," *IEEE J. Select. Areas Commun.*, vol. 20, no. 9, pp. 1677–1683, 2002.

[58] L. Zhang, Y. H. Chew, and W.-C. Wong, "Improving the performance of the time-of-arrival estimator in MIMO systems," in *Proc. 6th Int. Conf. on Signal Processing and Communication Systems (ICSPCS)*, pp. 1–5, Dec. 2012.

[59] D. Dardari, C. C. Chong, and M. Z. Win, "Threshold-based time-of-arrival estimators in UWB dense multipath channels," *IEEE Trans. Commun.*, vol. 56, no. 8, pp. 1366–1378, 2008.

[60] D. Dardari, A. Conti, U. Ferner, A. Giorgetti, and M. Z. Win, "Ranging with ultrawide bandwidth signals in multipath environments," *Proc. IEEE*, vol. 97, no. 2, pp. 404–426, 2009.

[61] T. M. Schmidl and D. C. Cox, "Robust frequency and timing synchronization for OFDM," *IEEE Trans. Commun.*, vol. 45, no. 12, pp. 1613–1621, 1997.

[62] H. Minn, V. K. Bhargava, and K. B. Letaief, "A robust timing and frequency synchronization for OFDM systems," *IEEE Trans. Wireless Commun.*, vol. 2, no. 4, pp. 822–839, 2003.

[63] C. W. Yak, Z. Lei, S. Chattong, and T. T. Tjhung, "Timing synchronization for ultra-wideband (UWB) multi-band OFDM systems," in *Proc. IEEE VTC-Fall*, pp. 1599–1603, Sept. 2005.

[64] H. Xu and L. Yang, "ToA estimation for MB-OFDM UWB by suppressing energy leakage," in *Proc. IEEE MILCOM*, pp. 2381–2386, Oct. 2010.

[65] H. Xu, C.-C. Chong, I. Guvenc, F. Watanabe, and L. Yang, "High-resolution TOA estimation with multi-band OFDM UWB signals," in *Proc. IEEE ICC*, pp. 4191–4196, May 2008.

[66] J. J. Caffery and G. L. Stuber, "Overview of radiolocation in CDMA cellular systems," *IEEE Commun. Mag.*, vol. 36, no. 4, pp. 38–45, 1998.

[67] J. J. Caffery, "A new approach to the geometry of toa location," in *Proc. IEEE VTC-Fall*, pp. 1943–1949, 2000.

[68] K. W. Cheung, H. C. So, W.-K. Ma, and Y. T. Chan, "Least square algorithms for time-of-arrival-based mobile location," *IEEE Trans. Signal Process.*, vol. 52, no. 4, pp. 1121–1128, 2004.

[69] Y.-T. Chan, H. Y. C. Hang, and P.-C. Ching, "Exact and approximate maximum likelihood localization algorithms," *IEEE Trans. Veh. Technol.*, vol. 55, no. 1, pp. 10–16, 2006.

[70] D. J. Torrieri, "Statistical theory of passive location systems," *IEEE Trans. Aerosp. Electron. Syst.*, vol. 20, no. 2, pp. 183–197, 1984.

[71] Y. T. Chan and K. C. Ho, "A simple and efficient estimator for hyperbolic location," *IEEE Trans. Signal Process.*, vol. 42, no. 8, pp. 1905–1915, 1994.

[72] H. C. So, Y. T. Chan, and F. K. W. Chan, "Closed-form formulae for time-difference-of-arrival estimation," *IEEE Trans. Signal Process.*, vol. 56, no. 6, pp. 2614–2620, 2008.

[73] L. Cong and W. Zhuang, "Hybrid TDOA/AOA mobile user location for wideband CDMA cellular systems," *IEEE Trans. Wireless Comm.*, vol. 1, no. 3, pp. 439–447, 2002.

[74] M. L. Bencheikh, Y. Wang, and H. He, "Polynomial root finding technique for joint DOA DOD estimation in bistatic MIMO radar," *Signal Process.*, vol. 90, no. 9, pp. 2723–2730, 2010.

[75] A. v. d. Veen, M. Vanderveen, and A. Paulraj, "Joint angle and delay estimation using shift-invariance techniques," *IEEE Trans. Signal Process.*, vol. 46, no. 2, pp. 405–418, 1998.

[76] H. Miao, M. Juntti, and K. Yu, "2-D unitary ESPRIT based joint AOA and AOD estimation for MIMO system," in *Proc. IEEE PIMRC*, pp. 1–5, Sept. 2006.

[77] M. Jin, G. Liao, and J. Li, "Joint DOD and DOA estimation for bistatic MIMO radar," *Signal Process.*, vol. 89, no. 2, pp. 244–251, 2009.

[78] K. Papakonstantinou and D. Slock, "ESPRIT-based estimation of location and motion dependent parameters," in *Proc. IEEE VTC-Spring*, pp. 1–5, 2009.

[79] M. Feder and E. Weinstein, "Parameter estimation of superimposed signals using the EM algorithm," *IEEE Trans. Acoust. Speech Signal Process.*, vol. 36, no. 4, pp. 477 –489, 1988.

[80] B. H. Fleury, D. Dahlhaus, R. Heddergott, and M. Tschudin, "Wideband angle of arrival estimation using the SAGE algorithm," in *Proc. IEEE Fourth Int. Symp. Spread Spectrum Techniques and Applications (ISSSTA)*, pp. 79–85, Sept. 1996.

[81] K. I. Pedersen, B. H. Fleury, and P. E. Mogensen, "High resolution of electromagnetic waves in time-varying radio channels," in *Proc. IEEE PIMRC*, pp. 650–654, Sept. 1997.

[82] B. H. Fleury, M. Tschudin, R. Heddergott, D. Dahlhaus, and K. I. Pedersen, "Channel parameter estimation in mobile radio environemnts using the SAGE algorithm," *IEEE J. Sel. Areas Commun.*, vol. 17, no. 3, pp. 434–450, 1999.

[83] B. Fleury, P. Jourdan, and A. Stucki, "High-resolution channel parameter estimation for MIMO applications using the SAGE algorithm," in *2002 Int. Zurich Seminar on Broadband Communications (IZS 2002)*, pp. 30–1–30–9, 2002.

[84] L. Zhang, Y. H. Chew, and W.-C. Wong, "A MAP-based channel estimation algorithm for SIMO systems over extended SV channel model," in *Proc. IEEE ICCS*, pp. 290–294, Nov. 2012.

[85] S. Venkatraman and J. Caffery, "Hybrid TOA/AOA techniques for mobile location in non-line-of-sight environments," in *Proc. IEEE WCNC*, pp. 274–278, Mar. 2004.

[86] N. Deligiannis and S. Louvros, "Hybrid TOA-AOA location positioning techniques in GSM networks," *Wireless Pers. Commun.*, vol. 54, no. 2, pp. 321–348, 2010.

[87] A.-C. Chang and J.-C. Chang, "Robust mobile location estimation using hybrid TOA/AOA measurements in cellular systems," *Wireless Pers. Commun.*, vol. 65, no. 1, pp. 1–13, 2012.

[88] N. J. Thomas, D. G. M. Cruickshank, and D. I. Laurenson, "Performance of a TDOA-AOA hybrid mobile location system," in *Proc. 2nd Int. Conf. 3G Mobile Communications Technologies*, pp. 216–220, 2001.

[89] J. Li, J. Conan, and S. Pierre, "Mobile station location estimation for MIMO communication systems," in *Proc. ISWCS*, pp. 561–564, Sept. 2006.

[90] H. Miao, K. Yu, and M. J. Juntti, "Positioning for NLOS propagation: Algorithm derivations and Cramer-Rao bounds," *IEEE Trans. Veh. Technol.*, vol. 56, no. 5, pp. 2568–2580, 2007.

[91] L. Zhang, Y. H. Chew, and W.-C. Wong, "Enhanced AoA estimation and localization through transmitter precoder design," *Int. J. Wireless Inf. Networks*, vol. 19, no. 4, pp. 315–325, 2012.

[92] A. Catovic and Z. Sahinoglu, "The Cramer-Rao bounds of hybrid TOA/RSS and TDOA/RSS location estimation schemes," *IEEE Commun. Lett.*, vol. 8, no. 10, pp. 626–628, 2004.

[93] R. I. Reza, *Data fusion for improved TOA/TDOA position determination in wireless systems.* PhD thesis, Virginia Tech., 2000.

[94] Y.-T. Chan, W.-Y. Tsui, H.-C. So, and P.-C. Ching, "Time-of-arrival based localization under NLOS conditions," *IEEE Trans. Veh. Technol.*, vol. 55, no. 1, pp. 17–24, 2006.

[95] I. Guvenc, C.-C. Chong, F. Watanabe, and H. Inamura, "NLOS identification and weighted least-squares localization for UWB systems using multipath channel statistics," *EURASIP Journal on Advances in Signal Processing*, vol. 2008, no. 1, pp. 1–14, 2008.

[96] W. Xu, *Multi-antenna non-line-of-sight identification techniques for target localization in mobile ad-hoc networks.* PhD thesis, Michigan Technological University, 2011.

[97] P. C. Chen, "A non-line-of-sight error mitigation algorithm in location estimation," in *Proc. IEEE WCNC*, pp. 316–320, Sept. 1999.

[98] L. Cong and W. Zhuang, "Non-line-of-sight error mitigation in TDOA mobile location," in *Proc. GLOBECOM*, pp. 680–684, 2001.

[99] C. Randell, C. Djiallis, and H. Muller, "Personal position measurement using dead reckoning," in *Proc. IEEE ISWC*, pp. 166–173, Oct. 2003.

[100] Y. K. Thong, M. S. Woolfson, J. A. Crowe, B. R. Hayes-Gill, and R. E. Challis, "Dependence of inertial measurements of distance on accelerometer noise," *Meas. Sci. Technol.*, vol. 13, no. 8, pp. 1163–1172, 2002.

[101] Q. Ladetto and B. Merminod, "In step with INS," *GPS World*, vol. 13, no. 10, pp. 30–38, 2002.

[102] C. Tepedelenlioglu, A. Abdi, G. B. Giannakis, and M. Kaveh, "Estimation of Doppler spread and signal strength in mobile communications with applications to handoff and adaptive transmission," *Wirel. Commun. Mob. Comput.*, vol. 1, no. 2, pp. 221–242, 2001.

[103] C. Tepedelenlioglu and G. B. Giannakis, "On velocity estimation and correlation properties of narrow-band mobile communication channels," *IEEE Trans. Veh. Technol.*, vol. 50, no. 4, pp. 1039–1052, 2001.

[104] H. Zhang and A. Abdi, "Space-time Doppler spread estimation in mobile fading channels," in *Proc. IEEE MILCOM*, pp. 1–5, 2006.

[105] J. M. Huerta, A. Giremus, J. Vidal, and J.-Y. Tourneret, "Joint particle filter and UKF position tracking under strong NLOS situation," in *Proc. IEEE/SP SSP*, pp. 537–541, Aug. 2007.

[106] C. Fritsche, U. Hammes, A. Klein, and A. M. Zoubir, "Robust mobile terminal tracking in NLOS environments using interacting multiple model algorithm," in *Proc. IEEE ICASSP*, pp. 3049–3052, Apr. 2009.

[107] C.-D. Wann, *Kalman Filtering for NLOS Mitigation and Target Tracking in Indoor Wireless Environment, Kalman Filter.* Vedran Kordic (Ed.), 2010.

[108] C.-D. Wann, Y.-J. Yeh, and C.-S. Hsueh, "Hybrid TDOA/AOA indoor positioning and tracking using extended Kalman filters," in *Proc. IEEE VTC-Spring*, pp. 1058–1062, May 2006.

[109] L. Zhang, Y. H. Chew, and W.-C. Wong, "A novel angle-of-arrival assisted extended Kalman filter tracking algorithm with space-time correlation based motion parameters estimation," in *Proc. IEEE IWCMC.* (to appear).

[110] R. Jirawimut, P. Ptasinski, V. Garaj, F. Cecelja, and W. Balachandran, "A method for dead reckoning parameter correction in pedestrian navigation system," *IEEE Trans. Instrum. Meas.*, vol. 52, no. 1, pp. 209–215, 2003.

[111] R. K. A. Owusu, "Particle filtering and information fusion of innovative location and tracking device targeting GPS hostile environments," in *Proc. ISABEL*, pp. 1–7, Oct. 2008.

[112] D. Kurth, G. Kantor, and S. Singh, "Experimental results in range-only localization with radio," in *Proc. IEEE/RSJ IROS*, pp. 974–979, Oct. 2003.

[113] F. V. Diggelen, *A-GPS : Assisted GPS, GNSS, and SBAS.* Artech House, 2009.

[114] E. D. Kaplan and C. Hegarty, *Understanding GPS: Principles and Applications, Second Edition.* Artech House, 2006.

[115] T. Cover and J. Thomas, *Elements of Information Theory.* New York: Wiley-Interscience, 1991.

[116] E. Visotsky and U. Madhow, "Space-time transmit precoding with imperfect feedback," *IEEE Trans. Inf. Theory*, vol. 47, no. 6, pp. 2632–2639, 2001.

[117] S. A. Jafar and A. Goldsmith, "Transmitter optimization and optimality of beamforming for multiple antenna systems," *IEEE Trans. Wireless Commun.*, vol. 3, no. 4, pp. 1165–1175, 2004.

[118] S. Venkatesan, S. H. Simon, and R. A. Valenzuela, "Capacity of a Gaussian MIMO channel with nonzero mean," in *Proc. IEEE VTC-Fall*, vol. 3, pp. 1767–1771, Oct. 2003.

[119] S. A. Jafar, S. Vishwanath, and A. Goldsmith, "Channel capacity and beamforming for multiple transmit and receive antennas with covariance feedback," in *Proc. IEEE Int. Conf. Commun.*, vol. 7, pp. 2266–2270, June 2001.

[120] M. Vu and A. Paulraj, "On the capacity of MIMO wireless channels with dynamic CSIT," *IEEE J. Sel. Areas Commun.*, vol. 25, no. 7, pp. 1269–1283, 2007.

[121] A. Paulraj, R. Nabar, and D. Gore, *Introduction to Space-Time Wireless Communications.* New York: Cambridge University Press, 2008.

[122] A. W. Marshall, I. Olkin, and B. Arnold, *Inequalities: Theory of Majorization and its Applications.* New York: Academic Press, 1979.

[123] G. Carter, *Coherence and Time Delay Estimation.* Piscataway, NJ: IEEE Press, 1993.

[124] A. L. Swindlehurst, "Time delay and spatial signature estimation using known asynchronous signals," *IEEE Trans. Signal Process.*, vol. 46, no. 2, pp. 449–462, 1998.

[125] H. Miao and M. J. Juntti, "Space-time channel estimation and performance analysis for wireless mimo-ofdm systems with spatial correlation," *IEEE Trans. Veh. Technol.*, vol. 54, no. 6, pp. 2003–2016, 2005.

[126] A. Scaglione, P. Stoica, S. Barbarossa, G. B. Giannakis, and H. Sampath, "Optimal designs for space-time linear precoders and decoders," *IEEE Trans. Signal Process.*, vol. 50, no. 5, pp. 1051–1064, 2002.

[127] S. Gezici, H. Celebi, H. V. Poor, and H. Arslan, "Fundamental limits on time delay estimation in dispersed spectrum cognitive radio systems," *IEEE Trans. Wireless Commun.*, vol. 8, no. 1, pp. 78–83, 2009.

[128] S. M. Alamouti, "A simple transmit diversity technique for wireless communications," *IEEE J. Sel. Areas Commun.*, vol. 16, no. 8, pp. 1451–1458, 1998.

[129] Q. H. Spencer, B. D. Jeffs, M. A. Jensen, and A. L. Swindlehurst, "Modeling the statistical time and angle of arrival characteristics of an indoor multipath channel," *IEEE J. Sel. Areas Commun.*, vol. 18, no. 3, pp. 347–360, 2000.

[130] A. Saleh and R. Valenzuela, "A statistical model for indoor multipath propagation," *IEEE J. Sel. Areas Commun.*, vol. 5, no. 2, pp. 128–137, 1987.

[131] A. P. Dempster, N. M. Laird, and D. B. Rubin, "Maximum likelihood from incomplete data via the EM algorithm," *J. Royal Statistical Soc., Ser. B*, vol. 39, no. 1, pp. 1–38, 1977.

[132] T. Moon, "The expectation-maximization algorithm," *IEEE Signal Process Mag.*, vol. 13, no. 6, pp. 47–60, 1996.

[133] B. Fleury, X. Yin, K. Rohbrandt, P. Jourdan, and A. Stucki, "Performance of a high-resolution scheme for joint estimation of delay and bidirection dispersion in the radio channel," in *Proc. IEEE VTC-Spring*, pp. 522–526, 2002.

[134] J. Wallace and M. Jensen, "Modeling the indoor MIMO wireless channel," *IEEE Trans. Antennas Propag.*, vol. 50, no. 5, pp. 591–599, 2002.

[135] N. Czink, X. Yin, H. Ozcelik, M. Herdin, E. Bonek, and B. H. Fleury, "Cluster characteristics in a MIMO indoor propagation environment," *IEEE Trans. Wireless Commun.*, vol. 6, no. 4, pp. 1465–1475, 2007.

[136] M. Matthaiou, D. I. Laurenson, and J. S. Thompson, "Detailed characterization of an indoor MIMO channel in the double directional spatial domain," *IET Microwaves Antennas Propag.*, vol. 3, no. 2, pp. 205–213, 2009.

[137] A. Abdi and M. Kaveh, "Parametric modeling and estimation of the spatial characteristics of a source with local scattering," in *Proc. IEEE ICASSP*, pp. 2821–2824, 2002.

[138] K. V. Mardia and P. E. Jupp, *Directional Statistics.* Chichester, England: Wiley, 2000.

[139] O. Besson and P. Stoica, "Decoupled estimation of DOA and angular spread for a spatially distributed source," *IEEE Trans. Signal Process.*, vol. 48, no. 7, pp. 1872–1882, 2000.

[140] T. Trump and B. Ottersten, "Estimation of nominal direction of arrival and angular spread using an array of sensors," *Signal Process.*, vol. 50, no. 1-2, pp. 57–69, 1996.

[141] S. Gezici, "A survey of wireless position estimation," *Wireless Pers. Commun.*, vol. 44, no. 3, pp. 263–282, 2008.

[142] F. Bai and A. Helmy, "A survey of mobility models in wireless adhoc networks," in *Wireless Ad Hoc and Sensor Networks*, Kluwer Academic Publishers, 2004.

[143] J. A. Fessler and A. O. Hero, "Space-alternating generalized expectation-maximization algorithm," *IEEE Trans. Signal Process.*, vol. 42, no. 10, pp. 2664–2677, 1994.

List of Publications

Journal papers

1. L. Zhang, Y. H. Chew, W.-C. Wong, "A novel angle-of-arrival assisted extended Kalman filter tracking algorithm with space-time correlation based motion parameters estimation", *Pervasive and Mobile Computing (Elsevier)* (as an extended version of the IWCMC paper, under review)

2. L. Zhang, Y. H. Chew, W.-C. Wong, "Transmitter precoder design to improve the performance of the MUSIC algorithm", *Signal Processing (Elsevier)*, vol. 93, no. 11, pp. 3202-3208, 2013

3. L. Zhang, Y. H. Chew, W.-C. Wong, "Enhanced AoA estimation and localization through transmitter precoder design", *International Journal of Wireless Information Networks*, vol. 19, no. 4, pp. 315-325, 2012

Conference papers

1. L. Zhang, Y. H. Chew, W.-C. Wong, "A novel angle-of-arrival assisted extended Kalman filter tracking algorithm with space-time correlation based motion parameters estimation", in *Proc. IEEE International Wireless Communications and Mobile Computing Conference (IWCMC)*, Jul. 2013

2. L. Zhang, Y. H. Chew, W.-C. Wong, "Improving the performance of the time-of-arrival estimator in MIMO systems", in *Proc. IEEE International Conference on Signal Processing and Communication Systems (ICSPCS)*, Dec. 2012

3. L. Zhang, Y. H. Chew, W.-C. Wong, "A MAP-based channel estimation algorithm for SIMO systems over extended SV channel model", in *Proc. IEEE International Conference on Communication Systems (ICCS)*, Nov. 2012

4. L. Zhang, Y. H. Chew, W.-C. Wong, "Precoder design for improving the performance of the MUSIC-based Angle-of-Arrival estimator", in *Proc. IEEE International Symposium on Personal, Indoor and Mobile Radio Communications (PIMRC)*, Sep. 2011